18th International Workshop on Optical Waveguide Theory and Numerical Modelling

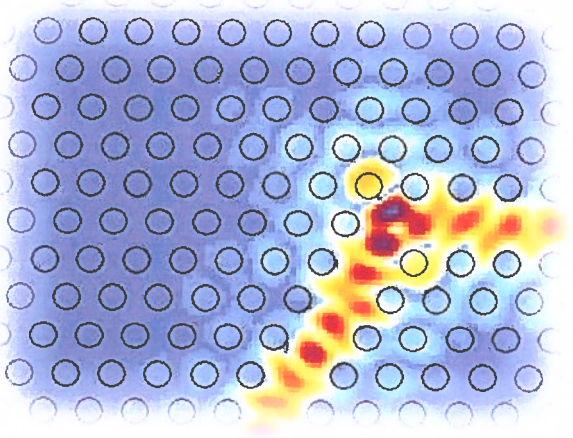

9th – 10th April 2010

Cambridge, UK

Hosted by:

The University of Cambridge, Department of Engineering

The George Green Institute for Electromagnetics Research
University of Nottingham

18th International Workshop on Optical Waveguide Theory and Numerical Modelling

9th – 10th April 2010

University of Cambridge

William Gates Building

Published by:

The George Green Institute for Electromagnetics Research
University of Nottingham
University Park
Nottingham
NG7 2RD
United Kingdom

ISBN 978-0-9541146-2-6

Technical Committee

Trevor Benson, University of Nottingham, UK
Peter Bienstman, Ghent University, Belgium
Jiri Ctyroky, Institute of Electronics and Photonics, Czech Republic
Anand Gopinath, University of Minnesota, USA
Hugo J.W.M. Hoekstra, University of Twente, Netherlands
Andrei V. Lavrinenko, COM-DTU, Lyngby Kgs., Denmark
Xavier Letartre, LEOM, Ecole Centrale de Lyon, France
Andrea Melloni, DEI-Politecnico di Milano, Italy
Reinhold Pregla, FernUniversität Hagen, Germany
Christoph Wächter, Fraunhofer IOF, Jena, Germany

Local Organising Committee

Trevor Benson, University of Nottingham, UK
Ahmed Al-Jarro, University of Nottingham, UK
Ruth Anderson, University of Nottingham, UK
Harshana Gihan Dantanarayana, University of Nottingham, UK
Steve Greedy, University of Nottingham, UK
Salah Obayya, University of Glamorgan, UK
Kathryn Sanderson, University of Nottingham, UK
Phillip Sewell, University of Nottingham, UK
Cattie Tuson, University of Cambridge, UK
Ana Vukovic, University of Nottingham, UK
Adrian Wonfor, University of Cambridge, UK

GIEMR, University of Nottingham, UK
-mail: Kathryn.Sanderson@Nottingham.ac.uk
hone : +44 115 84 68296

CONTENTS

POSTERS

WORKSHOP PROGRAMME

		Thursday 8th April
18:00 - 19:00		Welcome Reception and Registration CAPE Building (Centre for Advanced Photonics and Electronics)
		Friday 9th April
08:00 Onwards		Registration William Gates Building, Computer Laboratory
08:30 – 09:15	FrA	**Plenary: Evolution of Planar Waveguide Devices: Communication and Sensing Applications** *Katsunari Okamoto.* Location: LR1 (Lecture Room 1)
Session 1 **09:15 - 10:45**	**FrJA**	**ECIO / OWTNM Joint Session: Microresonators** **Chair: Trevor Benson, University of Nottingham, UK** Location: LR2 (Lecture Room 2)
09:15 - 09:45	FrJA1	**Analysis of Rotationally Symmetric Resonators (Invited)** *A. Vukovic, P. Sewell, T. M. Benson*
09:45 - 10:00	FrJA2	**3D Light Confinement in Air : The Photon Cage** *C. Sieutat, X. Letartre, P. Viktorovitch, J. L. Leclercq, A. Danescu, G. Grenet, H. Magoariec*
10:00 - 10:15	FrJA3	**Light Localization and Collection Systems Employing Micro/Nano-Spheres** *B. Stout, A. Devilez, N. Bonod*
10:15 - 10:30	FrJA4	**Modeling of Rare Earth Doped Microspheres** *A. Di Tommaso, M. De Sario, M. Ferrari, L. Mescia, T. Palmisano, G. C. Righini, F. Prudenzano*
10:30 - 10:45	FrJA5	**Modeling of Racetrack Resonator with Grating Assisted Coupling** *P. Orlandi, M. Gnan, A. Samarelli, G. Bellanca, A. Melloni, R. M. De La Rue, M. Sorel, P. Bassi*
10:45 - 11:15		**Coffee Break and Informal Viewing of Poster Presentations - Location: FW11**
Session 2 **11:15 - 12:45**	**FrJB**	**ECIO / OWTNM Joint Session: Quantum Phenomena** **Chair: Dominic Gallagher, Photon Design** Location: LR2 (Lecture Room 2)
11:15 - 11:30	FrJB1	**Quantum Random Walks Circuits with Photonic Waveguides** *A. Peruzzo, J. Matthews, A. Politi, M. Lobino, X-Q. Zhou, M. G. Thompson, J. O'Brien, N. Matsuda, N. Ismail, K. Wörhoff, Y. Bromberg, Y. Lahini, Y. Silberberg*
11:30 - 11:45	FrJB2	**Integrated Optics Implementation of Universal Quantum Gates, Bell States Preparation Circuit, Quantum Relay and Quantum LDPC Decoders** *I. B. Djordjevic*
11:45 - 12:00	FrJB3	**Monolithic Directional Optical Antennas for Funneling Photons to Single Emitters** *X-W. Chen, V. Sandoghdar, M. Agio*

12:00 - 12:15	FrJB4	**Tm:Ti:LiNbO$_3$ Waveguide for Quantum Memory Applications** *M. George, R. Ricken, W. Sohler, E. Saglamyurek ,N. Sinclair, C. La Mela, W. Tittel*
12:15 - 12:30	FrJB5	**A Compiled Version of Shor's Quantum Factoring Algorithm on a Waveguide Chip** *A. Politi, J. C. F. Matthews, J. L. O'Brien*
12:30 - 12:45	FrJB6	**Entangled Multi-Photon States in Waveguide for Quantum Metrology** *J. C. F. Matthews, A. Politi, D. Bonneau, J. L. O'Brien, A. Stefanov*
12:45 - 13:45		**Lunch Break - Department of Physics, Cavendish Laboratory**
Session 3 **13:45 - 15:30**	**FrE**	**Periodic Structures and Photonic Bandgaps** **Chair: John Love, The Australian National University, Canberra** Location: LR2 (Lecture Room 2)
13:45 - 14:00	FrE1	**Semi-Analytical Approach to the Analysis and Design of Photonic Crystal Cavities** *M. Felici, K. A. Atlasov, A. Surrente, K. F. Karlsson, E. Kapon*
14:00 - 14:15	FrE2	**Normalized Analysis for Large Tolerance Binary Gratings from a Modal Approach** *T. Kämpfe, E. Gamet, F. Pigeon, O. Parriaux*
14:15 - 14:30	FrE3	**Three-Dimensional Far Field Analysis for Photonic-Crystal Nanolasers** *J. Adam, K. A. Atlasov, E. Kapon, M. Gerken*
14:30 - 14:45	FrE4	**Optimizing Two-Dimensional Photonic Crystal Waveguide Bends** *Z. Hu, Y. Y. Lu*
14:45 - 15:00	FrE5	**Robust Topology Optimization of Photonic Crystal Waveguides with Tailored Dispersion Properties** *F. Wang, O. Sigmund, J. Søndergaard Jensen*
15:00 - 15:15	FrE6	**Optimal Tunability of Waveguides based on Silicon Photonic Crystals Infiltrated with Liquid Crystals** *J. Cos, J. Ferré-Borrull, J. Pallarés and L. F. Marsal*
15:15 - 15:30	FrE7	**Coupled-Resonator Optical Waveguides: *Q*-factor and Disorder Influence** *J. Grgić, E. Campaioli, S. Raza, N. A. Mortensen*
15:30 - 16:30		**Coffee Break and Formal Viewing of Poster Presentations - Location: FW11** **Authors are requested to man their posters**
		Poster Presentations
	P1	**Plasmonic Resonant Modes in Coupled and Overlapping Nanowires** *A. Stefanski, A. Manjavacas, V. Myroshnychenko, D. A. Pawlek, J. Garcai de Abajo*

	P33	**Synthesis of Gradient Refractive Index Profile Waveguides with Desired Propagation Properties** *N. E. Nikolaev*
	P34	**Effective-Index-Based Matrix Method: A Semi-Analytical Tool to Design Graded-Index Waveguides and Directional Coupler Devices** *P. Ganguly, J. C. Biswas, S. K. Lahiri, R. Chakraborty*
	P35	**Improved Variational Effective Index Approximation for Photonic Crystal Slabs** *P. Bindal, A. Sharma*
	P36	**Parallel Simulation of Non-Local Non-Linear Schrödinger Systems using Multithreaded Graphical Processing Unit** *M. Baregheh, V. Mezentsev, H. Schmitz*
	P37	**Fundamentals of Multi-Reflector Filtering Technology** *A. V. Tsarev*
	P38	**Numerical Simulation of Power Beam-Splitter based on Photonic Crystal Row of Holes and Brewster Effect** *A. V. Tsarev*
	P39	**Design and Simulation of Photonic Crystal Thin Film Photovoltaic Cells** *G. Gomard, E. Drouard, O. El Daif, X. Meng, A. Kaminski*
16:30 - 18:00	**FrF**	**Special Focus Session on Metamaterials** **Chair: Christoph Wächter, Fraunhofer Institut fuer Angewandte Optik und Feinmechanik Jena** Location: LR2 (Lecture Room 2)
16:30 - 17:00	FrF1	**Modelling Plasmonic Antennas and Related Metallic Nanostructures (Invited)** *O. J. F. Martin*
17:00 - 17:30	FrF2	**Perfect Imaging with Positive Refraction (Invited)** *U. Leonhardt*
17:30 - 18:00	FrF3	**Nonlinear and Switchable Photonic Metamaterials (Invited)** *N. I. Zheludev, V. A. Fedotov, K. F. MacDonald*
20:00		**Workshop Dinner - St Catharines College**
		Saturday 10th April
Session 4 **08:30 - 10:30**	**SaA**	**Methods** **Chair: Salah Obayya, Photonics Research Group, University of Glamorgan** Location: LR2 (Lecture Room 2)
08:30 - 09:00	SaA1	**Recent Developments on Wide Angle and Bidirectional Propagation Methods (Invited)** *A. Sharma, D. Bhattacharya*

- 09:15	SaA2	**Field Enhancement at a Graded-Index Interface between Positive- and Negative-Index Optical Materials** *I. Mozjerin, T. Gibson, E. P. Furlani, I. R. Gabitov, A. A. Hardy, N. M. Litchinitser*
- 09:30	SaA3	**Adaptive Spatial Resolution in Fourier Modal Methods for Modelling Guided-Wave Structures** *J. Čtyroký, I. Richter, P. Kwiecien*
- 09:45	SaA4	**Modified Padé Approximant Operators for Efficient Time-Domain Beam Propagators** *K. Q. Le, T. Benson, P. Bienstman*
- 10:00	SaA5	**Bio-Inspired Computing Applied to the Design of Novel Photonic Devices** *C. H. Silva-Santos, M. S. Gonçalves, H. E. Hernández-Figueroa*
- 10:15	SaA6	**Generalization of Aperiodic Rigorous Coupled Wave Analysis Technique to Ansiotropic Structures** *P. Kwiecien, I. Richter, J. Čtyroký*
- 10:30	SaA7	**Light Propagation in Metal-Clad, Dielectric-Core Multimode Fibres** *J. Love, J. Lambert, S. Law*
- 11:00		**Coffee Break**
on 5 - 12:45	SaB	**Modelling Techniques** **Chair: J. Čtyroký, Institute of Photonics and Electronics, Czech Republic** Location: LR2 (Lecture Room 2)
- 11:30	SaB1	**2D Finite Element Solution for the Maxwell's Equations (Invited)** *B. M. A. Rahman, A. Agrawal, S. M. Raiyan Kabir, K. T. V. Grattan*
- 11:45	SaB2	**Recent Advances in Time Domain Modelling of Photonics Devices** *S. S. A. Obayya*
5 - 12:00	SaB3	**Time-Domain Topology Optimization of Pulse-Shaping Filters** *L. Yang, O. Sigmund, A. V. Lavrinenko, J. M. Hvam*
0 - 12:15	SaB4	**A Multigrid Solver for the Steady-State Solution of Rate Equations Based Semiconductor Optical Amplifier Models** *J. Bos, R. Stoffer*
5 - 12:30	SaB5	**Photonic Crystal Fiber with Bends Based Biosensors** *A. Teyeb, F. AbdelMalek, S. S. A. Obayya, H. Bouchriha*
0 - 12:45	SaB6	**Investigation of CMOS Compatible Widely Tunable Multiplexers on SOI Technology** *A. V. Tsarev, F. De Leonardis, V. M. N. Passaro*
5 - 13:30		**Lunch Break**

Session 6 **13:30 - 15:00**	**SaC**	**Plasmonics** **Chair: Oliver Martin, EPFL, Lausanne** Location: LR2 (Lecture Room 2)
13:30 - 13:45	SaC1	**Simulating Plasmonic Ring Resonators using the Legendre Pseudospectral Time-Domain Method** *S-Y. Chung, C-Y. Wang, C-H. Teng, C-P. Chen, H-C. Chang*
13:45 - 14:00	SaC2	**Transmission Characteristics in Plasmonic Multimode Waveguides** *A. G. Edelmann, S. F. Helfert, J. Jahns*
14:00 - 14:15	SaC3	**Guiding and Focusing Electromagnetic Fields at the Nanoscale with Wedge and Channel Plasmon Polaritons** *S. G. Rodrigo, E. Moreno, S. I. Bozhevolnyi, L. Martín- Moreno, F. J. García-Vidal*
14:15 - 14:30	SaC4	**Plasmonic Waveguides Modelling: Density of Guided Modes Approach** *G. Colas des Francs, J. Grandidier, A. Bouhelier, J. C. Weeber, A. Dereux*
14:30 - 14:45	SaC5	**Computational Techniques for the Analysis and Design of Dielectric-Loaded Plasmonic Circuitry** *O. Tsilipakos, A. Pitilakis, A. C. Tasolamprou, T. V. Yioultsis, E. E. Kriezis*
14:45 - 15:00	SaC6	**Surface Plasmon Characterization Method based on Two-Groove Interference Pattern** *Y. Edlitz, S. Ruschin*
15:00 - 15:30		**Coffee Break**
Session 7 **15:30 - 16:45**	**SaD**	**Applications** **Chair: Andrea Melloni, Politecnico di Milano** Location: LR2 (Lecture Room 2)
15:30 - 16:00	SaD1	**Quantum Photonics using Guided Waves (Invited)** *I. A. Walmsley, N. Thomas-Peter, M. Hu, H. Coldenstrot-Ronge, T. Bartley, B. J. Smith*
16:00 - 16:15	SaD2	**Single-Shot 3D Reconstruction of Complex Dielectric Function of the Glass during the Femtosecond Laser Micro-Fabrication** *A. V. Turchin, M. Dubov, J. A. R. Williams*
16:15 - 16:30	SaD3	**A Guided Mode View on Near-Field Scanning Optical Microscopy Measurements of Optical Magnetic Fields with Slit Probes** *R. Stoffer, M. Hammer, O. V. Ivanova, H. J. W. M. Hoekstra*
16:30 - 16:45	SaD4	**Enhanced Transmission of Electromagnetic Radiation through Subwavelength Apertures beyond the Cutoff Wavelength** *S. Carretero-Palacios, S. G. Rodrigo, L. Martin-Moreno, F. J. Garcia-Vidal*
16:45		**Concluding Remarks and Close**

3D light confinement in air : the photon cage

C. Sieutat[1], X. Letartre[1], P. Viktorovitch[1], J.L. Leclercq[1], A. Danescu[1], G. Grenet[1], H. Magoariec[2]

[1] *Université de Lyon, Institut des Nanotechnologies de Lyon (INL), UMR CNRS 5270*
Ecole Centrale de Lyon, 36 avenue Guy de Collongue, F 69134 Ecully Cedex, France
xavier.letartre@ec-lyon.fr

[2] *Université de Lyon, Laboratoire de Tribologie et Dynamique des Systèmes (LTDS), UMR CNRS 5513*
Ecole Centrale de Lyon, 36 avenue Guy de Collongue, F 69134 Ecully Cedex, France

It is emphasing that Micro-Nano-Photonics can be defined as the control of photons within the tiniest possible space during the longest possible time. Optical microresonators are considered as the basic conceptual and technological bricks for that purpose. They are meant to provide strong spectral and spatial confinement of photons, which is essential for the efficient operation of a wide range of active micro-nano-photonic devices, including low threshold micro-lasers, non-linear optical devices and biochemical sensors. The general approach to achieve strong confinement of photons consists in high index contrast structuring of space at the wavelength scale. The progress in micro-nano-photonic integration technology has resulted in a large variety of photonic devices, fabricated along planar technological schemes, but mainly restricted to 2D operation. This way, multiple demonstrations have been made based on microdisk-, micropillar- and photonic crystals microcavities.

Significant progress for quasi 3D control of photons has been achieved in our group along a 2.5D nanophotonics approach which can be considered as an extension of planar 2D photonic crystal-based technology exploiting the vertical direction[1-4].

In this paper we propose a new concept for the 3D control of light in real 3D optical microresonators that can be assimilated to 'cages', where photons are trapped efficiently. The main attractive feature of this photon cages lies in their ability to result in a considerable enhancement of the electromagnetic field in the central part of the cage, that is in the air region, opening the way to new sensing or trapping of nanoparticles in fluidic (gas or liquid) ambiances.

We will present the basic concepts we exploit to confine photons in air using cylindrical or spherical structures based on a periodic lattice of pillars (or stripes). These structures act as 2D/3D mirrors to trap photons in a small volume of low index material (e.g. air). Numerical results, based on FDTD simulations, will illustrate this new idea. Finally, an original technological approach, based on mechanical relaxation of strained microstructures, will be proposed for the fabrication of such 'photon cages'.

References

[1] X. Letartre et al, *Journal of Lightwave Technology*, 21, 1691 (2003).
[2] B. Ben Bakir et al, *Appl. Phys. Lett.* 88, 081113 (2006) and *Virtual Journal on Nanoscale Science & Technology* (2006), 13 n°10.
[3] S. Boutami et al, *Appl. Phys. Lett.* 91, 071105 (2007)
[4] L. Ferrier et al, *Optics Express* 16, 3136-3145 (2008)

Light localization and collection systems employing micro/nano-spheres

Brian Stout* , Alexis Devilez, Nicolas Bonod
Institut Fresnel, Aix – Marseille université, Domaine universitaire de St Jérôme, 13397 Marseille, France
brian.stouts@fresnel.fr

Abstract

We demonstrate the utility of quasi-analytic calculations to accurately design light localization, collection, and emission systems using dielectric microspheres or metallic nano-spheres.

Dielectric microspheres can focus light in their near field with low divergence, A phenomenon called photonic nano-jets [1]. We have demonstrated the utility of analyzing the properties of these beams in reciprocal space. Notably, one can demonstrate that the illumination of the microsphere by a focused beam already containing large k-vectors enables the suppression the large z-axis extension of the emerging beam [2,3]. These subwavelength properties recommend photonic jets as a useful tool for high resolution nano-particles detection, fluorescence microscopy improvements and nano-patterning. Despite some their highly desirable properties of low loss and high directivity, systems involving dielectric systems are mico-meter scaled and largely limited by diffraction.
Truly sub-wavelength manipulation of light apparently require systems involving localized plasmon resonances.[4-6]. Recent investigations have been undertaken to move the localized EM field in the metallic structure by modulating the frequency, the polarization and more interestingly the phase of the excitation beam [7-11]. These studies nicely demonstrate that basic manipulation of the excitation beam can produce various field distributions in the near field of the metal structure. In this presentation, we demonstrate through simulations how antennas made of spherical nano-particles enable the control of light localization at nanometer scale. We demonstrate that by simply tuning the angle of illumination of an excitation plane wave, one can control the localization of the EM enhancement with a spatial resolution on the order of $\lambda/10$ [12].
An unfortunate drawback of nano-particles, particularly for nano-antenna applications is the high loss intrinsic to plasmonic systems. We address the issue of loss in a variety of antenna configurations and address issues concerning optimizing the directivity of emitted radiation and increasing intrinsic properties of the emitter such as its quantum efficiency [13].

References

1. A. Heifetz, S.-C. Kong, A. V. Sahakian, A. Taflove, V. Backman, "photonic Nanojets," J. Comput. Theor. Nanosci. **6**, 1979-1992 (2009).
2. A. Devilez, N. Bonod, J. Wenger, D. Gérard, B. Stout, H. Rigneault, E. Popov, "Three-dimensional subwavelength confinement of light using dielectric microspheres," Opt. Express **17**, 2089 – 2094 (2009).
3. A. Devilez, B. Stout, N. Bonod, E. Popov, "Spectral analysis of three-dimensional photonic jets," Opt. Express **16**, 14200 – 14212 (2008).
4. K. Li, M. I. Stockman, D. J. Bergman, "Self-similar chain of metal nanospheres as an efficient nanolens," Phys. Rev. B **91**, 227402 (2003).
5. W. Rechberger, A. Hohenau, A. Leitner, J. R. Krenn, B. Lamprecht, F. R. Aussenegg, "Optical properties of two interacting gold nanoparticles," Opt. Comm . **220**, 137 - 141 (2003).
6. H. Tamaru, H. Kuwata, H. T. Miyazaki, K. Miyano, "Resonant light scattering from individual Ag nanoparticles and particle pairs", Appl. Phys. Lett. **80**, 1826 (2002).
7. M. I. Stockman, S. V. Faleev, D. J. Bergman, "Coherent control of femtosecond energy localization in nanosystems," Phys. Rev. Lett. **88**, 067402 (2002).
8. M. Aeschlimann, M. Bauer, D. Bayer, T. Brixner, F. J. Garcia de Abajo, W. Pfeiffer, M. Rohmer, C. Spindler, F. Steeb, "Adaptative subwavelength control of nano-optical fields," Nature **446**, 301 (2007).
9. A. F. Koenderink, J. V. Hernandez, F. Rochibeaux, L. D. Noordam, A. Polman, "Programmable Nanolithography with plasmon nanoparticle arrays," Nanoletters **7**, 745 – 749 (2007).
10. J. Le Perchec, P. Quémerais, A. Barbara, T. Lopez-Rios, "Controlling strong electromagnetic fields at subwavelength scales," Phys. Rev. Lett. **97**, 036405 (2006).
11. G. Volpe, S. Cherukulappurath, R. J. Parramon, G. Molina-Terriza, R. Quidant, "Controlling the optical near field of nanoantennas with spatial phase-shaped beams," Nanoletters **9**, 3608 (2009).
12. A. Devilez, N. Bonod, B. Stout, "Far field control of light localization in nanoantennas," (submitted).
13. J-. J. Greffet, "Nanoantennas for light emission," Science 308, 1561 (2005).

Modeling of Rare Earth Doped Microspheres

A. Di Tommaso[1*], M. De Sario[2], M. Ferrari[3], L. Mescia[2], T. Palmisano[1], G.C. Righini[4], F. Prudenzano[1],

[1] *DIASS, Politecnico di Bari, 74100 Taranto, Italy*

* *ditommaso@deemail.poliba.it*

[2] *DEE, Politecnico di Bari, 70125 Bari, Italy;* [3] *CNR-IFN, CSMFO Lab., 38100 Trento, Italy*

[4] *CNR-IFAC, MDF Lab., 50019 Sesto Fiorentino, Italy*

Two computer codes for the design of active microspheres coupled with tapered fibers have been developed. The former code models the amplification of the Whispering-Gallery Modes (WGMs) propagating into rare earth doped microspheres. The latter code solves the rate equations and the power propagation equations in frequency domain (FD).

Introduction

High Q quality factor dielectric microspheres are very attractive for many applications: nonlinear optics, evanescent-wave sensing, amplification. In particular, active microspheres allow to design novel devices, e.g. in active biosensing area. In this work, two different versatile models are ad hoc developed/optimized for the design of rare earth doped dielectric microspheres. The design of an Er^{3+} doped silica microsphere, surrounded by air and coupled to a tapered silica fibre permits to show the code effectiveness. The tapered fibre can couple the light at both pump and signal wavelengths into low order WGMs closely confined to the sphere surface and equator. In the former home made computer code, the cavity resonances and the amplification due to rare earth have been modelled by means of an advanced FDTD (Finite Difference Time Domain) algorithm. The latter home made computer code takes into account the FD (Frequency Domain) analytical WGM solution, the coupling between microsphere and the tapered fiber, the rate equations, pertaining to ion population of the Er^{3+} energy levels and the power propagation equations, in the frequency domain. The simulated results are compared and their agreement validates each other both the codes.

Results

The investigated amplifying system consists of an erbium doped silica microsphere having radius R_s=15 μm. A tapered fibre having waist radius R_f=0.45 μm excites and extracts both the pump and the signal and it is far 300 nm from the microsphere. In this way the phase matching between the microsphere WGM at the signal wavelength and the fibre fundamental mode occurs. The fibre fundamental modes are considered for both signal and pump. The pump wavelength is 980 nm, the signal wavelength envelopes a sinusoidal carrier at 1.53 um. The pump power is 0.8 mW, because this value allows the complete ion population inversion. By means FDTD approach the transient response of the amplifying system to the CW input signal is simulated. In order to simplify the amplifying system model, a two-dimensional (2-D) approach can be used to study the WGMs along the sphere equator. The electromagnetic field profile of the microsphere WGMs are analytically calculated for both pump and signal. In steady state regime, the 2D FDTD method is less rigorous than 3D FD. Thus, the WGM electromagnetic field profiles and the propagation constants show a slight displacement. Nonetheless, by means of 2D FDTD approach it is possible to investigate other different structures.

Acknowledgements: The work has been developed within the COST ACTION MP0702: Towards Functional Sub-Wavelength Photonic Structures.

References L. Mescia, F. Prudenzano, M. De Sario, T. Palmisano, M. Ferrari, G.C. Righini, "Design of Rare Earth Doped Microspheres", accepted on Photonics Technology Letters.

Modeling of Racetrack Resonator with Grating Assisted Coupling

P.Orlandi[1], M.Gnan[1], A.Samarelli[2], G.Bellanca[3], A.Melloni[4], R.M.De La Rue[2], M.Sorel[2], P.Bassi[1]
[1] *DEIS, University of Bologna, Viale Risorgimento 2, I 40136, Bologna, Italy*
piero.orlandi@unibo.it
[2] *Electronics and Electrical Engineering Department, Glasgow University, Glasgow, UK*
[3] *Dipartimento di Ingegneria, University of Ferrara, Via Saragat 1, I 44100 Ferrara, Italy*
[4] *Dipartimento di Elettronica e Informatica, Politecnico di Milano, via Ponzio 34/5, I 20133, Milano, Italy*

We study the properties of Grating Assisted Couplers (GACs) included in a racetrack resonator geometry. A more detailed theoretical model of the coupling than is usually performed is shown to be necessary to describe correctly the behaviour of devices fabricated in SOI.

Introduction

The GAC is an optical component successfully applied in integrated optics ($LiNbO_3$) [1] and fibre optics [2]. Recently, it has been used in SOI to demonstrate channel dropping with dispersion control, with devices as long as 100 μm [3]. In order to reduce the device length and retain high selectivity, we have arranged it into a racetrack resonant cavity, thus obtaining a novel device. Such a device can be functional for add-drop behavior of a limited set of channels in DWDM systems.

Results

Using the simplified Coupled Mode Theory and the transfer matrix approach implemented by ASPIC modeling software [4], the inclusion of the GAC into the racetrack geometry limits the frequency range over which the resonance occurs (Fig.1). Characterization of devices fabricated in SOI having grating regions made by sinusoidal sidewall modulation shows an overall similarity to the simulated behavior, but also discrepancies that the model cannot encompass, such as coupling of the isolated port and split resonance peaks. In this paper, we shall show that correct device modeling requires accurate description of the modal coupling within the GACs. The hypotheses of weak coupling and weak perturbation of the high confinement modal regime will be progressively released and discussed in relation to the accurate modeling of the racetrack resonance.

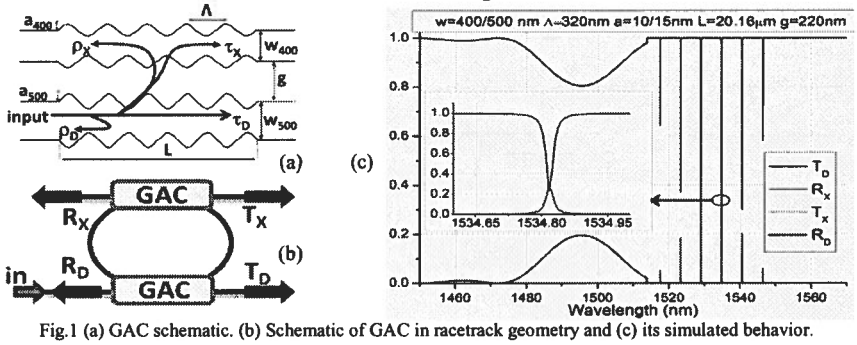

Fig.1 (a) GAC schematic. (b) Schematic of GAC in racetrack geometry and (c) its simulated behavior.

References

[1] P. Yeh and H.F. Taylor, *Appl. Optics,* **19**, 2848-2855, (1980).

[2] S. Orlov et al. *Opt. Lett.*, **22**, 688-690, (1997).

[3] D. Tan et al., *Appl. Phys. Lett.*, **95**, 141109, (2009).

[4] ASPIC, *www.aspicdesign.com*, Filarete, Italy.

Quantum Random Walks Circuits with Photonic Waveguides

Alberto Peruzzo, Jonathan Matthews, Alberto Politi, Mirko Lobino, Xiao-Qi Zhou, Mark G. Thompson, and Jeremy O'Brien
Department of Electrical and Electronic Engineering
University of Bristol, Bristol, United Kingdom

Nobuyuki Matsuda
Research Institute of Electrical Communication
Tohoku University, Sendai, Japan

Nur Ismail, Kerstin Wörhoff
Institute for Nanotechnology
University of Twente, Enschede, The Netherlands

Yaron Bromberg, Yoav Lahini, Yaron Silberberg
Department of Physics of Complex Systems, The
Weizmann Institute of Science, Rehovot, Israel

Abstract—**Arrays of 21 evanescently coupled waveguides are fabricated to implement quantum random walks and a generalized form of two-photon non-classical interference, which was observed via two photon correlation.**

Keywords-component; quantum optics; waveguides; quantum computing; quantum random walks.

I. INTRODUCTION

Quantum random walks, the quantum analogue of statistical random walks, have great potential for designing a new generation of quantum algorithms and can be regarded as a primitive for universal quantum computation. Derived from Richard Feynman's original proposal in the 1960s, physical observation of random walks based upon quantum mechanical behaviour has been an important pursuit in modern quantum physics. Demonstrations of discrete time quantum walks have so far included Nuclear Magnetic Resonance [1], the phase space of trapped ions [2], the position space of trapped ions [3], and the path of a single photon in a network of (bulk) linear optics [4].

Continuous time quantum walks (CTQW) have been demonstrated using NMR [5] and in a so called ``optical version of Galton's board" in the optical frequency space of an optical resonator [6] and in the tunnelling of light in coupled arrays of integrated waveguide structures [7].

The effective de-coherence free properties of photons make them an attractive test-bed for realizing quantum walks (as well as many other quantum mechanical behaviour). Quantum circuits are typically a series of nested interferometers (including [4]), which due to the nature of interferometry realized with bulk optics, is severely limited in size and complexity.

One of the most promising architectures for realizing CTQW is based on inherently stable integrated waveguide structures, already demonstrated in realizing optical circuits for quantum application [8-12].

For any circuit that would realize a quantum walk based on linear optics using an n-mode unitary, one could construct the circuit as a decomposition of 2-mode unitaries [13]. Decomposing circuits in this manner is, however, costly with respect to repeated bending circuitry into and out of interferometers. Instead, observation of larger CTQW (currently of the order 20-30 vertices) can be achieved using the direct tunnelling of light between coupled, ordered waveguide on a single array [7] (Fig. 1). By using this same architecture, the effects of Anderson localization on propagating quantum information [14] has been experimentally simulated using coherent light [15].

The statistics from measuring CTQW can be also predicted with a classical treatment. This provides motivation for the theoretical study into the distinctly non-classical effects of interfering more than one identical photon in an array of coupled waveguides [16]. This generalization of Hong-Ou-Mandel interference leads to various patterns of correlated statistics dependent upon the input state. While part of the model can be verified with classical correlation statistics (as they do in [16]), no experiment to date has been reported using quantum states of single photons to reproduce the full quantum correlation behaviour.

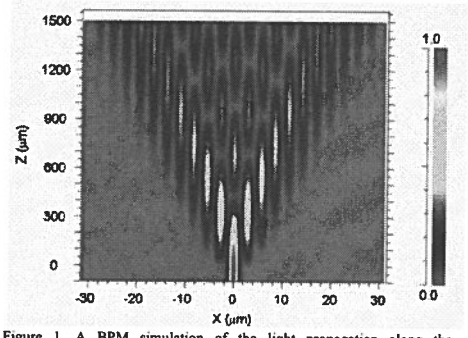

Figure 1. A BPM simulation of the light propagation along the waveguides array when the light is injected into the central waveguide.

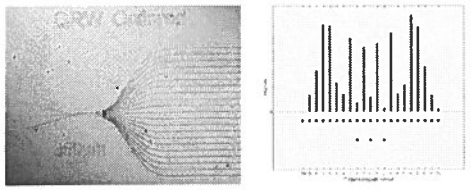

Figure 2 Left: An optical micrograph of a 21 waveguide quantum random walk device. Three input waveguides, initially separated by 250 micron, fan in to the 350 micron long coupling region, and 21 waveguides fan out to a 125 micron spacing. Right: Single photon quantum random walk data.

II. METHODS

For the device fabrication silicon oxynitride (SiON) layers are grown on thermally oxidized (8μm) Si <100> wafers (Fig. 2). The deposition is carried out in an Oxford parallel plate PECVD reactor utilizing SiH_4 and N_2O precursors. After annealing the channel waveguides are obtained by standard lithography and reactive ion etching in CHF_3 / O_2 chemistry. The channel structures are covered by a PECVD silicon oxide (SiO_2) cladding layer.

We coupled single photon pairs into the waveguides arrays and detected with silicon avalanche single photon detectors. To generate the single photon pairs a type I spontaneous parametric downconversion process was used. This is a $\chi^{(2)}$ nonlinear process where a bismuth borate BiB2O6 crystal is pumped by a 402 nm wavelength, 60 mW laser. The single photons are collected with polarization mantaining fibre arrays and injected into the waveguides. At the output a single mode fibre array was used to connect each waveguide to each detector.

The characterization of the QRW arrays has been done by measuring the single photon distribution (Fig. 2 left).

III. RESULTS AND CONCLUDING REMARKS

Fig. 2 left reports the output intensity when a single photon is injected into the central input waveguide.

When two photons are coupled into the waveguides, two photon correlation can be measured and the results are shown in Fig. 3. Remarkably the general behaviour of the quantum walks is demonstrated for the first time and it is in accordance with the predictions (Fig. 4). These results represent a first step highlighting the quality of these structures and their potential for quantum computing applications.

REFERENCES

[1] C. A. Ryan, M. Laforest, J. C. Boileau, R. Laflamme, PRA 72, 062317 (2005).

[2] H. Schmitz et al. arxiv.org/abs/0904.4214 (2009).

[3] M. Karski et. al. Science 325,174 (2009).

[4] B. Do et al., J. Opt. Soc. Am. B 22, 499 (2005).

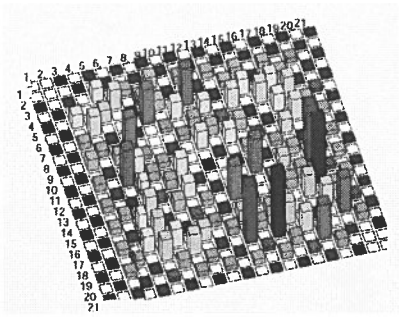

Figure 3. Measured 2-photons quantum correlation matrix when the photons are coupled to two adjacent waveguides.

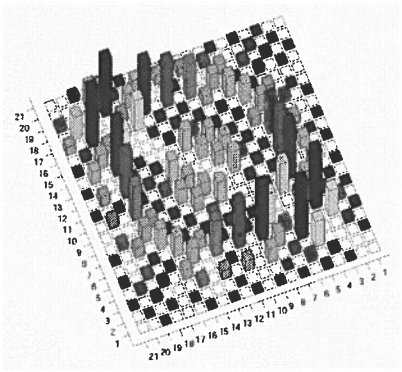

Figure 4. Simulation of the 2-photons quantum correlations when the photons are couple to adjacent waveguides.

[5] J. Du et. al. PRA 67, 042316 (2003).

[6] D. Bouwmeester, I. Marzoli, G. P. Karman, W. Schleich, J. P. Woerdman, PRA 61, 013410 (1999).

[7] H. B. Perets et al., PRL 100, 170506 (2008).

[8] A. Politi, et. al. Science 320, 646 (2008).

[9] J. C. F. Matthews, A. Politi, A. Stefanov, J. L. O'Brien Nature Photonics 3 346 (2009)

[10] A. Politi, J. C. F. Matthews, J. L. O'Brien Science 325, 1221 (2009).

[11] G. D. Marshall, A. Politi, J. C. F. Matthews, P. Dekker, M. Ams, M. J. Withford, J. L. O'Brien, Optics Express, 17, 15, 12546 (2009).

[12] A. Politi, J. C. F. Matthews, M. G. Thompson, J. L. O'Brien, IEEE Journal of Selected Topics in Quantum Electronics, 15, 6, 1673-1684 (2009).

[13] M. Reck, A. Zeilinger, H. J. Bernstein, P. Bertani PRL 73, 58 (1994).

[14] J. P. Keating, N. Linden, J. C. F. Matthews, A. Winter PRA, 76, 1, 012315 (2007).

[15] Y. Lahini, A. Avidan, F. Pozzi, M. Sorel, R. Morandotti, D. N. Christodoulides , Y. Silberberg, PRL 100, 013906 (2008).

[16] Y. Bromberg, Y. Lahini, R. Morandotti, Y. Silberberg, PRL, 102, 253904 (2009).

Integrated Optics Implementation of Universal Quantum Gates, Bell States Preparation Circuit, Quantum Relay and Quantum LDPC Decoders

Ivan B. Djordjevic
University of Arizona, Department of Electrical and Computer Engineering
1230 E. Speedway Blvd., Tucson, AZ 85721, USA
ivan@ece.arizona.edu

Abstract— **We show that arbitrary family of universal quantum gates can be implemented in integrated optics based on single optical hybrid/Mach-Zehnder interferometer/directional coupler and highly nonlinear optical fibers (HNLFs). We also show how to implement the Bell states preparation circuit and quantum relay, needed in quantum teleportation systems, using the same technology. Finally, we study the implementation of sparse-graph quantum decoders in integrated optics.**

Keywords- quantum teleportation; quantum information processing; integrated optics devices; quantum error-correction codes (QECCs); sparse-graph quantum codes

I. INTRODUCTION

Quantum information processing (QIP) is an active research area with numerous applications, including quantum teleportation and quantum computing [1]. In order to perform an arbitrary quantum computation operation a minimum number of gates, known as universal quantum gates [1],[2]-[4], is needed. In this paper, we show that arbitrary single-qubit gate can be implemented based on single optical hybrid (OH)/Mach-Zehnder interferometer (MZI)/directional coupler (DC). We also show how to implement the deterministic CNOT gate based on OH/MZI/DC and highly nonlinear optical fiber (HNLF), which completes the implementation of arbitrary set of universal quantum gates in all-fiber technology. Two basic quantum circuits needed in quantum teleportation are Bell states preparation circuit and quantum relay. We also show how to implement them in integrated optics. The QIP, unfortunately, relies on delicate superposition states, which are sensitive to interactions with environment, resulting in decoherence. Moreover, the quantum gates are imperfect and the use of quantum error correction coding (QECC) is essential to enable the fault-tolerant computing and to deal with quantum errors [1]. In our recent paper [5] we proposed several structured quantum LDPC codes based on the balanced incomplete block designs (BIBDs), which offer a number of advantages thanks to the sparness of their quantum check-matrix. We show that encoder/decoder for arbitrary quantum LDPC code can be implemented in integrated optics as well.

II. INTEGRATED OPTICS IMPLEMENTATION OF UNIVERSAL QUANTUM GATES AND PAULI GATES

In what follows, the logical "0" is represented by a horizontal (H) photon $|H\rangle=[1\ 0]^T$ and the logical "1" is represented by a vertical (V) photon $|V\rangle=[0\ 1]^T$. An arbitrary single-qubit gate can be implemented in integrated optics based on OH, MZI or DC as shown in Figs. 1 (a)-(c), respectively. By expressing the power splitting ratio of OH as $k=\cos^2(\gamma/2)$ where angle γ is used to parameterize the power splitting ratio, the output qubit $[\psi_{H,o}, \psi_{V,o}]^T$ is related to the input qubit $[\psi_H, \psi_V]^T$ by

$$\begin{bmatrix}\psi_{H,o}\\ \psi_{V,o}\end{bmatrix}=U\begin{bmatrix}\psi_H\\ \psi_V\end{bmatrix},\ U=\begin{bmatrix}\cos\left(\frac{\gamma}{2}\right)e^{j(\alpha-\beta/2-\delta/2)} & -\sin\left(\frac{\gamma}{2}\right)e^{j(\alpha-\beta/2+\delta/2)}\\ \sin\left(\frac{\gamma}{2}\right)e^{j(\alpha+\beta/2-\delta/2)} & \cos\left(\frac{\gamma}{2}\right)e^{j(\alpha+\beta/2+\delta/2)}\end{bmatrix}. \quad (1)$$

The matrix U in eq. (1) represents the matrix representation of an arbitrary single-qubit quantum gate according to the Z-Y decomposition theorem (see equation (4.12) in [1]). The same equation holds for MZI-based and DC-based single-qubit quantum gate (see Figs. 1(b,c)). By setting $\gamma=\delta=0$ rad, $\alpha=\pi/4$ and $\beta=\pi/2$ rad U-gate described by (1) operates as the phase gate; by setting $\gamma=\delta=0$ rad, $\alpha=\pi/8$ and $\beta=\pi/4$ rad the U-gate operates as $\pi/8$ gate; while by setting $\gamma=\pi/2$, $\alpha=\pi/2$, $\beta=0$ rad and $\delta=\pi$, the U-gate operates as Hadamard gate.

To complete the implementation of the following set of universal quantum gates {Hadamard, phase, $\pi/8$, CNOT}, the implementation of CNOT-gate is needed. The authors in [2] proposed the use of directional couplers to implement the CNOT-gate. However, in that proposal, the control output qubit is affected by input target qubit, which violates the definition of CNOT-gate operation (control qubit must be unaffected by target qubit) [1]. The CNOT gate from [2] operates correctly only with probability of 1/9, and is essentially a probabilistic gate. In Fig. 2 we show the deterministic implementation of CNOT-gate based on optical hybrid shown in Fig. 1 and HNLF. By using the quantum-mechanical description provided in [1], it can be shown that output control $|C_o\rangle=[c_{H,o}\ c_{V,o}]^T$ and target qubits $|T_o\rangle=[t_{H,o}\ t_{V,o}]^T$ are related to corresponding input qubits by:

$$\begin{bmatrix}c_{H,o}\\ c_{V,o}\\ t_{H,o}\\ t_{V,o}\end{bmatrix}=\underbrace{\frac{1}{\sqrt{2}}\begin{bmatrix}1&1&0&0\\1&-1&0&0\\0&0&1&1\\0&0&1&-1\end{bmatrix}}_{I\otimes H}\underbrace{\begin{bmatrix}1&0&0&0\\0&1&0&0\\0&0&1&0\\0&0&0&-1\end{bmatrix}}_{K}\underbrace{\frac{1}{\sqrt{2}}\begin{bmatrix}1&1&0&0\\1&-1&0&0\\0&0&1&1\\0&0&1&-1\end{bmatrix}}_{I\otimes H}\begin{bmatrix}c_H\\ c_V\\ t_H\\ t_V\end{bmatrix} \quad (2)$$

$$=U_{CNOT}\begin{bmatrix}c_H\\ c_V\\ t_H\\ t_V\end{bmatrix},\ U_{CNOT}=\begin{bmatrix}1&0&0&0\\0&1&0&0\\0&0&0&1\\0&0&1&0\end{bmatrix}$$

This paper was supported in part by the NSF under Grant IHCS-0725405.

The Kerr nonlinearity device in Fig. 2 performs the controlled-Z operation. In the absence of control c_V-photon the target qubit is unaffected because $H^2=I$ (identity operator). In the presence of control c_V-photon, thanks to the cross-phase modulation in HNLF, the target vertical photon experience the phase shift χL, where χ is the third order nonlinearity susceptibility coefficient and L is the HNLF length. By selecting appropriately the fiber length we obtain $\chi L=\pi$ and the overall action on target qubit is $HZH=X$, which corresponds to the CNOT gate action.

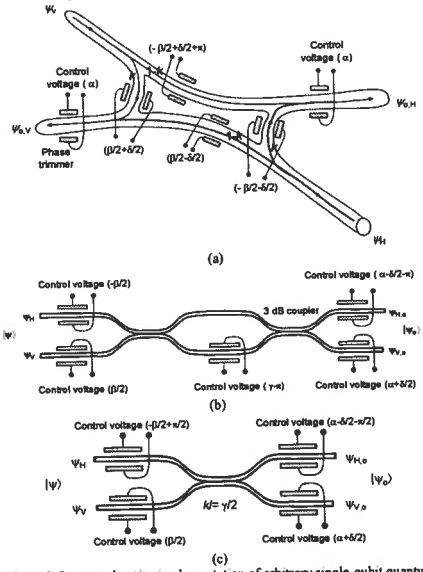

Figure 1. Integrated optics implementation of arbitrary single-qubit quantum gate based on single: (a) optical hybrid, (b) Mach-Zehnder interferometer and (c) directional coupler (k-the coupling coefficient, l-the coupling region length).

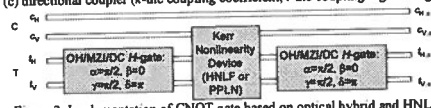

Figure 2. Implementation of CNOT gate based on optical hybrid and HNLF. OH/MZI/DC H-gate: OH/MZI/DC based Hadamard gate, PPLN: periodically poled LiNbO3.

With small modifications in (1) and by using similar approach to that described in Fig. 2, we can easily obtain the Barenco gate; while Deutsch gate can be obtained by employing three control qubits, instead of one used in Fig. 2.

By using the U-gate shown in Fig. 1 and by appropriately setting the phase shifts α, β, γ, and δ we can obtain the corresponding Pauli gates. The Y-gate is obtained by setting $\gamma=\pi$, $\beta=\delta=0$ rad and $\alpha=\pi/2$; the Z-gate is obtained by setting $\gamma=\delta=0$ rad, $\alpha=\pi/2$ and $\beta=\pi$; while the X-gate is obtained by setting $\gamma=\pi$, $\delta=0$ rad, $\alpha=\pi/2$ and $\beta=-\pi$.

III. Integrated Optics Implementation of Bell States Preparation Circuit and Quantum Relay

We further describe the implementation of Bell states preparation circuit based on OH/MZI/DC, which is shown in Fig. 3(a). The upper OH/MZI/DC circuit operates as Hadamard gate, while the rest of the circuit operates as CNOT gate. In Fig. 3(b) we describe how to implement the quantum relay based on Bell states preparation circuit (shown in Fig. 3(a)), Hadamard, controlled-X and controlled-Z gates described above. We employ the principle of differed measurement and perform corresponding measurements only in last intermediate node, which is a key difference with various quantum relay architectures described in [6]. The measurements circuits in Fig. 3(b) represent avalanche photodetectotors (APDs), which are used to detect the presence of c_V-photons in corresponding control qubits. The detection of c_V-photons triggers the application of required control voltages on phase trimmers to perform controlled-X and controlled-Z operation.

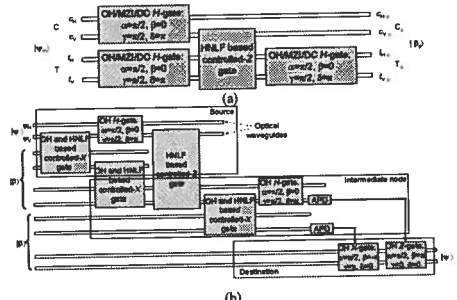

Figure 3. Integrated optics implementation of: (a) Bell states preparation circuit, and (b) quantum relay.

IV. Integrated Optics Implementation of Quantum LDPC Encoders/Decoders

The QECC encoders/decoders are essentially based on Pauli gates, whose implementation in integrated optics is already described in previous section. We have recently shown [5] that encoders and decoders for quantum LDPC codes can be implemented based on Hadamard and CNOT gates only. Therefore, arbitrary quantum LDPC encoder and decoder can be implemented in integrated optics based on OH/MZI/DC.

References

[1] M. A. Neilsen, and I. L. Chuang, *Quantum Computation and Quantum Information*. Cambridge University Press, 2000.

[2] T. C. Ralph *et al.*, "Linear optical controlled-NOT gate in the coincidence basis," *Phys. Rev. A*, vol. 65, paper 062324, 2002.

[3] A. Barenco, "A universal two-bit quantum computation," *Proc. R. Soc. London. A*, vol. 449, pp. 679-683, 1995.

[4] D. Deutsch, "Quantum computational networks," *Proc. R. Soc. London. A*, vol. 425, pp. 73-90, 1989.

[5] I. Djordjevic, "Photonic quantum dual-containing LDPC encoders and decoders," *IEEE Photon. Technol. Lett.*, vol. 21, pp. 842-844, 2009.

[6] S.-T. Cheng *et al.*, "Quantum communication for wireless wide-area networks," *IEEE J. Sel. Areas Comm.*, vol. 23, pp. 1424-1432, 2005.

Monolithic directional optical antennas for funneling photons to single emitters

Xue-Wen Chen, Vahid Sandoghdar and Mario Agio
Laboratory of Physical Chemistry, ETH Zurich, 8093 Zurich, Switzerland
mario.agio@phys.chem.ethz.ch

An emerging strategy for achieving efficient coupling of single emitters with photons relies on optical antennas. Here, we propose a class of metal nanostructures that feature directionality, strong field enhancement, and low losses for applications in quantum photonics and quantum nano-optics.

Introduction

Coupling single photons with single quantum emitters has become central to nanophotonics, for the implementation of integrated quantum networks and computing, but also for improving classical ways of processing information such as optical switching [1]. Progress in nano optics has shown that optical antennas [2] and plasmonic waveguides [3] can lead to large coupling efficiencies with broadband operation and better miniaturization in comparison to micro-resonators. However, optical antennas suffer from dipolar radiation patterns, which require high numerical-aperture optics for achieving strong couplings, and directional antenna arrays imply accurate handling of each individual element at the nanoscale [4]. On the other hand, practical exploitations of plasmonic waveguides need a rapid and effective conversion of surface plasmon-polaritons (SPPs) into photons, especially in the near infrared spectral range. Here, we propose a class of optical antennas that combines the high directionality of plasmonic waveguides with the performances and simplicity of dipole antennas.

Results

The figure below illustrates the concept of integrated monolithic directional antennas, where a finite metal nanostructure acts as an efficient light-matter interface between a nearby quantum emitter and photons, as well as a mode converter for coupling to a lossless waveguide. As an illustrative example, we consider metal nanowires butt-coupled to a dielectric fiber. Under appropriated conditions, we show that more than 95% of the incident guided photons are converted into SPPs and vice versa. The mechanism that boosts the coupling efficiency relies on the formation of a weak resonance at the nanowire-fiber interface, which entails a relationship between the operating wavelength and the nanowire and fiber radii. When we replace the nanowire with a truncated metal cone, SPPs nanofocus towards the cone tip to yield intensity enhancements of more than three orders of magnitude and, when propagating backward, collection efficiencies above 70% in the near infrared spectral range [5,6].

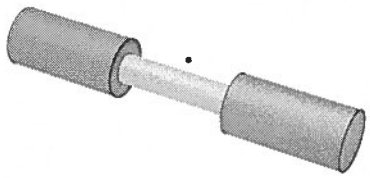

References

[1] J. L. O'Brien, A. Furusawa, J. Vučković, *Nat. Photonics*, **3**, 687-695, (2009)

[2] S. Kühn, U. Håkanson, L. Rogobete, V. Sandoghdar, *Phys. Rev. Lett.*, **97**, 017402, (2006)

[3] D. E. Chang, A. S. Sørensen, P. R. Hemmer, M. D. Lukin, *Phys. Rev. Lett.*, **97**, 053002, (2006)

[4] J. Li, A. Salandrino, N. Engheta, *Phys. Rev. B*, **76**, 245403, (2007)

[5] X.-W. Chen, V. Sandoghdar, M. Agio, *Nano Lett.*, **9**, 3765-3761, (2009)

[6] X.-W. Chen, V. Sandoghdar, M. Agio, *submitted*, (2010)

Tm:Ti:$LiNbO_3$ Waveguide for Quantum Memory Applications

M. George, R. Ricken and W. Sohler
Angewandte Physik, Department Physik
Universität Paderborn, Paderborn, Germany
mathew.george@uni-paderborn.de

E. Saglamyurek, N. Sinclair, C. La Mela and W. Tittel
Institute for Quantum Information Science,
and Department of Physics and Astronomy
University of Calgary, Calgary, Canada

Abstract—**We report fabrication and characterization of a Tm:Ti:$LiNbO_3$ optical waveguide, single mode around 800 nm wavelength, in view of photon-echo quantum memory applications. In particular, room- and low-temperature properties were investigated via loss and absorption measurements, spectral hole burning, photon echo, and Stark spectroscopy.**

Keywords: rare-earth-ion doped crystal; optical waveguide; lithium niobate; photon-echo; quantum memory.

I. Introduction

Quantum memories are key elements for quantum repeaters, which promise overcoming the distance barrier of quantum communication [1]. A currently extensively studied approach relies on photon echoes [2,3]. Tm:Ti:$LiNbO_3$ optical waveguides combine interesting features arising from the specific rare-earth dopant, the host material, as well as the waveguide. Specifically, thulium features a transition at 795 nm (Fig. 1), a wavelength where air is transparent, entangled photons are conveniently generated in non-linear crystals or optical fibres, and high-efficiency and easy-to-operate single photon detectors are commercially available. Furthermore, when implemented into Lithium Niobate, its electronic states acquire permanent electric dipole moments, allowing for modification of the transition frequencies through the application of an electric field [4]. Finally, the use of a waveguide where travelling wave electrodes can be spaced closely and light intensities can be large, promise simple integration with fibre optics and quantum networks, sub-ns Stark frequency control, and large Rabi frequencies, which benefits the optical pumping procedure required for spectral tailoring of the inhomogeneously broadened absorption line [2,3].

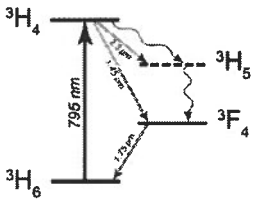

Figure 1. Simplified energy level diagram of Tm:$LiNbO_3$ showing the electronic levels relevant to this work.

II. Waveguide Fabrication and Characterization

A. *Tm diffusion doping of $LiNbO_3$*

Commercially available 0.5 mm thick Z-cut wafers of undoped optical grade congruent lithium niobate were Tm-doped near the +Z-surface before waveguide fabrication. A vacuum deposited Tm layer of 19.6 nm thickness was in-diffused at 1130 ^{0}C during 150 hrs in an argon-atmosphere followed by a post treatment in oxygen (1 h). The diffusion profile was determined by secondary neutral mass spectroscopy (Fig. 2). The maximum Tm concentration of about 1.35 x 10^{20} cm^{-3} corresponds to a concentration 0.74 mole %.

B. *Ti indiffused waveguides in Tm:$LiNbO_3$*

On the Tm-doped surface 3.0 µm wide, 40 nm thick Ti-stripes were deposited and subsequently in-diffused at 1060 ^{0}C for 5 hrs to form 30 mm long optical strip waveguides. In the wavelength range around 775 nm, these waveguides are single mode for TE and TM-polarization (see also Fig. 2).

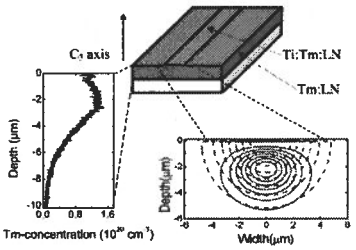

Figure 2. Scheme of the waveguide geometry with the measured Tm concentration profile on the left and the calculated intensity distribution of the fundamental TM-mode superimposed on the profile of the extraordinary index of refraction induced by the Ti-doping. The latter data are for 795 nm wavelength. Iso-intensity lines are plotted for both, the index and the mode profile, corresponding to 100%, 87.5%, 75% etc. of the maximum index increase ($\Delta nmax = 4.0 \times 10^{-3}$) and mode intensity, respectively.

C. *Characterization*

The total waveguide propagation losses, consisting of absorption and scattering loss, were measured around 800 nm wavelength at room temperature by the Fabry-Perot method [5]. In addition, the waveguide propagation loss was determined at 729 nm wavelength where negligible absorption by the Tm-

ions is expected. In this way the scattering loss was determined alone; it is 0.2 dB/cm for both polarizations.

Moreover, polarization dependent transmission spectra of a 30 mm long waveguide were measured, yielding the inhomogeneously broadened spectrum depicted in Fig. 3.

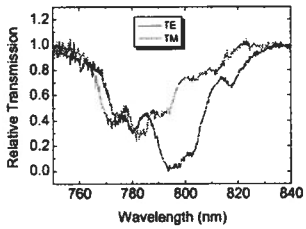

Figure 3. Relative transmission through the Tm:Ti:$LiNbO_3$ waveguide for TM- and TE-polarization, respectively, as a function of wavelength.

III. Thulium Spectroscopy

To characterize Tm:Ti:$LiNbO_3$ waveguides for photon-echo based quantum memories, we studied a large variety of low-temperature (3K) properties (for more information see [6,7]).

First, we repeated the measurement of the inhomogeneously broadened $^3H_6 \leftrightarrow {}^3H_4$ absorption line at 3.5 K, which confirmed the strong polarization dependence that we already found at room temperature. Furthermore, the measurement reflected the temperature dependent distribution of atomic population in the ground state Stark levels, and enhanced absorption for transitions starting in the ground state Stark level.

Next, we investigated relaxation avenues and population dynamics of the $^3H_4$ and $^3F_4$ atomic. This impacts on the possibility to tailor the inhomogeneously broadened absorption line by frequency selectively transferring absorbers to long-lived states. Figure 4 depicts the results of time-resolved spectral hole burning, yielding radiative lifetimes of 82 μs and 2.4 ms for the $^3H_4$ and $^3F_4$ levels, respectively, and a branching ratio from the $^3H_4$ into the $^3F_4$ level of ~ 44%.

We repeated these studies under application of magnetic fields between 100 and 1250 Gauss, oriented parallel to the crystal C_3-axis. This led to the appearance of two atomic ground state sub-levels with lifetimes exceeding 1 second.

An important property that determines the storage time of quantum states in optical atomic is the width of the sharpest spectral feature that can be generated. It depends on the homogeneous linewidth of the $^3H_6 \leftrightarrow {}^3H_4$ transition (which itself is limited by the inverse radiative lifetime) as well as on spectral diffusion, which leads to time dependent broadening. Using two- and three-pulse photon echoes, we found an effective homogeneous linewidth of 1.082 MHz, and hence a minimum spectral feature of around 2 MHz.

Finally, in order to control dephasing and rephrasing of atomic coherence through electric fields [2], we measured the DC Stark effect, again using spectral hole burning techniques. We observed a linear frequency shift (reflecting the symmetry properties of Tm in $LiNbO_3$) of 24.6 ± 0.7 kHz·cm/V.

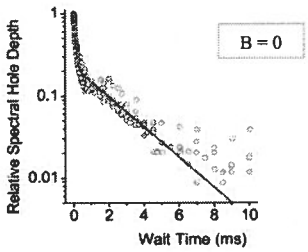

Figure 4. Spectral hole decay under zero magnetic field. Plotted circles denote the normalized spectral hole depth as a function of the waiting time between burning and reading pulses. Two exponential decays are easily identified, yielding radiative lifetimes of 82μs and 2.4 ms for the $^3H_4$ and $^3F_4$ levels, respectively. The branching ratio into the $^3F_4$ level is approximately 44%.

IV. Conclusions

Our findings demonstrate the suitability of Tm:Ti:$LiNbO_3$ waveguides cooled to 3 K for implementations of photon-echo quantum memory protocols. Level structure, lifetimes, and branching ratios allow tailoring of the natural, inhomogeneously broadened absorption profile. The minimum width of spectral holes of ~2 MHz, as determined by spectral diffusion, will limit storage of quantum information in optical coherence to roughly a hundred nanoseconds. While longer times may be achievable at lower temperature, this is still sufficient for mapping coherence onto long-lived ground state coherence, as Rabi frequencies exceeding hundred MHz can be obtained, due to the high power densities achievable inside waveguiding structures. Finally, the existence of a linear Stark shift, together with the possibility to space electrodes closely, allows shifting of resonance frequencies by more than 100 MHz within sub-nanosecond times, thus enabling novel phase control techniques. The first demonstration of a quantum memory protocol, using this waveguide, will be reported elsewhere [8].

References

[1] H. J. Briegel, W. Dür, J. I. Cirac and P. Zoller, "Quantum repeaters: The role of imperfect local operations in quantum communications," Phys. Rev. Lett. 81, 5932 (1998).

[2] W. Tittel *et al.*, " Photon-echo quantum memory in solid state systems" Laser and Photonics Rev. DOI 10.1002/lpor.200810056.

[3] H. de Riedmatten *et al.*, "A solid-state light-matter interface at the single-photon level, " Nature 456, 773 (2008).

[4] R. Macfarlane, "Optical Stark spectroscopy of solids", J. Lumin. 125, 156 (2007).

[5] R. Regener and W. Sohler, "Loss in low-finesse Ti:$LiNbO_3$ waveguide resonators". App. Phys. B, vol 36 p 143 (1985).

[6] N. Sinclair *et al.*, "Spectroscopic investigations of a Ti:Tm:$LiNbO_3$ waveguide for photon echo quantum memory", J. Lumin., in press.

[7] C.W. Thiel *et al.*, "Optical Decoherence and Persistent Spectral Hole Burning in Tm^{3+}:$LiNbO_3$", J. Lumin., in press.

[8] E. Saglamyurek et al., "Integrated quantum memory for quantum communication", to be presented at OFC 2010.

A compiled version of Shor's quantum factoring algorithm on a waveguide chip

Alberto Politi, Jonathan C. F. Matthews & Jeremy L. O'Brien
Centre for Quantum Photonics, H. H. Wills Physics Laboratory & Department of Electrical and Electronic Engineering,
University of Bristol,
Bristol, UK,
Jeremy.Obrien@Bristol.ac.uk

Abstract—**Realization of a compiled version of Shor's quantum factoring algorithm is realized on a waveguide chip. Utilizing quantum and classical interference, multiple quantum gates are integrated within silica-on-silicon waveguide to realize a proof-of-principle of quantum computation within a single optical chip. This demonstration illustrates the importance of integrated optics for future quantum technology.**

Keywords-component; quantum information; algorithm; single photons; integrated waveguides

I. INTRODUCTION

Realizing computation based on quantum physics is one of the main goals for modern science and engineering. Fifteen years ago, Peter Shor proposed an algorithm [1] that would harness the unique quantum mechanical properties of superposition and entanglement to efficiently factorize a product of two large prime numbers [2]. To date, no known algorithm exists using conventional classical computation to solve this problem in time less than exponentially large in the input, making factorization intractable and forms the basis for most modern cryptographic security.

Progress towards proof-of-principle demonstration of Shor's factoring algorithm have included liquid state nuclear magnetic resonance [2] and bulk optical implementations using simplified quantum logic gates [3,4]. While the latter demonstrate the necessary use of entanglement required for improvement over classical computation, they cannot be scaled to the required large number of quantum gates and quantum bits (qubits). Instability and physical size remain as amongst the largest of limitations in complexity implementing practical quantum technology.

Recent demonstrations of using both lithographic and directly written monolithic waveguide circuits for quantum optical experiments [5,6,7,8,9] allows the use of integrated optics as an important platform for future quantum optical schemes. We report the subsequent application of waveguide quantum gates to realize a circuit implementing a compiled version of Shor's quantum algorithm to factorize 15 [10].

This work was supported by Engineering and Physical Sciences Research Council, Quanutm Information Processing Interdisciplinary Research Collaboration, Intelligence Advanced Research Projects Activity, and the Leverhulme Trust. J.L.O'B acknowledges a Royal Society Wolfson Merit Award.

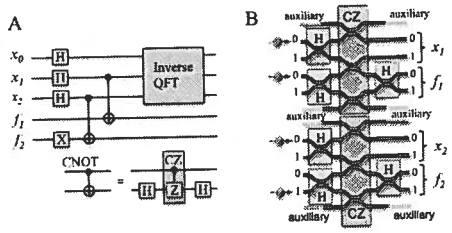

Figure 1: Realizing a compiled version of Shor's algorithm on a waveguide chip. (A) The quantum circuit compiled to factorize 15. (B) Schematic of the waveguide circuit including photonic inputs.

II. METHOD

The full process of Shor's algorithm can be partitioned into conventional classical processing and a quantum sub-routine known as order finding [1,3,4]. Figure 1A shows the quantum circuit for the compiled order finding routine designed specifically to factorize 15 with designed success rate of 1/2. The circuit comprises of a number of single qubit rotations (Hadamard (H), NOT (X)) and two two-qubit entangling gates (controlled π-phase shift (C-Z)) acting on qubits in two registers known as the argument (x_i) and function (f_i). An inverse quantum fourier transform (QFT) acting on the argument register is achieved for certain compiled circuits using classical post-processing [4]. The integrated waveguide version of this circuit consists of directional couplers to realize the quantum optical gates [5] and is shown schematically in figure. The 3.5μm core waveguides, designed to guide the fundamental mode for λ=790nm, are defined by doped silica on a silicon substrate and are fabricated using standard lithographic techniques [5].

Photonic quantum bits are encoded using the path of four 790nm photons simultaneously prepared via spontaneous parametric down-conversion. A 157fs Ti:sapphire laser tuned

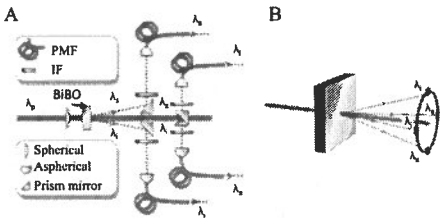

Figure 2: The down conversion based photon source. (A) Schematic of the down conversion source pumped by 390nm light to produce two pairs of 790nm photons, filtered by high transmission interference filters (IF) and collected in four spacial modes (B) into polarization maintaining fibre (PMF).

to 790nm is up-converted using a 2mm thick nonlinear bismuth borate BiB_2O_6 (BiBO) crystal (cut for second harmonic generation) to produce a beam of λ_p=385nm. This is then focused down onto a second BiBO crystal cut for spontaneous parametric down-conversion, producing pairs of signal and idler photons $\lambda_s=\lambda_i$=790nm, which are first filtered through high transmission interference filters (λ_0=790nm), before being collected in polarization maintaining fibres as shown in figure 2.

The photons are injected into the waveguide chip using butt-coupled arrays of polarization maintaining fibre matched to the dimensions of the waveguide circuit, and detected after the waveguide circuit using single photon counting avalanche photodiodes to yield the outcome of the quantum algorithm.

III. Results & Concluding Remarks

Detecting photons in the argument registers yields the outcome of the order finding routine. The two expected failure and two success events are predicted to occur with equal probability (1/4). Our experimental results (given in figure 3) agree with this with a similarity 99±1%. Together with final steps of classical processing, the factors of 15 are correctly determined [10].

While complete scalability of using photons to realize quantum computation is still an open area of research, needing efficient single photon sources and efficient single photon detectors, the ongoing progress in these fields together the use of ultra-stable and miniaturized integrated optical circuits, will

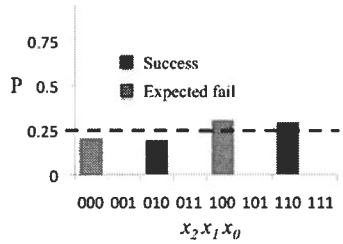

Figure 3: argument register outputs are normalized to a statistical distribution. With classical post-processing, these results reveal the factors of 15 to be 3 and 5 with success rate ½ [4,10]. The dashed line shows the ideal level of the four possible outcomes of the value, while the blue and red bars display expected success and failure outcomes of the circuit.

allow the development of sophisticated quantum circuits and the implementation of large-scale quantum algorithms.

Acknowledgment

We thank R. Jozsa, A. Laing, A. Montanaro, S. Takeuchi, M. G. Thompson and X.-Q. Zhou for helpful discussions.

References

[1] P. W. Shor, in *Proceedings of the 35th Annual Symposium on the Foundations of Computer Science* (IEEE Computer Science Press, Los Alamitos, CA, 1994), pp. 124-134.

[2] L. M. K. Vandersypen *et. al.*, *Nature* **414**, 883 (2001).

[3] C.-Y. Lu, D. E. Browne, T. Yang, J. W. Pan, *Phys. Rev. Lett.* **99**, 250504 (2007).

[4] B. P. Lanyon *et. al.*, *Phys. Rev. Lett.* **99**, 250505 (2007).

[5] A. Politi, M. J. Cryan, J. G. Rarity, S. Yu, and J. L. O'Brien, *Science* **320**, 646 (2008).

[6] A. Politi, J. C. F. Matthews, M. G. Thompson, J. L. O'Brien, *IEEE Journal of Selected Topics in Quantum Electronics*, **15**, 6, 1673-1684 (2009).

[7] G. D. Marshall, et al., *Optics Express*, **17**, 12546 (2009).

[8] J. C. F. Matthews, A. Politi, A. Stefanov and J. L. O'Brien, *Nature Photonics*, **3**, 346 (2009).

[9] B. J. Smith, D. Kundys, N. Thomas-Peter, P. G. R. Smith, I. A. Walmsley *Opt. Exp.* **17**, 13516 (2009).

[10] A. Politi, J. C. F. Matthews and J. L. O'Brien, *Science*, **325**, 1221 (2009).

Entangled Multi-Photon States in Waveguide for Quantum Metrology

Jonathan C. F. Matthews, Alberto Politi,
Damien Bonneau & Jeremy L. O'Brien
Centre for Quantum Photonics, H. H. Wills Physics Laboratory & Department of Electrical and Electronic Engineering,
University of Bristol, Bristol, UK
Jeremy.Obrien@Bristol.ac.uk

André Stefanov
Now at: Federal Office of Metrology METAS,
Bern-Waberm, Switzerland

Abstract—**Entangled photonic states known as "NOON" states are manipulated within monolithic waveguide circuitry. The resulting quantum interference has sufficient visibility to measure phase beyond the shot noise limit using integrated waveguide. We also demonstrate a scheme for heralding two- and four-photon entangled states which can be generalized to arbitrarily large NOON states.**

Keywords-component; quantum metrology; integrated waveguides; single photons

I. INTRODUCTION

Harnessing quantum superposition and quantum entanglement of single photon is already providing enhanced security with quantum cryptography [1] and is one of the leading platforms for other technologies derived from quantum information science, including quantum computation [2], quantum lithography [3] and quantum metrology [4].

In each of these technologies, quantum mechanics offers additional improvement over what can be achieved by applying classical physics alone. Quantum metrology uses large superposition states of photons, entangled in number and one other type of (typically path or polarization), known as "NOON" states. Related to so-called "Schrödinger cat states", NOON states of photon number N are mathematically defined by

$$|N::0\rangle = \frac{1}{\sqrt{2}}\left(|N\rangle_a |0\rangle_b + |0\rangle_a |N\rangle_b\right) \qquad (1)$$

where $|n\rangle_j$ represents the Fock state of n photons populating a mode labeled j. These states have an increased sensitivity to relative phase relative to un-entangled light, allowing a precision in phase measurement towards the Heisenberg limit (HL) $\Delta\phi \sim 1/N$, beyond the classical shot noise limit (SHL) of $\Delta\phi \sim 1/\sqrt{N}$ [4].

Previous experiments to demonstrate the increased resolution in phase sensitivity gained by NOON states have been demonstrated using bulk optics by encoding the quantum states in polarization and path (for example [5] and [6]

This work was supported by IARPA, EPSRC, QIP IRC and the Leverhulme Trust

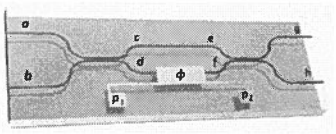

Figure 1: An integrated waveguide Mach-Zehnder interferometer used to manipulate entangled states of light using a resistive heater (labeled ϕ).

respectively). We present here the manipulation of NOON states in integrated waveguide circuits and experimentally implement a theoretical proposal to herald the creation of NOON states of up to four photons using only linear optics and projective measurements [8].

II. MANIPULATING NOON STATES

A. Method

The waveguide circuit for manipulating path entanglement is a Mach Zehnder interferometer with lithographically patterned thermal resister to control the internal phase as shown in figure 1. The 3.5μm core waveguides are lithographically patterned from doped Silica fabricated on a Silicon substrate using standard methods and are designed for single mode operation in the 780nm region. On applying a voltage across the thermal resister, the relative optical phase of quantum states guided through the interferometer is varied in a stable, controlled manner.

Multi photon states of two- and four-photons are produced by pumping spontaneous parametric down conversion (SPDC). A Ti:sapphire pulsed laser (157fs) laser is tuned to 780nm and upconverted to 390nm via second harmonic generation in a 2mm thick nonlinear Bismuth Borate BiB_2O_6 (BiBO) crystal. This is then focused onto a second BiBO crystal cut for non-collinear down-conversion to produce pairs of signal and idler photons with wavelength 780nm. The pairs are filtered spectrally using high transmission interference filters and spatially into two modes by focusing onto polarization maintaining fibres (PMF). The photons are injected into the chip using butt-coupled arrays of PMF pitched to match those of the waveguide. Coincidental events are then detected using

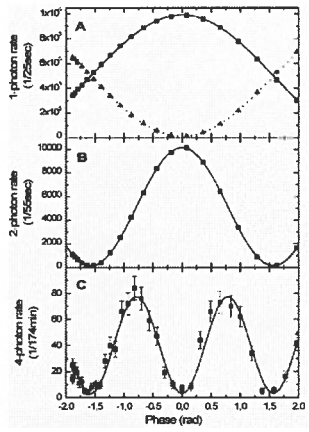

Figure 2: Quantum interference inside a waveguide interferometer. (A) The single photon interference patterns from inputting single photons in waveguide *a* (see figure 1); black squares are plotted from detecting photons on output *h*, red triangles correspond to detections at output *g*. (B) Two photon interference pattern of a two-photon NOON state. (C) Four photon interference pattern on post-selecting a four-photon NOON state inside the interferometer. All plots use sinusoids as a best fit.

commercially available silicon avalanche photo diode single photon counting modules (SPCM).

B. Results

Figure 1A displays the single photon interference fringe obtained on inputting single photons into mode *a* and detecting them independently at modes *g* and *h* with respect to variation of phase inside the interferometer. While this interference pattern is equivalent to the pattern observed from inputting classical light, the contrast of 0.982±0.003 indicates an average fidelity of 0.99984±0.00004 for manipulating single bits of quantum information (qubits) encoded across two spatial modes—the natural encoding for integrated waveguide circuitry[cite integrated quantum circuits].

On inputting two coherent identical photons on inputs *a* and *b* deterministically yields a two photon NOON state; varying the phase of the device by □ causes the two photon NOON state to be shifted in phase by 2□. On post selecting two photon coincidences across the outputs of *g* and *h* allows an interference pattern of twice the resolution of the single photon case to be observed. The fringe given in figure 2B has a contrast of 0.972±0.004, sufficient to beat the standard quantum limit (assuming high efficiency photon sources and perfect detectors).

Producing four photon NOON states is not so straightforward as the two photon case and cannot be achieved by using non-classical interference of Fock states alone. To observe a four-fold interference fringe, we use a method to post select the presence of a four photon NOON state inside the interferometer, hence allowing the observation of a four-photon interference fringe with four times the resolution of the single photon case [6]. The plot given in figure 2C has a contrast of 0.92±0.04, which despite the detection scheme required to post select the four photon NOON state, is sufficient to beat the standard quantum limit (again, assuming high efficiency detectors and photon sources).

III. HERALDING NOON STATES

The generation of large photon number NOON states is unlikely to be achieved by using non-classical interference alone. It has been theoretically proposed [8] that using linear optics and projective measurements, large photon number NOON states can be constructed from Fock states. Demonstrate this experimentally in waveguide circuit designed to herald the presence of two- and four-photon NOON states with, in principle, perfect fidelity. This requires two extra ancillary photons for each case. Using projective measurements in this manner can also be generalized to yield arbitrarily large NOON states [9].

IV. CONCLUDING REMARKS

The inherent stability and near perfect mode-overlap of lithographic waveguide architecture is ideal for the application to quantum metrology. They have already been demonstrated to yield high levels of non-classical interference for components for quantum computation [10,11,12], and the results presented here highlight their potential for quantum metrology realized in an integrated optics platform.

ACKNOWLEDGMENT

We thank A. Laing, T. Nagata, S. Takeuchi, X. Q. Zhou, J. P. Hadden, A. Lynch and J. G. Rarity for helpful discussion.

REFERENCES

[1] N. Gisin, G. Ribordy, W. Tittel, H. Zbenden, *Rev. Mod. Phys.* **74**, 145-195 (2002).

[2] M. A. Nielsen, I. L. Chuang, *Quantum Computation and Quantum Information* (Cambridge Univ. Press, 2000).

[3] A. N. Boto *et. al. Phys. Rev. Lett.* **85**, 2733-2736 (2000).

[4] V. Gioveannetti, S. Lloyd, L. Maccone, *Science* **306**, 1330-1336 (2004).

[5] M. W. Mitchell, J. S. Lundeen, A. M. Steinberg *Nature* **429**, 161-164 (2004).

[6] T. Nagata, R. Okamoto, J. L. O'Brien, K. Sasaki, S. Takeuichi, *Science* **316**, 726-729 (2007).

[7] J. C. F. Matthews, A. Politi, A. Stefanov, J. L. O'Brien, *Nature Photon.* **3** 346 (2009).

[8] H. Lee, P. Kok, N. J. Cerf, J. P. Dowling *Phys. Rev. A* **65** 030101 (2002).

[9] P. Kok, H. Lee, J. P. Dowling, *Phys. Rev. A* **65** 052104 (2002).

[10] A. Politi, M. J. Cryan, J. G. Rarity S. Yu, J. L. O'Brien *Science*, **320**, 646-649 (2008).

[11] A. Politi, J. C. F. Matthews and J. L. O'Brien, *Science*, **325**, 1221 (2009).

[12] A. Politi, J. C. F. Matthews, M. G. Thompson, J. L. O'Brien, *IEEE Journal of Selected Topics in Quantum Electronics*, **15**, 6, 1673-1684 (2009).

Semi-analytical approach to the analysis and design of photonic crystal cavities

Marco Felici[1], Kirill A. Atlasov[1], Alessandro Surrente[1], Karl Fredrik Karlsson[1], and Eli Kapon[1]
[1] *Laboratory of Physics of Nanostructures, Ecole Polytechnique Fédérale de Lausanne (EPFL), CH-1015 Lausanne, Switzerland*
marco.felici@epfl.ch

By expressing the modes of line-defect PhC cavities in terms of the Bloch states of a W1 waveguide, we can (*i*) shed light on the 0D→1D transition occurring for increasing cavity length; (*ii*) design PhC cavities with the desired mode structure. As an example, we present a PhC cavity supporting a Gaussian mode with Q~10^7.

Introduction

Currently, most methods for the design of photonic crystal (PhC) cavities rely on extensive, computationally demanding parameter-space searches. In the present work we take a different approach to the problem, by seeking to establish a direct, *semi-analytic relationship* between the target electromagnetic field distribution and the dielectric constant ε of the PhC structure supporting it. We find that for line-defect PhC cavities such a relationship can be derived if it is assumed that the cavity modes can be reconstructed through linear combinations of the 1D Bloch eigenmodes of a PhC W1 waveguide.

Results

As a test for the validity of our basic hypothesis, the expansion in waveguide eigenmodes is applied to the modes of L_N-type cavities of varying length ($3 \leq N \leq 35$). It is found that L_N-cavity modes can be correctly reconstructed through such an expansion for $N \geq 5$. This confirms that a well-defined "waveguide-like" character is acquired by L_N cavities as soon as the cavity length exceeds a few unit cells, thus supporting recent theoretical predictions [1] and experimental findings.[2] The possibility to write PhC cavity modes in terms of W1 Bloch states allows us to define a direct relationship between a given field distribution and the ε of the corresponding PhC cavity. As shown in Fig. 1, this method can be used to design a cavity supporting the desired mode, *e.g.*, a mode with Gaussian envelope function and ultra-low radiative losses (quality factor of 6.8 10^6).

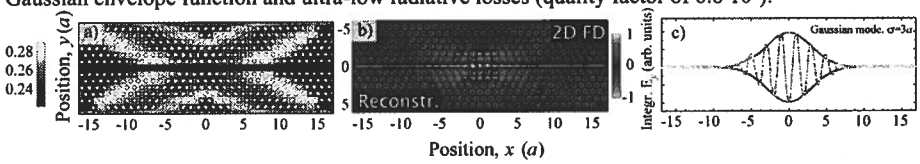

Figure 1. (a) False-color mapping of the *r/a* of the holes forming the PhC cavity defined in the text. The holes are also shown, as circles of radius proportional to the actual *r/a*. (b) Spatial distribution of the E_y component of the Gaussian mode supported by the PhC cavity shown in (a). The upper half shows the fundamental mode of the cavity, as obtained from 2D FD computations. The mode with Gaussian envelope function ($\sigma=3a$) is displayed in the lower half. (c) Integral along y of the E_y component of the mode shown in (b). The black [red] curve refers to the mode obtained from 2D FD computations [to the reconstructed mode with Gaussian envelope function]. Two Gaussian curves (in red and blue, $\sigma=3a$) are shown for comparison.

References

[1] V. S. C. Manga Rao et al., Phys. Rev. Lett. 99, 193101 (2007).

[2] K. A. Atlasov et al., Opt. Express 18, 117 (2010).

Normalized analysis for large tolerance binary gratings from a modal approach

Thomas Kämpfe, Emilie Gamet, Florent Pigeon, Olivier Parriaux
Laboratoire Hubert Curien UMR CNRS 5516, Université Jean Monnet, 42000 Saint Etienne, France
thomas.kampfe@univ-st-etienne.fr

The analysis and broadening of the tolerances of dielectric, binary gratings on the basis of a modal representation using ultimately normalized parameters (duty cycle, wavelength/period, index contrast) leads to physically meaningful comprehensive 3D-charts. The example given relates to duty cycle tolerance.

Introduction

1D binary surface relief gratings with a rectangular profile have many applications, e.g. beam-splitting, polarization control, total reflection. The optimization of the diffraction efficiencies can be done using rigorous methods, e.g. RCWA, to scan the parameter space. However, designing gratings with large tolerance to parameter variations is not straightforward [1]. To that end, the transmission through the segmented membrane is represented in terms of the interplay of the propagating grating modes. Using the parameters as depicted in Fig. 1 and assuming perpendicular incidence the dispersion equation is:

$$\cos k_{g1} r_1 \cos k_{g2} r_2 - 0.5\left(k_{g1}/k_{g2} - k_{g2}/k_{g1}\right)\sin k_{g1} r_1 \sin k_{g2} r_2 = 1 \qquad (1)$$

with $k_{gi} = \sqrt{n_i k_0^2 - \beta_q^2}$ defining the propagation constants β_q of the modes whose excitation is governed by the overlap integral with the incident field and an impedance mismatch term. The diffraction orders can be understood as an interference between the modes [2], allowing an intelligible analysis of the effect of the variation of the normalized parameters.

Results

Exemplarily we consider the tolerance to duty cycle d for a grating suppressing the 0th transmission order under normal incidence. In this case, the 0th and 2nd grating modes only are excited and a large parameter tolerance requires the change of the difference of the propagation constants $\beta_{02}=\beta_2-\beta_0$ to be minimal ($\partial\beta_{02}/\partial d=0$), which can be analytically evaluated using Eq.(1), leading to a subset of the generalized parameter space (Fig. 2). To achieve complete destructive interference the mode coupling must be equal, leading to the second subset in Fig. 2. The second derivative ($\partial^2\beta_{02}/\partial d^2$) indicates, when minimal, the largest tolerance to d and selects the optimal parameters within the intersection of both subsets. Concrete examples of large duty cycle tolerant gratings will be shown and the extension of the approach to functional parameters will be suggested.

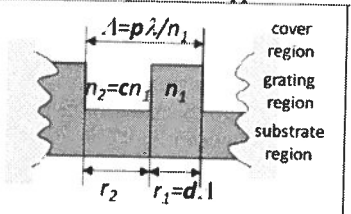

Fig. 1: Physical grating parameters and generalized parameters

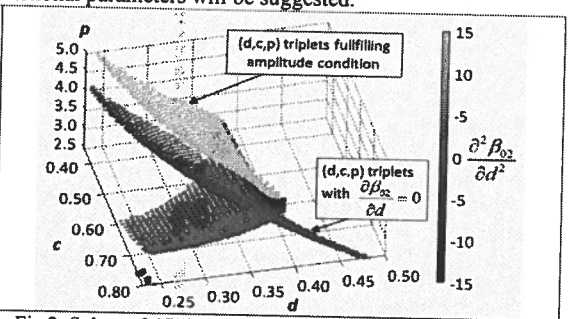

Fig.2: Subsets fulfilling phase and amplitude condition, further qualified by the second derivative (gray level)

References

[1] E. Gamet et al., "Duty cycle tolerant binary grating...," *J. Europ. Opt. Soc. Rap. Public.* **4** (2009)
[2] T. Clausnitzer et al. "An intelligible explanation of highly-efficient..." *Opt. Exp.* **13**, (2005)

Three-Dimensional Far Field Analysis for Photonic-Crystal Nanolasers

Jost Adam[1], Kirill A. Atlasov[2], Eli Kapon[2] and Martina Gerken[1]

[1] Integrated Systems and Photonics, Institute of Electrical and Information Engineering, Christian-Albrechts-Universität zu Kiel, Germany. e-mail: ja@tf.uni-kiel.de

[2] Laboratory of Physics of Nanostructures, Ecole Polytechnique Fédérale de Lausanne (EPFL), Switzerland

We present a spherical-multipole based near-to-far field transformation technique in conjunction with the three-dimensional finite difference time-domain method. It is applied to calculate the radiated far field of quantum-wire based photonic-crystal microcavity lasers.

Summary

Far field calculations are necessary for a broad range of applications concerning emissive electromagnetic components and emerging novel micro and nanoscale optoelectronic devices. Recently, there has been significant interest concerning emitters based on photonic-crystal (PhC) microcavities, in particular, PhC nanocavity semiconductor lasers [1]. Proper design of such PhC structures allows not only for control of spontaneous emission thus, enhancing the quantum-electrodynamics effect of such lasers and hence their efficiency, but also for tailoring of the far field emission characteristics. In this contribution we present calculations on recently demonstrated quantum-wire PhC lasers [2]. Since the PhC cavities are of a complex geometry, numerical modeling is mandatory. Classical modeling approaches such as the three-dimensional (3-D) finite difference time-domain (FDTD) method in conjunction with field monitors are highly memory and calculation power consuming and hence are not practical. Near-to-far field transformations help to overcome this problem as they allow for (semi-)*analytical* treatment. Thus, this is a powerful tool and is essential if not only a device simulation is required but also its optimization. In particular it could be further applied to design cavity geometries that allow for desired emission directionality.

Based on a recently proposed and verified spherical-multipole based near-to-far field transformation technique [3], 3-D radiation patterns of L3 (see Fig. 1(a)) and L6 PhC cavities are calculated and the preliminary results are shown in Fig. 1(b). The presented method is useful for efficient calculations of novel nanophotonic devices, and promising in its use for optimization of their performance.

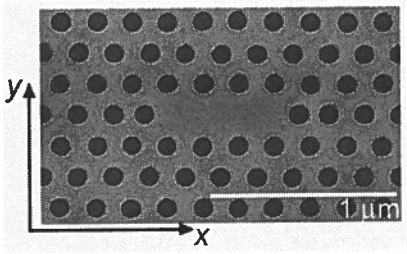

(a)

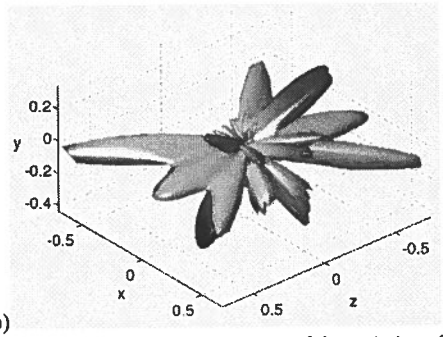

(b)

Fig. 1. (a) SEM top-view image of L3 PhC nanocavity laser [2] ; (b) 3-D radiation pattern of the emission of the fundamental cavity mode (normalized radiated power).

References

[1] S. Noda, Science 314, 5797 (2006).

[2] K. A. Atlasov et al, Optics Express 17, 18187-18183 (2009).

[3] J. Adam, L. Klinkenbusch, Adv. Radio Sci. 7, 43–48 (2009).

Optimizing Two-dimensional Photonic Crystal Waveguide Bends

Zhen Hu[1] and Ya Yan Lu[2]

[1]*Department of Mathematics, Hohai University, Nanjing, Jiangsu, China*
[2]*Department of Mathematics, City University of Hong Kong, Kowloon, Hong Kong*

New optimal waveguide bends in two-dimensional photonic crystals are obtained by solving optimization problems using the radii of certain dielectric rods or air-holes around the centers of the bends as free parameters. These bends outperform previous designs with similar configurations.

Introduction

For photonic integration, it is important to develop PhC waveguide bends with high transmission and wide bandwidth [1]. Many authors have optimized PhC waveguide bends based on various assumptions [2,3]. Using a recently develop efficient numerical method [4], we consider the optimization with respect to the radii of a few dielectric rods (for 90° bends) or air-holes (for 60° bends).

Results

For 90° bends in a square lattice of dielectric rods (same parameters as in [1,2]), we obtain an optimal design as shown in the figure (upper-left panel). The corresponding transmission spectrum is given in the lower-left

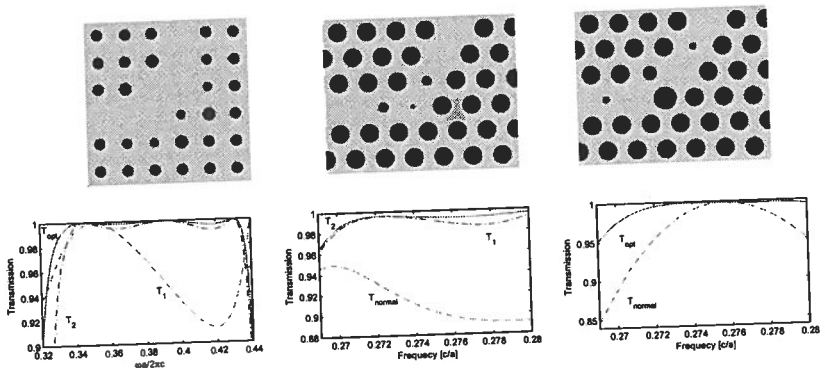

panel as T_{opt} and it is compared with the transmission spectra of the bends in [1] (curver T_1) and [2] (curve T_2). For 60° bends in a 2D PhC with a triangular lattice of air-holes (same parameters as in [3]), we consider two cases: (a) adding three air-holes in the bend, (b) adding five air-holes and modifying one original air-hole. T_2 and T_{opt} in the lower-middle and lower-right panels correspond to the designs shown in the upper-middle and upper-right panels, respectively. T_1 in the lower-middle panel corresponds to a bend with only two additional air-holes. T_{normal} in the lower-middle and lower-right panels correspond to the bends in [3] (additional air-holes are identical).

References

[1] A. Mekis, J. C. Chen, I. Kurland, *et al.*, Phys. Rev. Lett. 77, 3787-3790 (1996).
[2] J. Smajic, C. Hafner and D. Erni, Opt. Express. 11, 1378-1384 (2003).
[3] A. Chutinan, M. Okano and S. Noda, Appl. Phys. Lett. 80, 1698-1700 (2002).
[4] Z. Hu and Y. Y. Lu, Optics Express, **16**, 17383-17399 (2008).

Robust topology optimization of photonic crystal waveguides with tailored dispersion properties

Fengwen Wang[12], Ole Sigmund[1] and Jakob Søndergaard Jensen[1]
[1] *Department of Mechanical Engineering, Technical University of Denmark, Nils Koppels Allé Building 404, 2800 Kgs. Lyngby, Denmark*
[2] fwan@mek.dtu.dk

A robust topology optimization approach is used to design photonic crystal waveguides. By optimizing the material distribution we design waveguide dispersion curves with constant low group velocity. The formulation ensures good performance also if the structure is slightly dilated or eroded corresponding to an over- or underetching.

Introduction

Photonic crystals with line defects facilitate propagation of a guided mode within the band gap [1]. This can be used to manipulate the propagation properties, e.g. creating slow light. Previously, it was demonstrated that the dispersion curve can be tailored through perturbation of air holes adjacent to the waveguide core [2], and recently it was shown that topology optimization can be applied to create novel waveguide designs with enhanced dispersion properties [3]. Here, we base the optimization on a finite element eigenvalue analysis of a super-cell and tailor the dispersion curve by minimizing the difference between the computed group velocity and a prescribed velocity v_g^* through several discrete Bloch wavenumber k_n:

$$\min_{\rho_i}: \max_{k_n} \left(\frac{\omega_n^m - \omega_{n+1}^m}{k_{n+1} - k_n} - v_g^* \right)^2 \qquad (1)$$
$$s.t.: \ 0 \le \rho_i \le 1$$

The design is parametrized by elementwise continuous variables ρ_i that govern the local dielectric properties. The eroded and dilated structures are created by morphology operations and the performance is considered simultaneously using the formulation in Eq. (1).

Results

We illustrate the optimization procedure by designing a photonic crystal with constant group velocity: c/25. We obtain a group velocity within 7% tolerance for $k \in [0.3825, 0.45]a/2\pi$. The eroded and dilated structures (not shown) perform equally well.

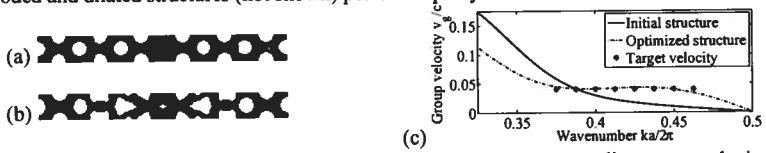

Figure 1. (a) Initial design. (b) Optimized design. (c) Corresponding group velocity.

References

[1] J. D. Joannopoulos, et al., Photonic Crystals – Modeling the Flow of Light, Princeton University Press, 2008, ISBN: 978-0-691-12456-8.

[2] L. H. Frandsen, et al., *Opt. Express*, **14**, 9444-9450, (2006).

[3] R. Stainko and O. Sigmund, *Waves in Random Complex Media*, **17**, 477-489, (2007).

Optimal tunability of waveguides based on Silicon Photonic Crystals infiltrated with Liquid Crystals

Joaquín Cos, Josep Ferré-Borrull, J. Pallarès and L. F. Marsal
D.E.E.E.A., Universitat Rovira i Virgili, Avda. Països Catalans 26, 43007 Tarragona, Spain
lluis.marsal@urv.net

In this work we study the optimization of the tunability range in waveguides based on silicon Photonic Crystal infiltrated with Liquid Crystal. To this end, we use the plane-wave expansion method considering anisotropy and modelling supercells to account for the lattice defects that define the waveguide.

Introduction

Tunability is a necessary feature for many photonic crystal-based devices such as multiplexers or modulators. Among the possibilities for tuning the properties of 2D Si-based photonic crystals (nonlinear materials, nonlinearities of the Si caused by changes in carrier concentration), liquid crystals (LCs) represent a very suitable material: the easy control of the anisotropy by means of external applied electric fields provides such tuning[1]. However, the infiltration of the LC in the Si pores reduces the index contrast with the consequence of a decrease in the performance of the devices (smaller band gaps, non-existence of complete band gap, small tunability range). Furthermore, the LCs usually used in the display industry have a small birefringence in its anisotropic state, which results in an even smaller tunability range. Therefore, an optimal design of the structures is determinant for a proper working of the devices.

Results

We have studied the tunability range of a Si-based photonic waveguide with a triangular lattice where a line of scatterers in the direction Γ–K has been infiltrated with E7 liquid crystal (Fig. 1 inset). The liquid crystal director is always in the plane of the cylinders, thus guided modes are tuned by changing the angle between the direction Γ–K and the LC director, α. The tunability range can be maximized by finding the optimal radius for the infiltrated scatterers, while the radius of the rest of scatterers has been chosen so that the bandgap is maximum ($R=0.44a$). In order to model the structure we have considered a 7x1 supercell and 1225 plane-waves. Fig. 1 shows the tunability range versus the radius of the infiltrated scatterers of two guided modes [2] at points Γ and K.

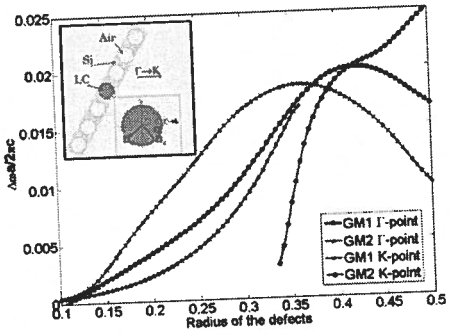

Fig. 1: Maximum tunability range of the guided modes versus the radius of the infiltrated line of scaterers in the Γ–point and the K-point. 7x1 Supercell of a 2D PC with a triangular lattice, the central line is infiltrated with LC and. optical axis orientation (inset).

References

[1] S. Weiss, H. Ouyang, J. Zhang, and P. Fauchet, *Opt. Express*, **13**, 1090-1097, (2005).

[2] H. Takeda and K. Yoshino, *Phys. Rev. B*, **67**, 073106, (2003).

Acknowledgements: This work was supported by Spanish Ministry of Ciencia e Innovacion (MICINN) under grant number TEC2009-09551, HOPE CSD2007-00007 (Consolider-Ingenio 2010) and AECID-A/024560/09.

Coupled-resonator optical waveguides: *Q*-factor and disorder influence

Jure Grgić, Enrico Campaioli, Søren Raza, and Niels Asger Mortensen
Department of Photonics Engineering, DTU Fotonik, Technical University of Denmark, DK-2800 Kongens Lyngby, Denmark

jgrg@fotonik.dtu.dk

Introduction

We are exploring coupled-resonator optical waveguides (CROW) dispersion properties in the presence of finite Q factors and disorder. Numerical results are obtained with the aid of a Green function approach. Finite Q, small fluctuations of resonance frequencies and varying coupling occur in all real structures. Such inevitable effects should be considered when assessing potential advantageous of slow light propagation. As a general result, we find that the maximal group delay is bound by the photon life-time of a single resonator, and it remains roughly constant over the entire bandwidth of the CROW. Here, we extend this work and treat slow light, damping, and disorder-driven localization in CROWs on an equal footing.

Results

To access the influence of fluctuations in Ω (from resonator to resonator) we analyze CROWs made of 100 resonators where the resonant frequency has 2% standard deviation and Q=1000. In general, the practical length L is now bounded by the localization length (associated with the exponential suppression of the transmission T) and the maximal group delay now becomes

$$\tau_{\max}(\omega) \approx \frac{\xi(\omega)}{v_g(\omega)} = -\pi\rho(\omega)\ln[T(\omega)] \qquad (3)$$

We employ a Green function method calculate the transmission and the DOS and by brut-force ensemble averaging (10000 different realizations) we arrive at ensemble-averaged properties of the maximal group delay, as illustrated by the blue solid line in Fig. 1. Notice that we always have $\tau_{\max} < \tau_p$ in the presence of disorder. The red trace shows the results for one particular member of the ensemble, indicating pronounced sample-to-sample fluctuations in the group delay and localization properties.

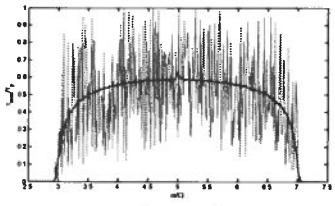

Fig. 1 Ensemble averaged group-delay properties of a disordered CROW (blue line). Each CROW is displaying significant sample-to-sample fluctuations (red curve).

In the context of practical applications involving the group delay, we note that the maximal attainable group delay appears as a balance between the reduced group velocity and the decay length. Explicit calculations show that irrespectively of the underlying band structure, the maximal group delay is limited by the photon life time of the resonators. This illustrates the importance of addressing propagation loss, localization, and slow-light on an equal footing when applying CROW concepts in design of optical buffers and delay-line architectures.

References

[1] A. Yariv, Y. Xu, R. K. Lee, and A. Scherer, Opt. Lett. **24** 711-713 (1999).
[2] S. Mookherjea and A. Oh, Opt. Lett. **32** 289-291 (2007).
[3] S. Raza, J. Grgić, S. Xiao, and N. A. Mortensen, J. Europ. Opt. Soc. Rap. Public. **5**, 10009 (2010).

Modelling Plasmonic Antennas and Related Metallic Nanostructures

Olivier J. F. Martin

[1]*Nanophotonics & Metrology Laboratory, Swiss Federal Institute of Technology Lausanne (EPFL)*
Olivier.Martin@epfl.ch

In my presentation I will focus on our on-going work on the modelling of realistic plasmonic nanostructures, both individual and in periodic arrays. Although I will emphasize the modelling aspects, I will also touch on the nanofabrication and characterization issues.

Perfect imaging with positive refraction

Ulf Leonhardt[1]
[1] *School of Physics and Astronomy, University of St Andrews, North Haugh, St Andrews KY16 9SS, UK*
ulf@st-andrews.ac.uk

Perfect imaging has been believed to rely on negative refraction [1], but in the lecture I show that an ordinary positively-refracting optical medium may form perfect images as well. In particular, I prove that Maxwell's fish eye [2] in two-dimensional integrated optics makes a perfect instrument with a resolution not limited by the wavelength of light [3,4]. I also show how to modify the fish eye such that perfect imaging devices can be made in practice [3,4].

References

[1] J.B. Pendry, *Phys. Rev. Lett.* **91**, 099701 (2003).

[2] J.C. Maxwell, *Cambridge and Dublin Math. J.* **8**, 188 (1854).

[3] U. Leonhardt, *New J. Phys.* **11**, 093040 (2009).

[4] U. Leonhardt and T.G. Philbin, *Phys. Rev. A* **81**, 011804 (2010).

ɾecent Developments on Wide Angle and Bidirectional Propagation Methods

Anurag Sharma and Debjani Bhattacharya
Physics Department, Indian Institute of Technology Delhi, New Delhi-110016, India
asharma@physics.iitd.ac.in

: discuss the recently developed finite difference based split-step nonparaxial methods for scalar and ıivectorial beam propagation. The methods solve the second order wave equation directly and are very :ient in terms of speed and accuracy. Applications to reflecting structures are also discussed.

ımmary

: have recently developed a finite-difference split-step non-paraxial method, which is based on : solution of the wave equation without paraxial or one-way approximation [1,2]. The method has :n shown to give very good accuracy and stability, even with relatively large propagation steps. e algorithm of the method can be written as

$$\Phi(z+\Delta z) = \mathbf{P}\,\mathbf{Q}(z)\,\mathbf{P}\,\Phi(z) + O\left((\Delta z)^3\right) \qquad (1)$$

ıere $\Phi(z)$ is the column vector containing the field and its derivative, **P** is a constant matrix ɔresenting propagation through a reference medium of index n_r, **Q**(z) is a sparse matrix defining : index distribution as a function of z, which is the general direction of propagation. Thus, one ıgle step requires only multiplication of a square (dense) matrix with a complex column vector d of a sparse matrix with a column vector, and hence, is computationally efficient. The one-time mputation of matrix **P** requires diagonalization and square root operation of a dense matrix **S**, ıich is the finite-difference representation of the operator, $k_0^2 n_r^2 + \partial^2/\partial x^2$ (for 2D propagation). In r method a higher order series of the central difference approximation is used for the ɔresentation of $\partial^2/\partial x^2$. We have also developed a procedure for analytical evaluation of the ıtrix **P**, using the analytical diagonalization of the tridiagonal matrix for the central difference erator [3]. This is a very big advantage in terms of computational speed and efficiency. In 3D ɔpagation matrix **S** involves the operator $k_0^2 n_r^2 + \partial^2/\partial x^2 + \partial^2/\partial y^2$ and the matrices involved now come large block matrices. However we have shown that by suitably altering the matrix ɔresentations, the diagonalization of matrix **P** can be done analytically even in this case [4].

In devices with high index contrast, the electric field becomes discontinuous and hence a mivectorial method is required. For semivectorial method, we have devised an alternate splitting ɛthod [5], which maintains the required continuity of field and derivatives in the semivectorial uation [6]. In other semivectorial methods [7,8], the continuity conditions at an interface are used modify the finite difference operators in the scalar wave equation. These methods are very ficient for mode calculation but for wide-angle propagation these may not be suitable.

The methods discussed above are bidirectional and can be used to study diffraction, reflection, d total internal reflection very efficiently. Applications of the method to study waveguide Bragg atings and other reflecting geometries will be discussed.

This work was partially supported by a grant from the Council of Scientific and Industrial Research 'SIR), Govt. of India and through UKIERI Major Project. One of the authors (DB) would also like to knowledge financial support from the CSIR, Govt. of India.

eferences

] A. Sharma and A. Agrawal, *IEEE Photon. Technol. Lett.* **18**, 944 (2006). [OWTNM 2005]
] A. Sharma and A. Agrawal, *Opt. Quantum Electron.* **38**, 19 (2006). [OWTNM 2005]
] A. Sharma, D. Bhattacharya and A. Agrawal, *Opt. Quantum Electron.* **39**, 623 (2007). [OWTNM 2006]
] D. Bhattacharya and A. Sharma, *Opt. Quantum Electron.* **39**, 865 (2007). [OWTNM 2007]
] D. Bhattacharya and A. Sharma, *Applied Opt.* **48**, 1878-1885 (2008). [OWTNM 2008]
] D. Bhattacharya and A. Sharma, *Opt. Quantum Electron.* **40**, 933-942 (2008). [OWTNM 2008]
] R. Stoffer, H.J.W.M. Hoekstra, *Opt. Quantum Electron.* **30**, 375-383 (1998).
] J. Yamauchi, *Propagating Beam Analysis of Optical Waveguides*, Research Studies Press, Hertfordshire, UK (2003).

Field enhancement at a graded-index interface between positive- and negative-index optical materials

Irene Mozjerin[1], Tolanya Gibson[1], Edward P. Furlani[2], Ildar R. Gabitov[3], Amos A. Hardy[4] and Natalia M. Litchinitser[1]

[1] *Department of Electrical Engineering, University at Buffalo, The State University of New York, Buffalo, New York 14260, USA*

irenemoz@buffalo.edu

[2]*The Institute for Lasers, Photonics and Biophotonics, University at Buffalo, The State University of New York, Buffalo, New York 14260, USA*

[3]*Department of Mathematics, University of Arizona, Tucson, Arizona, 85721, USA*

[4]*Department of Physical Electronics, Tel Aviv University, Tel Aviv 69978, Israel*

The effect of electromagnetic enhancement in a graded-index transition between positive- and negative-index optical materials is studied based on realistic values of material parameters deduced from those experimentally obtained for a negative-index metamaterial.

Summary

Recent study of interfaces with smooth and gradual transitions from positive-index to negative-index materials has revealed the electromagnetic enhancement phenomenon to occur near the point where the real part of the refractive index changes its sign [1]. Such field enhancement takes place for both TE- and TM-waves when the incident wave vector makes an angle with the interface. The metamaterials were assumed to be lossless. In this case, the effective dielectric permittivity ε and magnetic permeability μ are real-valued, and the electric field amplitude for the TM-wave, or magnetic field amplitude for the TE-wave, tends to infinity at the zero-index point.

Now we investigate the field enhancement and the related field confinement in graded-index transitions between regular dielectric optical materials and negative-index metamaterials. Since optical metamaterials based on plasmonic nanostructures are lossy, ε and μ are complex-valued. In lossy graded-index transitions the electromagnetic field is finite everywhere and the enhancement may be completely eliminated when the imaginary parts of ε and μ are sufficiently large. Another important property of lossy transitions is that the enhancement factor may be different for TE- and TM-waves if the relative ε and the relative μ are unequal. Furthermore, the enhancement peak may be shifted from the zero-index point towards the positive-index region. The field enhancement for the TE-wave is demonstrated in Fig. 1. We study the dependence of the field profile near the zero-index point on the parameters of the transition. Our study is based on full-wave field simulations using realistic values of the material parameters deduced from those reported for a silver-based negative-index metamaterial at a telecommunication wavelength [2].

The phenomenon of electromagnetic enhancement in graded-index transitions holds potential for applications in low-intensity nonlinear optics, subwavelength light sources and polarization sensitive optical devices.

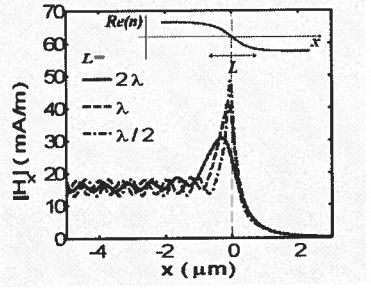

Fig. 1 Variation of the absolute value of the x-component of the magnetic field along the x-axis that is normal to the interface. The inset shows variation of the real part of the refractive index along the x-axis. Material parameters are deduced from those given in [2].

References

[1] N. M. Litchinitser, et al., *Opt. Lett.* **33**, 2350 (2008)

[2] G. Dolling, et al., *Opt. Lett.* **31**, 1800 (2006)

Adaptive Spatial Resolution in Fourier Modal Methods for Modelling Guided-Wave Structures

Jiří Čtyroký[1], Ivan Richter[2], and Pavel Kwiecien[2]
[1] *Institute of Photonics and Electronics AS CR, v.v.i., Chaberská 57, 182 51 Praha 8, Czech Republic*
ctyroky@ufe.cz
[2] *Czech Technical University in Prague, Faculty of Nuclear Sciences and Physical Engineering Department of Physical Electronics, Břehová 7, 11519 Prague 1, Czech Republic*

Implementation of Adaptive Spatial Resolution algorithm into two independent versions of a bi-directional Fourier modal method is briefly described and its performance is described and critically assessed.

Introduction

Fourier modal methods (FMM) became efficient tools for numerical modelling diffraction gratings and waveguide devices [1, 2]. Nonlinear coordinate transformation has been used as an efficient boundary condition of the PML type in these methods [2]. Another nonlinear coordinate transformation known as adaptive spatial resolution (ASR) has been recently introduced into FMM, too [3-6], aimed at reducing the number of expansion terms required to reach required accuracy.
We have implemented the ASR transformation into two independent versions of 2-D FMM – the Aperiodic Rigorous Coupled Wave Analysis (ARCWA), and the bi-directional mode expansion propagation method using harmonic expansion (BEXX) [7]; in both methods, the nonlinear complex transformation [5] is used as PML. In this contribution, the implementation of ASR will be briefly described and its advantages and problems will be critically assessed.

Results

Results of FMM modelling of various structures obtained with and without ASR will be presented and mutually compared. The figures below demonstrate the improvement of the convergence of the modal back-reflection from the double groove in a strongly guiding waveguide [2] with increasing number of expansion terms.

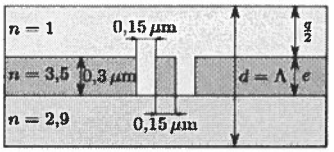

$\lambda = 0.975\ \mu m,\ \Lambda = d = 1.1\ \mu m$
$e = 0.3\ \mu m,\quad \frac{q}{2} = 0.4\ \mu m$
$R_0^{TE} = 0.3952113445$
$R_0^{TM} = 0.3554782782$

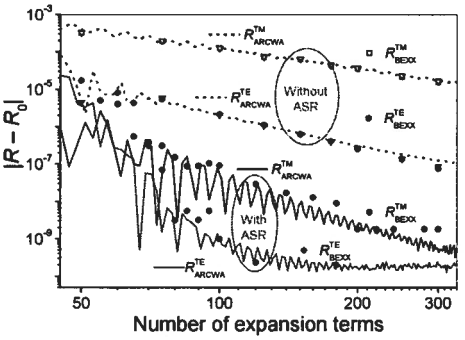

References

[1] E. Silberstein, P. Lalanne et al., *JOSA A*, **18**, 2865-2875, (2001).
[2] J. P. Hugonin and P. Lalanne, *JOSA A*, **22**, 1844-1849, (2005)
[3] G. Granet, *JOSA A*, **16**, 2510-2516 (1999)
[4] T. Vallius and M. Honkanen, *Optics Express* **10**, 24-34, (2002)
[5] P. Debackere, P. Bienstman, and R. Baets, *Optical and Quantum Electron.* **38**, 857-867, (2006)
[6] T. Weiss, G. Granet, et al., *Optics Express*, **17**, 8051 (2009)
[7] J. Čtyroký, *J. Lightwave Technol.* **27**, 2575-2582, (2009)

Modified Padé Approximant Operators for Efficient Time-Domain Beam Propagators

Khai Q. Le[1], Trevor Benson[2] and Peter Bienstman[1]
[1] *Photonics Research Group, Department of Information Technology, Ghent University-IMEC, Belgium*
khai.le@intec.ugent.be
[2] *George Green Institute for Electromagnetics Research, University of Nottingham, UK*

The usefulness of the recently introduced modified Padé approximant operators for the solution of time-domain beam propagation problems is presented. We show this both for a wideband method which can take reflections into account, and for a split-step method for the modeling of ultrashort unidirectional pulses. The resulting approaches achieve high-order accuracy not only in space but also in time.

Introduction

Many Time Domain Beam Propagation Methods (TD-BPMs) are based on the slow-wave approximation, and ignore the second order derivative with respect to time. If this derivative term is included, it is commonly approximated by rational real Padé approximant operators [1]. These incorrectly propagate evanescent modes in the frequency domain leading to additional errors and instability problems. We proposed modified Padé approximant operators to overcome these problems [2]. Here TD-BPMs based on the modified Padé operators are used to investigate an optical grating and to simulate ultra-short pulse propagation in a Y-branch waveguide structure.

Results

For the grating problem the relative error (RE) of the field profile at a reference point, i.e. the error with respect to the field profile obtained at the smallest time step used of 0.1fs, is calculated as a function of time. Fig. 1 shows this error for the conventional (cPade) and modified (mPade) Padé schemes with various time step resolutions (0.5fs, 1fs, 2fs). The REs obtained using the modified Padé(1,1) operator are much smaller than those obtained by the conventional one for the same accuracy, with an associated reduction in computational effort.

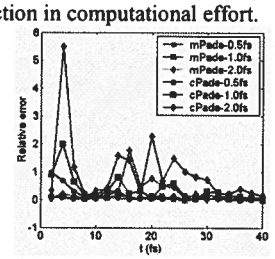

Fig. 1. Relative error of the field monitored at the reference point calculated by the modified (red lines) and conventional (blue lines) Padé-based TD-BPM with various time steps using the field at 0.1 *fs* as a reference

Calculations for pulses propagating in a Y-branch waveguide using conventional and modified Padé-based TD-BPM with various propagation step resolutions also show that REs obtained using the modified approach are much smaller than those obtained by the conventional one for the same propagation step.

References

[1] J. Shibayama, A. Yamahira, T. Mugita, J. Yamauchi and H. Nakano, "A finite-difference time-domain beam-propagation method for TE- and TM-wave analyses," J. Lightwave Technol. **21**, 1709-1715 (2003).
[2] Khai Q. Le, T. M. Benson, and P. Bienstman: Application of the modified Padé approximant operators for time-domain beam propagation method, J. Opt. Soc. Am. B., vol. 26, pp. 2285-2289 (2009).

Bio-Inspired Computing Applied to the Design of Novel Photonic Devices

Carlos H. Silva-Santos, Marcos S. Gonçalves and Hugo E. Hernández-Figueroa
[1] *University of Campinas, Albert Einstein Avenue 400, 13083-852, Campinas, Brasil*
henrique@dmo.fee.unicamp.br

The design of two novel band-gap-type photonic devices based on three different bio-inspired optimization algorithms is presented in detail.

Introduction

The development of new and sophisticated devices is in general a complex task. Here, we show that the integration between three bio-inspired algorithms (Genetic Algorithm, Evolution Strategy and Artificial Immune System) and a 2D Finite Element Method solver prove to be effective numerical tools for such a complex design. Two new complex photonic devices are taken as examples. In both cases the optimization is applied to a full crystal structure, whose basic elements were kept or removed towards maximization of the device performance.

Results

The first device is an unbalanced high index-contrast Y power splitter with expected outputs of 30% and 70% related to the input power. The structure to be optimized appears in Fig. 1(a). The optimized structure produced by the bio-inspired algorithms is illustrated in Fig. 1(b), with output powers of 22% and 69% as shown in Fig. 1(c) over a quite wideband: from 1.4 to 1.60 μm.

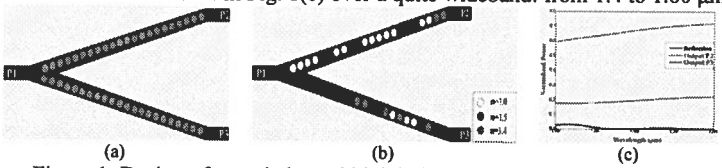

(a) (b) (c)

Figure 1. Design of an unbalanced high index-contrast Y power splitter.

The second device is a high index-contrast coupler between a micro and nano waveguides with widths of 2 μm and 0.2 μm, respectively, separated of 10 μm. The structure to be optimized is depicted in Fig. 2(a). In this case the optimized structure, illustrated in Fig. 2(b), presents losses of 0.97dB or 74.97% of coupling at λ=1.55 μm. Fig. 2(c) shows the electric field distribution. In both optimizations the Artificial Imune System presented best convergence.

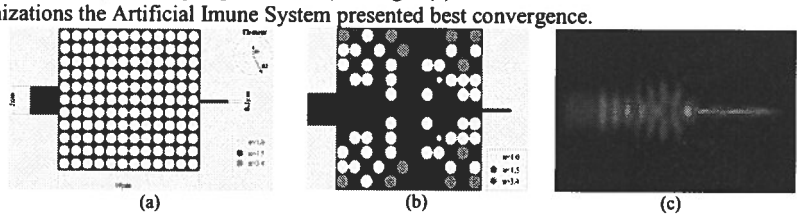

(a) (b) (c)

Figure 2. Design of a high index-contrast micro-nano waveguide coupler.

References

[1] J. Brianeze, C. H. Silva-Santos, H. E. Hernández-Figueroa, *Revista Chilena de Ingeniare,* December 2009, Vol.17, N.3, pp. 288-298, ISSN 0718-3305.

[2] P. Cheben, *et al.*, *Optics Express,* May 2006, Vol. 14, N. 11, pp. 4695-4702.

Generalization of Aperiodic Rigorous Coupled Wave Analysis Technique to Anisotropic Structures

Pavel Kwiecien[1], Ivan Richter[1], and Jiří Čtyroký[2]

[1] *Czech Technical University in Prague, Faculty of Nuclear Sciences and Physical Engineering Department of Physical Electronics, Břehová 7, 11519 Prague 1, Czech Republic*
pavel.kwiecien@fjfi.cvut.cz, ivan.richter@fjfi.cvut.cz

[2] *Institute of Photonics and Electronics AS CR, v.v.i., Chaberská 57, 182 51 Praha 8, Czech Republic*
ctyroky@ufe.cz

The aperiodic rigorous coupled wave analysis method with the complex coordinate transformation and adaptive spatial resolution technique is generalized for application to electrically or magnetically anisotropic structures. Several results for electrically anisotropic 2D photonic structures will be presented and discussed.

Summary

Currently, as photonic and plasmonic structures, especially with high-index contrast and subwavelength feature sizes, are becoming very attractive components for integrated optics and photonics devices, among others, new exploitation of anisotropic and / or magneto-optic materials is becoming quite promising, especially due to their new functionalities. Having in mind several possible modeling applications in our laboratories, including, e.g., studies of magneto-optic structures, or even negative-index metamaterials, in this contribution, we have first concentrated into a generalization of our efficient aperiodic rigorous coupled wave analysis (ARCWA) code for 2D structures made with anisotropic inclusions. Since our tool has already shown itself quite efficient and robust for various computationally demanding 2D isotropic photonic and / or plasmonic structures [1,2], including e.g. photonic crystal waveguides, surface-plasmon resonance sensors, plasmonic subwavelength apertures and slit-groove diffraction problems, etc., we have seen its potential in proficient functioning even for birefringent structures. Within this first step, especially electrically anisotropic materials have been on interest, although the technique enables us to easily switch to magnetically anisotropic problems as well. Hence, the anisotropy was newly applied within our method to the 1D periodic RCWA technique, following the original idea of Li [3], concentrating especially to the correct Fourier factorization scheme which ensures the fast and correct convergence, even for problems with a high permittivity contrast. Next, following the idea of introducing an artificial periodicity of a single aperiodic structure [4], and efficient application of the nonlinear coordinate transformation as the absorbers, we have successfully transformed the anisotropic 1D RCWA method into the ARCWA variant. Among the testing examples, the original technique for analyzing the light propagation in step-index LiNbO3 waveguides [5] was used in order to compare ARCWA rigorous results. Finally, the additional efficient technique, known as the adaptive spatial resolution (ASR) algorithm [6,7], have been included into the code, too. In the paper, several interesting practical examples of our anisotropic ARCWA generalization will be presented and discussed.

References

[1] J. Čtyroký, I. Richter, P. Kwiecien, *Proceedings of SPIE*, **7099**, 70991K:1-11, (2008).
[2] J. Čtyroký, I. Richter, P. Kwiecien, SPP4 Conference, Amsterdam, The Netherlands (2009).
[3] L. Li, *Journal of Modern Optics*, **45**, 1313 (1998).
[4] E. Silberstein et al., *JOSA A*, **18**, 2865 (2001).
[5] J. Čtyroký, *Journal of Optical Communication*, **5**, 16 (1984).
[6] G. Granet, *JOSA A*, **16**, 2510-2516 (1999).
[7] T. Weiss et al., *Optics Express*, **17**, 8051 (2009).

Light Propagation in Metal-Clad, Dielectric-Core Multimode Fibres

John Love[1], Jamil Lambert[2] & Sue Law[3]

[1] *Optical Sciences Group, Research School of Physics & Engineering, The Australian National University, Canberra, ACT 0200, Australia*
E-mail: John.Love@anu.edu.au
[2] *School of Physics, The University of Sydney, NSW 2006, Australia*
[3] *Department of Physics & Engineering, Macquarie University, NSW 2109, Australia*

An approximate analytical expression is derived for the fraction of light propagating along a fully excited multimode fibre with a dielectric core and a metal cladding and is compared with experimental measurements.

Introduction

Light propagation in dielectric core-cladding multimode fibres can be readily described quantitatively using either bound-ray tracing or bound-mode superposition [1]. The overall attenuation in such fibres is necessarily zero, provided only that the fibre constituent materials are lossless in terms of material absorption and scattering and the fibre remains straight.

Propagation in metal clad air- or dielectric-core fibres first received attention theoretically in 1964 as a possible candidate for the long-distance, high-capacity telecommunications transmission of light pulses prior to the advent of the all-conquering single-mode glass fibre [2]. The use of metal-clad fibres at optical wavelengths for data transmission may seem at first contradictory because of the very high attenuation introduced by the metal at optical wavelengths, as is the case with surface wave polaritons. However, it is the light confining effect of the metal due to the very large and negative real part of its dielectric constant relative to that of the core that makes low-loss guided transmission of at least the fundamental mode possible over long distances [2]. The Achilles heel in this case, however, is the unacceptably high bend loss induced over such distances by even extremely large radius bends.

Biomedical Applications

Recently, a prototype radiation dosimeter has been developed for biomedical application that uses an air core and a silver-coated cladding to transmit light over short distances [3, 4]. This arrangement eliminates the background Cerenkov radiation signal that would otherwise be present if solid core conventional fibres are employed for this purpose.

Results

In this paper we develop a simple model of the air-core metal-clad fibre and derive a closed-form analytical expression for the transmission loss and compare it with measured experimental results. Away from the beginning of the fibre, the power remaining in the core is shown to decrease relatively slowly as the inverse square root of the distance along the fibre.

References

[1] A.W.Snyder & J.D. Love, Optical Waveguide Theory, Chapman & Hall (London), 1983
[2] E. Marcatili et al, Bell Sys. Tech. J, **43**, 1763-1809 (1964).
[3] J. Lambert et al, Phys. Med. Biol, **53**, 3071-3080 (2008)
[4] J. Lambert et al, Phys. Med. Biol, **55**, 1115-1126 (2010)

2D Finite Element Solution for the Maxwell's Equations

B. M. A. Rahman, Arti Agrawal, S. M. Raiyan Kabir
and K T V Grattan

School of Engineering and Mathematical Science, City University London, United Kingdom

email:b.m.a.rahman@city.ac.uk

This paper presents a novel finite element technique to solve the Maxwell equations in 2D. This method can be used to simulate photonic devices and subsystems, including devices with left handed materials which may also be dispersive.

Introduction

The Finite Difference Time Domain (FDTD) methods are widely used for solving the Maxwell equations. To approximate a complex photonic structure the grid has to be very dense. For a dense grid, the time step has to be small. As a result, the FDTD is computationally very expensive in memory and also in time. On the other hand, the finite element discretization is more efficient in discretizing the computational domain. For this reason the number of nodes needed to approximate the structure is much lower than the finite difference grid. In this paper an efficient two-dimensional finite element method with two interrelated meshes for solving the Maxwell equations is presented.

FETD Technique

The computational domain is discretized using triangular elements in which the first mesh contains all the **E**(or **H**) field components. The second mesh is composed of triangles generated by taking the centroid of the elements from the first mesh as its nodes and represents the **H**(or **E**) field components. The Maxwell equations in 2D was discretized with the finite element method. The Drude model is used to calculate the complex permeability and permittivity of the associated materials. For the TM mode, the electric field components are calculated at the nodes of first mesh and the magnetic field components are calculated at the nodes of second mesh. In this approach, an efficient non-uniform mesh can be used. Complex photonic structures with curve or arbitrary interfaces like rings etc. can be discretized with the lower mesh density.

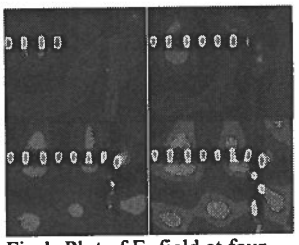

Fig 1. Plot of E_z field at four different time steps.

Results

The FETD technique can be used to simulate complex photonic structures. This method can be used to design planar integrated optic circuits and even dispersive left-handed materials. Figure 1 shows an example of a 90° bent waveguide. The source in this simulation was a point source at the centre of the waveguide.

Conclusions

As this new approach does not require denser mesh for curved geometry, the technique is efficient in its memory usage. All the components of same electric (or magnetic) field can be calculated at the first (or second) nodal discretization, which would facilitate launching a given field profile and the approach can also be used to simulate dispersive and left-handed materials.

Recent advances in time domain modelling of photonics devices

S.S.A. Obayya
Integrated Communications Research Centre, Faculty of Advanced Technology, University of Glamorgan, Pontypridd CF37 1DL, UK, Email: sobayya@glam.ac.uk

Numerical modelling of photonic devices is becoming of extreme importance for the design of new structure for a wide range of applications. In this work accurate and efficient modelling techniques for the simulation of last generation photonic devices are presented.

Introduction

Since light has become the transmission medium of modern communication, the increased demand for advanced optical communication systems has continually redirected the research efforts towards the design of new and more efficient photonic devices Structures based on these design concepts require the use of efficient electromagnetic simulators, which naturally demand huge computer resources: RAM memory and speed. For this reason, parallel to the technology development, also the electromagnetic computation has been required to offer appropriate and efficient numerical modelling techniques.

The Finite Element Method (FEM) presents great meshing flexibility which can be use to efficiently decrease the need of memory for the discretisation of computational domains. Moreover, a full-vectorial BPM algorithm based on the numerically efficient finite element method (VFEBPM) have been presented [1]. This algorithm considers only two transverse magnetic field components, hence it is more numerically efficient than the vectorial propagation algorithm which considers all the three magnetic field components.

The Finite Difference Time Domain (FDTD) technique stands for one of the most popular techniques for the modelling of a wide range of photonic devices. Research efforts have been spent on FDTD to make it more efficient in terms of computational burdens, and these efforts have given rise to the complex-envelope finite-difference time-domain (CE–ADI–FDTD) method [2] which allows to dramatically reduce the number of time step required for a given simulation.

It is well known that numerical dispersion effect demands the choice of a grid resolution with typical cell size as low as 15-20 times the minimum simulated wavelength. This requirement together with the existence of the Courant stability criterion for FDTD algorithms increase exponentially the need of computer resources. The Multi-Resolution Time Domain (MRTD) method has proved to show a strong linear dispersion so that a much less grid resolution is required [3]. Typically, in MRTD scheme the spatial discretisation is limited only by the Nyquist sampling limit which makes of MRTD a promising method to model nonlinear devices.

The finite volume time domain (FVTD) method has attracted a great attention in numerical modelling environment in computational electromagnetic problems [4]. The beauty of FVTD is that it combines the versatile and flexible meshing capabilities of the FEM in addition to being explicit where only field updates are performed at each time step as in FDTD. Its meshing capabilities result from the method being based on triangular elements which can discretise curved boundaries with great accuracy using fewer elements compared to other methods whose formulation is based on orthogonal grids.

References

[1] S.S.A. Obayya, et al., *J. Lightw. Technol.*, **18**, 409-415, (2000)
[2] D. Pinto, and S.S.A. Obayya, *J. Lightw. Technol.*, **25**, 440-447, (2007)
[3] R. Letizia, and S.S.A. Obayya, *IET Optoelectronics*, **2**, 241-253, (2008)
[4] D. Pinto, and S.S.A. Obayya, *IEEE Photon. Technol. Lett.*, **20**, 339-341, (2008)

Time-Domain Topology Optimization of Pulse-Shaping Filters

Lirong Yang[1], Ole Sigmund[2], Andrei V. Lavrinenko[1] and Jørn M. Hvam[1]

[1] *Department of Photonics Engineering, Technical University of Denmark, Ørsteds Plads, Building 343, 2800 Kgs. Lyngby, Denmark*
lirong.yang@fotonik.dtu.dk

[2] *Department of Mechanical Engineering, Technical University of Denmark, Nils Koppels Allé, Building 404, 2800 Kgs. Lyngby, denmark*

Time-domain topology optimization (TO) is used here to design optical pulse-shaping filters in 2D planar waveguides in silicon-on-insulator (SOI).

Introduction

Shaping optical pulses into arbitrary wave forms is desirable in many applications including optical communication, nonlinear optics and biomedical imaging. Time-domain TO is chosen because a single transient analysis can cover a wide frequency span while the frequency-domain analysis requires a broad range and fine intervals of the sampled frequencies. This is suitable for the case of pulse shaping filter designing. One-dimensional (1D) designs of a thin-film square-pulse shaping filter were reported in [1] and here we extend the method to 2D SOI structures.

Results

An input Gaussian pulse with a full width at half maximum (FWHM) of 26fs and a carrier wavelength of $1.55\mu m$ is to be converted to a square pulse by going through a silicon waveguide filter section with air holes. The resulting target square pulse (Fig. 1a) has a FWHM of 90fs with its amplitude decreased compared to that of the un-filtered pulse. The design domain is a $3.75\mu m$ by $1.5\mu m$ region with the inlet and outlet waveguides both with the width of $400nm$. The calculation domain is uniformly discretized into grids spaced by $25nm$. Throughout the iterations the optimization algorithm redistributes Si and air in the design domain to fulfil the square pulse filtering. The heaviside step function [2] combined with the morphology open operator with a diameter of 3 elements [3] were used to control the minimum feature size of the design and to ensure a solid-void topology (Fig. 1b).

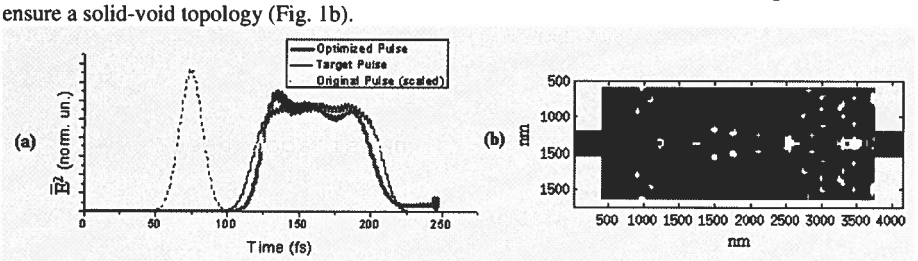

Fig. 1. Square pulse shaping. (a) The optimized output pulse (solid grey) vs. the target pulse (solid black) as well as the scaled input Gaussian pulse (dotted black); (b) The resulting filter topology with Si (black) and air (white).

References

[1] L. Yang, et al., Appl. Phys. Lett., **95**, (2009)
[2] J. K. Guest, et al., Int. J. Numer. Meth. Engng., **61**, 238-254, (2004)
[3] O. Sigmund, et al., Struct. Multidisc. Optim., **33**, 401-424, (2007)

A Multigrid Solver for the Steady-State Solution of Rate Equations Based Semiconductor Optical Amplifier Models

Jan Bos and Remco Stoffer
PhoeniX Software, P.O. Box 545, 7521PA Enschede, The Netherlands
jan.bos@phoenixbv.com

Rate equation based SOA models model the signal gain and noise spectrum as a large set of coupled non-linear first order ODEs. The coefficients in these equations depend on the amount of carriers and the material gain model. Given a carrier distribution the ODE's are trivially solved, so the problem reduces to solving the carrier distribution from the carrier density equation which balances the emission/absorption of photons and the carrier density locally in the SOA. Discretizing the carrier distribution along the propagation direction then leads to a set of non-linear equations that can be solved by means of Newton-Raphson (NR). Since a single local change in the carrier distribution causes the photon densities to change everywhere in the SOA, and more so the farther away due to gain, this means that the Jacobian is full and non-diagonally dominant. The non-local effect of pointwise updates can be circumvented by a 2nd order distributive relaxation, that is by applying net zero simultaneous updates of a site and it's adjacent sites of the form $\delta[-1\ 2\ -1]/2$. Such updates, while locally satisfying the carrier density equation, leave the photon densities and thus the carrier densities away from the update location unchanged making the relaxation a local one. Furthermore it has good smoothing properties, a prerequisite for multigrid methods to be effective. This paper describes the details of a multigrid solver employing the distributive relaxation for a problem described in the literature [1] that is complex enough to greatly benefit from the described approach.

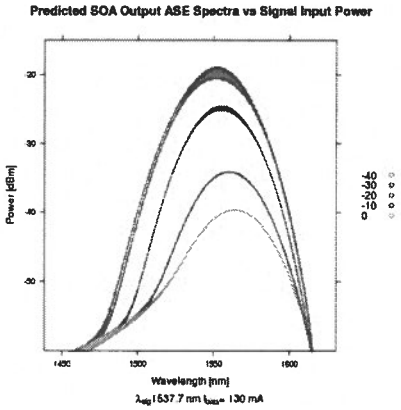

Table 1: *Calculation times(in seconds) for: Full Newton-Rhapson (NR) / Full Multigrid with two F(1,1) cycles per level (FMG). Nz is the number of elements in the propagation direction, Nf is the number of frequency slices. Clearly, FMG scales much better than NR.*

Nz \ Nf	128	256	512
128	14.8 / 1.4	28.7 / 2.5	56.2 / 4.7
256	55.2 / 2.2	105 / 4.3	205 / 8.4
512	211 / 4.7	392 / 8	756 / 15.7

References

[1] M.J. Connelly, *Journal of Quantum Electronics* **37**, nr 3, 239-447 (2001)

This work was carried out with the support of the APACHE-project („Agile Photonic Integrated Systems-on-Chip enabling WDM Terabit Networks"), a Specific Targeted Research Project funded by the European Commission through the 7th ICT-Framework Programme.

Photonic crystal fiber with bends based biosensors

A.Teyeb[1], F. AbdelMalek[1], S.S.A. Obayya[2], H. Bouchriha[3]
[1] *National Institute of Applied Sciences and Technology, BP 676,Cedex 1080, Tunis, Tunisia*
[2] *Faculty of Advanced Technology, University of Glamorgan, Pontypridd CF37 1DL, Wales, UK*
[3] *Unité de Physique Quantique et de Photonique, Faculté des Sciences de Tunis, Campus universitaire 2092 Manar II Tunisia*
Email: sobayya@glam.ac.uk

Introduction

Photonic crystal fibres (PCFs) with solid core offer more design possibilities by varying the number of air holes in the cladding and lattice constant, leading to many applications that can not be achieved with traditional optical fibers [1]. The demand for either chemical or biochemical sensing of low index materials is increasing, also, sensing of bulk materials and surface sensing will increase even in future because of tremendous progress in telecommunication, materials processing, health services [2].
A novel PCF based sensor is proposed. In order to increase the interaction between the light and analytes, the PCF is bent. The proposed PCF sensor consists of three circles surrounding the core. The active region is the middle circle of a varying radius. The sensor operates when the circle is filled with either liquids or gas. The sensitivity, the field plots, real and imaginary parts of the refractive index are calculated. By careful selection of the design parameters such as the radius of the sensing circle, the diameter of air holes in the core region and hole to hole spacing, Λ the sensitivity towards various analytes is determined. The field is calculated with and without bending and are shown in Fig.1(a) and Fig.1(b). The electric field is concentrated in the sensing circle for the PCF without bending, however, it fluctuates and tends to fellow the curvature.

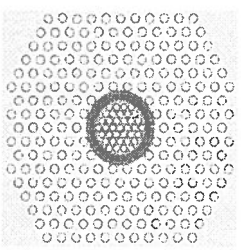
Fig.1(a)

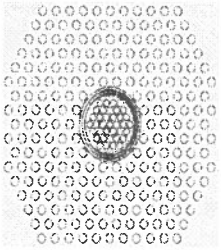
Fig.1(b)

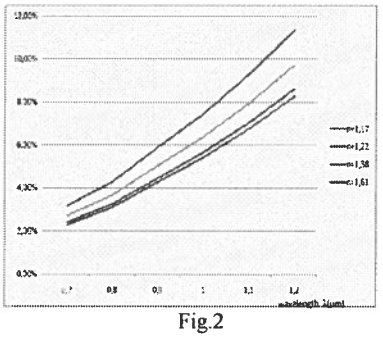
Fig.2

Also, the sensitivity is performed, findings show that the proposed PCF sensor is sensitive to gas of refractive index 1.61, however the selectivity towards dry air and CO is low at small wavelength as it is shown in Fig.2.

References

[1] P. Petropoulos, et al., *Opt. Lett.* **26**, 1233-1235 (2001)
[2] Y. L. Hoo, et al., *Opt. Eng.*, **41**, 8-9 (2002)

Investigation of CMOS Compatible Widely Tunable Multiplexers on SOI Technology

Andrey V. Tsarev
Laboratory of Optical Materials and Structures
Institute of Semiconductor Physics SB RAS
Novosibirsk, 630090, Russia
tsarev@isp.nsc.ru

Francesco De Leonardis
Dipartimento di Ingegneria dell'Ambiente e per lo Sviluppo
Sostenibile, Politecnico di Bari, Taranto, Italy
f.deleonardis@poliba.it

Vittorio M. N. Passaro
Dipartimento di Elettrotecnica ed Elettronica
Politecnico di Bari, Bari, Italy
passaro@deemail.poliba.it

***Abstract*—We present analysis of widely tunable multiplexers based on multi-reflector filtering approach. It implements novel wide CMOS-compatible silicon-on-insulator heterogeneous waveguides with thermo-optic phase shifters. Structure design has been performed by numerical modeling by FEM, BPM and FDTD methods.**

Keywords-component: Integrated optics; Silicon Photonics; Reconfigurable Add/Drop Multiplexer (ROADM); Multi-Reflector Filtering Technology.

I. INTRODUCTION

Silicon photonics belongs to rapidly growth science and technology [1]. A great progress has been done on application of this technology for development of reconfigurable Add/Drop multiplexers (ROADM) based on silicon-on-insulator (SOI) structures with thin (~ 220 nm) silicon core. Manufacturing of these devices is compatible with semiconductor CMOS technology [2]. Unfortunately, currently used silicon photonics has the principal limitation in the number of tunable wavelength channels of ROADM, hardly larger than 50.

Our research has proposed alternative multi-reflector (MR) filtering technology [3-6], which overcome this limitation in the number of tunable wavelength channels and open the way to increase its number up to 200 or 400. Unfortunately, MR technology has not yet been experimentally demonstrated. This work describes general properties of MR-ROADM and show its advantages related to other well known technologies.

II. ROADM IN THIN SOI

The general view of future ROADM is presented in Fig.1 [6]. Wavelength filtering takes place due to interference effect among multiple sub-beams reflected by the partial reflection mirrors which form the beam expanders for In, Drop, Add and Through channels. Use of thermo optic phase shifters for wide and fine tuning provides wavelength filtering in any desired tuning range by appropriate electrical signals applied to the local heaters over the channel optical waveguides. These waveguides have to be single mode and also have wide cross section in order to suppress parasitic signals. Thus, we propose to use in the design heterogeneous [4-7] (see Fig. 2) or strip and grating loaded [8] waveguides. Heterogeneous waveguides provide single mode behavior due to mode-dependent optical loss induced by side p^+n^+-regions with high concentration of free carriers [4-7]. Partial reflectors are made by deeply etched slots with typical widths of about 40 nm.

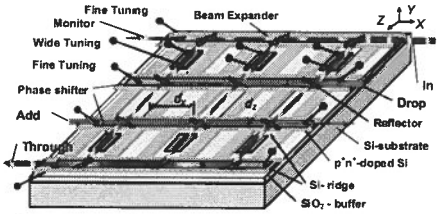

Figure 1. General view of thermo-optic MR-ROADM on thin SOI.

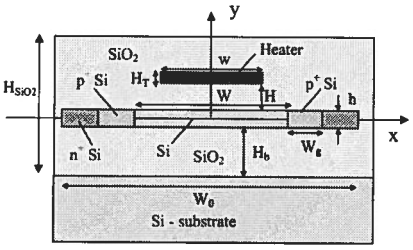

Figure 2. Heterogeneous SOI waveguide.

Thermo-optic phase shifters have been investigated in wide quasi-single mode heterogeneous waveguide by using FEM

(for heating) and BPM (for optical propagation) techniques [4]. Our simulations show that it is possible to provide small switching power $P_\pi < 40$ mW for π phase shift and low switching time < 10 μs (see Fig. 3).

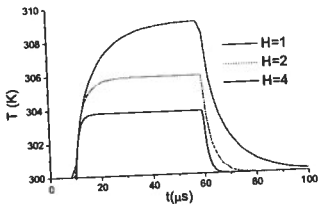

Figure 3. FEM simulations of time response of temperature in the waveguide center for different buffer heights; inward heat flux has a step impulse function of 50 μs duration and amplitude 10^{+7} W/m^2. h = 220 nm, H_b = 4 μm, w = 8 μm, W = 10 μm, W_0 = 35 μm, H = 0.1 μm, H_T = 0.2 μm.

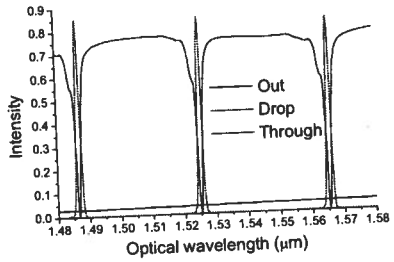

Figure 4. 2D FDTD simulation of frequency response of MR-ROADM with 32 slanted reflectors (incident angle φ = 45°). FWHM = 1.5 nm. FSR = 40 nm. Variable reflector width from 40 nm to 110 nm.

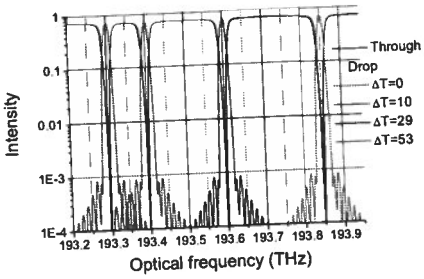

Figure 5. Simulated frequency response of the 25 GHz ROADM (intended for 200 tunable wavelength channels, φ = 45°). N_r = 380.

The typical simulation of MR-ROADM by 2D FDTD is shown in Fig. 4. The width d and shift of position of every reflector has been optimized to achieve the desired frequency response with high side-lobe suppression. It demonstrates the proof-of-concept of MR-filtering technology and shows that device can realize the required Drop/Through function. Better performance is provided by device with a larger number of reflectors (N_r) and variable reflector coefficients (see Fig. 5). Simulation of this device has been carried out by a ray-tracing model and taking into account phase delays of all reflected and transmitted sub-beams [6]. This variant of device is tuned in the range FSR/8 by temperature change ΔT in fine tuning phase shifters, with maximum power $P_f = P_\pi * N_r$ = 15.2 W. The total FSR (40 nm) is digitally switched by wide tuning elements with maximum power $P_w = P_\pi * N_r /2$. Thus, our simulations prove that MR-ROADM can be implemented for 25 GHz or smaller ITU grids, handling wavelength channels as large as 200 or more.

III. Conclusions

Paper presents advanced simulations of multi-reflector ROADM based on heterogeneous SOI waveguide structures with thermo-optic phase shifters. The local heaters are studied by FEM and BPM. Filtering properties of ROADM are examined by 2D FDTD simulations for a small number of partial reflectors (N_r = 32). Devices with a larger number of reflectors are investigated by in-house software and demonstrate wide tuning of 200 wavelength channels with FSR = 40 nm. To provide better performance every reflector has variable, optimized reflection coefficient and position. Thus, novel multi-reflector ROADMs are proved to be CMOS compatible and could be manufactured on thin SOI wafers.

Acknowledgment

The authors thank Company RSoft Design Group, Inc. for providing user license for BPM and FTDT software. This work was partially supported by II Engineering Faculty of Politecnico di Bari with funds by Provincia di Taranto, Taranto, Italy.

References

[1] G.T. Reed, Silicon Photonics. State of the art (John Wiley & Sons, Ltd, 2008).

[2] W. Bogaerts, R. Baets, P. Dumon, V. Wiaux, S. Beckx, D. Taillaert, B. Luyssaert, J. Van Campenhout, P. Bienstman, D. Van Thourhout, "Nanophotonic waveguides in silicon-on-insulator fabricated CMOS technology," J. Lightwave Technol. Vol. 23, pp. 401-412, 2005.

[3] A. V. Tsarev, "Tunable optical filters," United States Patent No 6,999,639, February 14, 2006.

[4] F. De Leonardis, A.V. Tsarev, V.M.N. Passaro, "Optical properties of new wide heterogeneous waveguides with thermo optical shifters," Opt. Express, vol. 16, pp. 21333–21338, 2008.

[5] A.V. Tsarev, F. De Leonardis, and V.M.N. Passaro, "Thin heterogeneous SOI waveguides for thermo-optical tuning and filtering," Opt. Express, vol. 16, pp. 3101-3113, 2008.

[6] A.V. Tsarev, "Thin heterogeneous optical silicon-on-insulator waveguides and their application in reconfigurable optical multiplexers," Quantum Electronics, vol. 38, pp. 445-451, 2008.

[7] A.V. Tsarev, "New type of heterogeneous nanophotonic silicon-on-insulator optical waveguides," Quantum Electronics, vol. 37, pp. 775-776, 2007.

[8] A.V. Tsarev, "New wide strip and grating loaded quasi-single-mode waveguide on SOI," Opt. Express, vol. 17, pp. 13095-13101, 2009.

Simulating Plasmonic Ring Resonators Using the Legendre Pseudospectral Time-Domain Method

Shih-Yung Chung[1], Chih-Yu Wang[1], Chun-Hao Teng[2], Chung-Ping Chen[1], and Hung-chun Chang[3]
[1] *Graduate Institute of Electronics Engineering and Department of Electrical Engineering, National Taiwan University, Taipei, Taiwan 10617, R.O.C.*
[2] *Department of Applied Mathematics, National Chiao Tung University, Hsinchu, Taiwan 30010, R.O.C.*
[3] *Department of Electrical Engineering, Graduate Institute of Photonics and Optoelectronics, and Graduate Institute of Communication Engineering, National Taiwan University, Taipei, Taiwan 10617, R.O.C.*
hcchang@cc.ee.ntu.edu.tw

The high-accuracy Legendre pseudospectral time-domain (PSTD) method is employed to simulate transmission characteristics of two-dimensional (2-D) plasmonic ring resonators based on the metal-insulator/metal (MIM) waveguide structure. Both Drude and Drude-Lorentz material dispersion models for the metal are considered.

Introduction

We simulate and study subwavelength metal waveguide ring resonators operating under the phenomenon of surface plasmon polaritons (SPPs) [1]. The finite-difference time-domain (FDTD) method has been a popular numerical analysis and simulation method for studying such structures and other plasmonic problems. However, due to its stair-casing approximation of the often occurring curved material interface, the FDTD calculation of the electromagnetic field near the interface is difficult to offer high accuracy. Recently, a high-order accurate Legendre PSTD algorithm was developed based on a penalty scheme and a multi-domain approach [2] and has been applied to obtain high-accuracy fields near silver nanorod arrays [3]. In this paper, we consider 2-D PSTD method and use it to simulate ring resonators formed by MIM waveguide structures, as shown in Fig. 1(a). Curvilinear quadrilateral sub-domains are properly designed so that possible curved metal/insulator boundaries can be well fit and boundary conditions can be correctly imposed, avoiding the stair-casing approximation as in the FDTD scheme.

Results

We study several ring resonators having different ring shapes, including the circular ring as in Fig. 1(a), the elongated ring (racetrack shape), the rectangular ring, and the hexagonal ring. Figure 1(b) shows the transmittance spectra for the circular-ring resoantor of Fig. 1(a) with R=500 nm, W=100 nm, and G=20 nm. Both Drude and Drude-Lorentz material dispersion models for silver are considered. We believe the obtained results possess very good accuracy.

References

[1] S. I. Bozhevolnyi, et al., Nature, **440**, 508–511 (2006).

[2] C. H. Teng, et al., *J. Sci. Comput.*, **36**, 351–390 (2008).

[3] B. Y. Lin, et al., *Opt. Express*, **17**, 14211–14228 (2009).

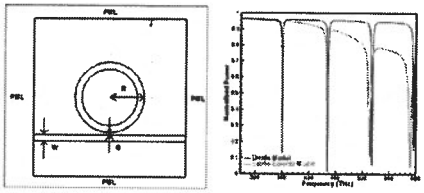

(a) (b)

Fig. 1. (a) Schematic plot and (b) PSTD calculated transmission spectra of an MIM circular-ring-resonator.

Transmission characteristics in plasmonic multimode waveguides

André G. Edelmann, Stefan F. Helfert and Jürgen Jahns
FernUniversität in Hagen, Chair of Optical Information Technology, Universitätsstr. 27
58084 Hagen, Germany
andre.edelmann@fernuni-hagen.de

We analyze the transmission characteristics related to the self–imaging effect in plasmonic multimode waveguides. As result the correlation between the input field and the field at the self–imaging distance of a central wavelength is computed.

Introduction

Plasmons are electromagnetic waves propagating at optical frequencies along a dielectric metallic interface [1]. In plasmonic multimode waveguides interesting self–imaging effects can be observed [2]. We study the transmission characteristics related to this self–imaging effect. For the analysis the Method of Lines (MoL) [3] was used.

Results

In Figure 1a we see the plasmonic field propagation at the top of a metallic structure in the plasmonic multimode waveguide. We can clearly see the field repetition at the self–imaging distance $L_{si} \approx 15.8\mu$m. The transmission characteristics were obtained by determining the correlation between the input field and the field at the self–imaging distance L_{si}. In our studies we consider the symmetric (even) and antisymmetric (odd) modes. Figure 1b show the results for the central wavelengths $\lambda_0 = 0.6\mu$m resp. $\lambda_0 = 0.7\mu$m. The curves for the central wavelength $\lambda_0 = 0.7\mu$m were smoother compared to those for $\lambda_0 = 0.6\mu$m.

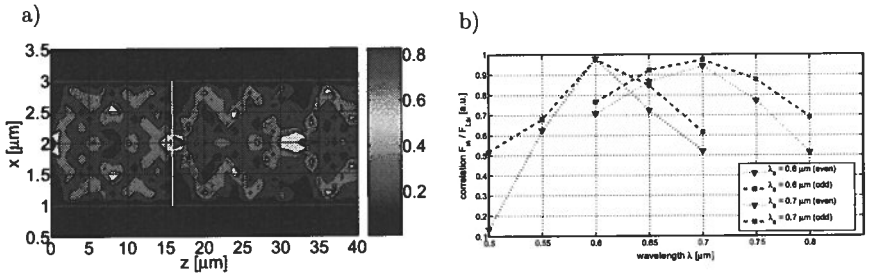

Fig. 1. a) Field distribution at the top of a metallic structure in the plasmonic multimode waveguide (the losses of the metal were neglected). b) Transmission characteristics for even and odd excitation at the wavelengths $\lambda_0 = 0.6\mu$m resp. $\lambda_0 = 0.7\mu$m.

References

[1] H. Raether, *Surface plasmons on smooth and rough surfaces and on gratings* (Springer, Berlin, 1988).
[2] A. G. Edelmann, S. F. Helfert, and J. Jahns, "Analysis of the self–imaging effect in plasmonic multimode waveguides", to appear in Appl. Opt. **49** (2010).
[3] R. Pregla, *Analysis of electromagnetic Fields and Waves: The Method of Lines* (John Wiley & Sons, Ltd., West Sussex, England, 2008).

Guiding and focusing electromagnetic fields at the nanoscale with Wedge and Channel Plasmon Polaritons

Sergio G. Rodrigo[1], E. Moreno[2], S. I. Bozhevolnyi[3], L. Martín-Moreno[1] and F.J. García-Vidal[2]

[1]*Instituto de Ciencia de Materiales de Aragón (ICMA) and Departamento de Física de la Materia Condensada, CSIC-Universidad de Zaragoza, E-5009 Zaragoza, Spain*
sergut@unizar.es
[2] *Dpto de Física Teórica de la Materia Condensada, Universidad Autónoma de Madrid, E-28049 Madrid, Spain.*
[3]*Institute of Sensors, Signals and Electrotechnics (SENSE), University of Southern Denmark, Niels Bohrs Allé 1, DK-5230 Odense M, Denmark*

Introduction

Optical circuits promise to be a feasible way to downscaling in micro and nanotechnology. However, guiding and focusing light at subwavelength scales still remains a major issue. Electromagnetic (EM) fields confined in metallic channels or wedges are though to be one of the best suited candidates for on-chip miniaturization.

Results

Surface Plasmon Polaritons (SPPs) are electromagnetic modes perpendicularly confined to a metal surface. A main design difficulty is finding structures that support electromagnetic fields also with small "lateral" modal size while featuring long propagation lengths. The EM fields supported by V-shaped grooves carved in a metal, called Channel Plasmon Polaritons (CPPs) **[1]**, and the EM modes supported by metallic wedges, that is, the so-called Wedge Plasmon Polaritons (WPPs) **[3]**, fulfill these requisite at telecom wavelengths **[2,3]** and devices based upon them have been experimentally demonstrated **[4,5]**.

We will present a theoretical study based on the Finite-Difference Time-Domain (FDTD) method demonstrating that efficient WPP to SPP conversion can be achieved by modifying the wedge geometry along the mode propagation direction, from an initial wedge-shaped profile to that of the flat surface **[3]**. This makes such a device promising to be used as SPP ←→ WPP coupler. Interestingly, a similar building scheme based on CPPs does not display good conversion performance, but intense EM field enhancement is found in the tapered section of the waveguide for optimized configurations **[6,7]**, which will be explained from the theoretical standpoint.

References

[1] I. V. Novikov and A. A. Maradudin, *Phys. Rev. B* 66, 035403 (2002).

[2] E. Moreno, F. J. García-Vidal, S.G. Rodrigo, L. Martín-Moreno, and S.I. Bozhevolnyi. *Opt. Lett.*, 31, 3447-3449 (2006).

[3] E. Moreno, S.G. Rodrigo, S. I. Bozhevolnyi, L. Martín-Moreno, and F. J. García-Vidal, *Physical Review Letters* 100, 023901 (2008).

[4] S. I. Bozhevolnyi, V. S. Volkov, E. Devaux, J. Y. Laluet, and T. W. Ebbesen, *Nature* 440, 508 (2006).

[5] A. Boltasseva, V. S. Volkov, R. B. Nielsen, E. Moreno, S. G. Rodrigo, and S. I. Bozhevolnyi, *Opt. Express* 16, 5252-5260 (2008).

[6] V.S. Volkov, S.I. Bozhevolnyi, S.G. Rodrigo, L. Martín-Moreno, F. J. García-Vidal, E. Devaux, and T.W. Ebbesen. *Nano Letters*, 9, 1278-1282 (2009).

[7] V.S. Volkov, S. I. Bozhevolnyi, J. Gosciniak, S. G. Rodrigo, L. Martín-Moreno, F. J. García-Vidal, E. Devaux, , and T. W. Ebbesen, *New J. Phys.* 11, 113043 (2009).

Plasmonic waveguides modelling : density of guided modes approach

G. Colas des Francs, J. Grandidier, A. Bouhelier, J.C. Weeber and A. Dereux

[1] *Laboratoire Interdisciplinaire Carnot de Bourgogne (CNRS/Université de Bourgogne)*

Faculté des Sciences Mirande, 9, av. Savary, BP 47870, 21078 Dijon Cedex

Introduction

Surface plasmon polariton (SPP) waveguiding is the subject of intense research since it could combine the electronic circuitry miniaturization with the large photonic bandwidth. SPP couples metal free electrons oscillations with an electromagnetic wave and present reduced mode effective volume promising for achieving light matter interaction at a sub-wavelength scale. Recently, strong efforts have been push forward active control of the guided SPP, with particular attention for gain-assisted propagation.

We will present a mode solver based on the density of guided modes (DOS) evaluation[1]. We will also discuss the interest of this formulation to properly describe stimulated emission in a plasmonic waveguide[2]. Specifically, we will focus on the two competitive processes for the gain medium relaxation: coherent stimulated emission and incoherent non radiative coupling to the metal[3].

Results

We present on fig.1a, the three partial DOS calculated near a guided mode resonance. Guided mode effective index, propagation length and polarization state are directly deduced from DOSs resonance profiles. Interestingly, although we calculated the 2D-DOS associated with the waveguiding structure, we fully characterize the 3D supported mode (Fig1b-d). We will also compare this method with the 2D differential method and the effective index model.

Finally, we will discuss how DOS evaluation allows to precisely describe gain-assisted propagation in a plasmonic waveguide. Particularly, we will focus on the competition between spontaneous and stimulated relaxation by coupling to the plasmon mode.

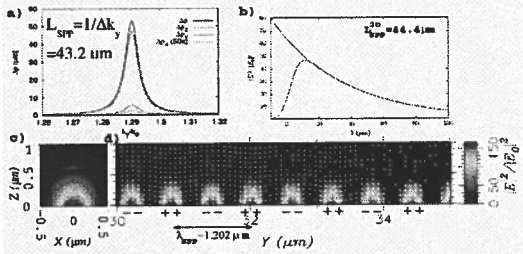

Fig. 1 a) Partial density of states variations near a guided mode resonance. b) Mode decay length under 2D gaussian beam excitation. c-d) Mode intensity profile. The plasmonic waveguide consists in a 600 nm x 600 nm polymer stripe deposited on a 100 nm thick gold film, free space wavelength is λ=1.55 µm .

[1] Colas des Francs *et al*, Physical Review B **80**, 115419 (2009).

[2] Grandidier *et al*, Nano Letters **9**, 2935 (2009).

[3] de Leon, Berini, Physical Review B **78**, 161401(R) (2008).

Computational Techniques for the Analysis and Design of Dielectric-Loaded Plasmonic Circuitry

Odysseas Tsilipakos, Alexandros Pitilakis, Anna C. Tasolamprou,
Traianos V. Yioultsis, and Emmanouil E. Kriezis
Department of Electrical and Computer Engineering, Aristotle University of Thessaloniki, Thessaloniki GR-54124, Greece
otsilipa@auth.gr, mkriezis@auth.gr

Guided-wave plasmonic components based on the dielectric-loaded plasmonic (DLSPP) waveguide are theoretically investigated by utilizing the finite element (FEM) and the beam propagation method (BPM).

Introduction

Plasmonic components are a prime candidate for nanophotonic circuits, combining the bandwidth of photonics along with nanoscale dimensions. The recently proposed DLSPP waveguide [1] is technologically simple and exhibits strong guiding properties. It is therefore suitable for densely integrated plasmonic circuits. Among the DLSPP-based components that have been demonstrated [2], microring resonator filters [2-3] and Mach-Zehnder interferometers are of substantial interest since they can provide the basis for the realization of switchable plasmonic circuits.

Results

Microring and microdisk resonator filters are investigated (Fig. 1) by utilizing the vectorial 3D finite element method. This choice is very natural given the resonant nature of these components, where the response is shaped by multiple interference effects between the circulating modes. For larger structures, such as Mach-Zehnder interferometers, a FEM solution becomes computationally expensive and in many instances prohibitive. In such cases, the presence of a clear direction of propagation along with the minimal level of reflections renders the BPM a favorable alternative. Though not as commonly utilized in plasmonics, our results indicate that it is a robust and valuable tool for the numerical analysis of such DLSPP-based components.

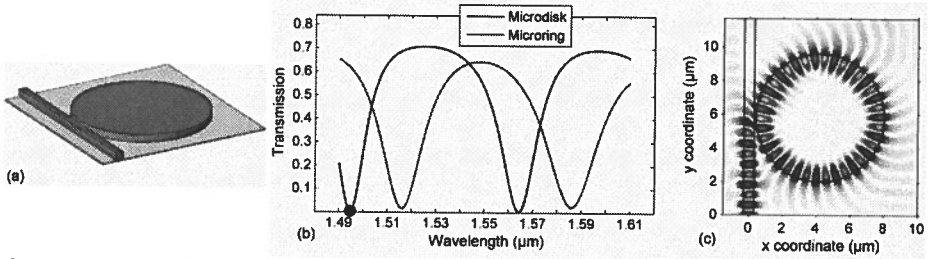

Figure 1: (a) Schematic of the simulated microdisk resonator filter, (b) Transmission versus wavelength for a microdisk (R = 3.5 μm) and a microring resonator filter of the same footprint (R = 3.8 μm), and (c) Real part of E_z at the transmission minimum marked in (b).

References

[1] T. Holmgaard and S. I. Bozhevolnyi, *Phys. Rev. B*, **75**, 245405, (2007)

[2] T. Holmgaard, *et al.*, *Appl. Phys. Lett.*, **94**, 051111, (2009)

[3] O. Tsilipakos, T. V. Yioultsis, and E. E. Kriezis, *J. Appl. Phys.*, **106**, 093109, (2009)

Surface plasmon characterization method based on two-groove interference pattern

Yochai Edlitz[1] and Shlomo Ruschin[2]
[1] *Raymond and Beverly Sackler School of physics Tel-Aviv University Tel Aviv 69978, Israel*
[2]*Department of Electrical Engineering—Physical Electronics, Tel Aviv University, Tel Aviv 69978, Israel*
ruschin@eng.tau.ac.il

Introduction

The modeling of a simple non-contact method for full characterization of surface plasmon modes is presented. It is based on the analysis of the interference pattern originating in two sub-wavelength grooves in a metallic film. Real and imaginary parts of the SP propagation constants are extracted.

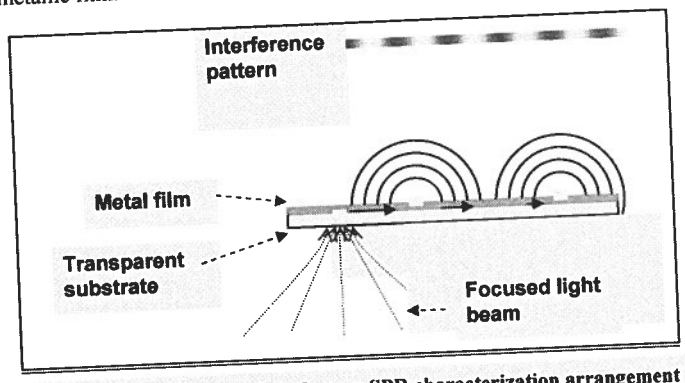

Figure 1: Two-groove interference SPR characterization arrangement

Method description and results

Practically all reported methods for SP modes characterization require substantial disturbances of the guiding field like prism proximity, grating structuring, or near-field techniques. The present method is based on the findings of Kuzmin et. Al. [1] who showed that in a two-slit arrangement in a metallic film, the illumination of one slit is sufficient to create an interference pattern. According to the present method (Figure 1), a SP wave is excited in a metallic film and made to propagate along it. Two sub-wavelength grooves are milled in the film, which scatter part of the SP wave. Light scattered by the groves propagates in free space and creates a typical Young interference fringe pattern. The analysis of the pattern properties: fringe position and contrast furnishes the desired characterization of the SP wave. Furthermore, delineating non-parallel grove lines with varying distance and sliding the SP input position, allows canceling out the influence of the scattering efficiency from the calculation. The simulation includes the entire process of light propagation both in the film and free-space and calculation of the grove scattering efficiency by modal expansion. The model was successfully verified by comparison with experimental data reported in ref. [1]. Sensitivity and dynamic range of the method were analyzed, and its application for SPR sensing is suggested.

References

1. [1] Kuzmin, N., et al. "Enhancement of spatial coherence by surface plasmons". Optics Letters. Vol. 32, 5, pp. 445-447. (March 2007)

Quantum Photonics using Guided Waves

Ian A. Walmsley, Nick Thomas-Peter, Michael Hu, Hendrik Coldenstrot-Ronge,
Tim Bartley and Brian J. Smith
Clarendon Laboratory, University of Oxford, Parks Road, Oxford, OX1 3PU, UK
walmsley@physics.ox.ac.uk

Photonics provides a promising route to implementing quantum-enhanced technologies. Underpinning this technology lies the generation, manipulation and stabilization of multi-photon entangled states. Waveguide structures provide important physical features that enable these, as well as convenient structures for scaling to larger numbers of photons.

Introduction

Quantum technologies promise to enhance the capabilities of transmission and processing of information beyond what is possible using classical physics. Applications are envisaged to communications, cryptography, metrology, imaging and computation. All-optical versions of these technologies exist in principle, based on uniquely quantum features such as reduced noise, increased correlations and measurement back-action that are fundamentally different that those used in the design of classical optical analogues of these processing devices. The distribution of photonic entangled quantum states and their application to real-world processing tasks is therefore a central element of quantum information science. The key capabilities that enable this technology are the preparation of appropriate photonic quantum states, the manipulation of these in response to external controls, the storage of the outputs of the processing and the measurement of these outcomes. Each of these benefits by the use of waveguiding structures.

Results

The key features of waveguides that are critical for such development include control of dispersion by means of the guide size,[1] controllable birefringence,[2] stability of multiple-nested interferometers,[3] and flexibility of configuration.[4] Particularly useful examples can be found in both photonic-crystal fibers as well as standard polarization preserving single mode fibers. The relative merits of these sources are predicated on the quality of the structure fabrication and the ease of coupling multiple sources together. Further, integrated photonic circuits enable concatenation of multiphoton interferometers that can be used both to prepare states, and as sensing devices.

References

[1] O. Cohen et al. Phys. Rev. Lett. 102, 123603 (2009)

[2] B. J. Smith et al., Opt. Exp., 17, 23589-23602 (2009)

[3] B. J. Smith et al., Opt. Express 17,13516 (2009)

[4] G. Puentes et al., Phys. Rev. Lett., 102, 080404 (2009)

Single-shot 3D Reconstruction of Complex Dielectric Function of the Glass during the Femtosecond Laser Micro-Fabrication

A.V. Turchin [1,2], M. Dubov [1], and J.A.R. Williams [1]
[1] *Aston University, Aston Triangle, Birmingham, B4 7ET, United Kingdom;*
m.dubov@aston.ac.uk
[2] *Institute of Physics, NASU, Nauky av. 46, Kyiv 680028, Ukraine*

Introduction

To reconstruct 3D dielectric function of glass during direct laser micro-fabrication we suggest to measure the complex value of field scattered by the volume subject to femtosecond laser induced plasma, theoretically justify and numerically solve the inverse scattering problem. The optical layout we suggest has common features with DIC-microscopy, where both "reference" and "probe" beams (with orthogonal polarizations) pass almost the same optical path, sometimes through the micro-objectives with high NA. Our approach has also similarities with Digital Holographic Microscopy, where one records two-beam interference pattern and reconstructs of the distribution of the refractive index (for phase object) using Fresnel diffraction integrals in scalar approximation.

Results

Experimental set-up (Fig. 1, a) includes femtosecond laser operated at 800 nm and specially designed optical cuvette (Fig. 1, b) to minimize parasitic reflections. First demonstration was done with DPSS CW laser illumination.

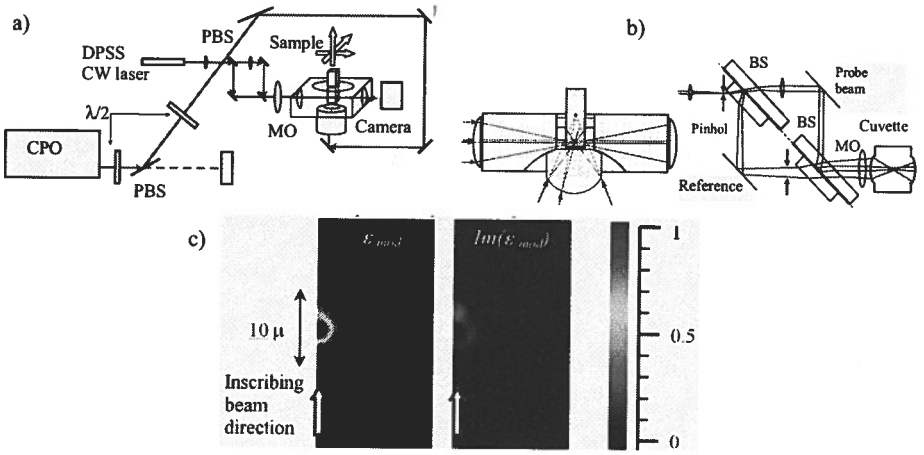

Figure 1. (a) Experimental set-up includes DPSS laser or other source. The inscribing beam is delivered from the bottom of the cuvette made of BK7 glass as well, while diagnostics beam (shown online in green) passes from the left side on both a side and a top view (b). In the cuvette two beams do not overlap; the probe beam is collimated and centred on the inscribed region, while the reference beam is transmitted over unmodified glass and it is tightly focused so that an interference pattern on the camera forms parallel fringes.

We present an example of reconstructed of dielectric function, normalized to max, on Fig.1, c). In conclusion, our method can be used to measure both ultrafast and slow dynamics of $Re(\varepsilon_{mod})$ and $Im(\varepsilon_{mod})$ – with time resolution ranging from sub-ps to ms range.

A guided mode view on Near-field Scanning Optical Microscopy measurements of optical magnetic fields with slit probes

Remco Stoffer[1], Manfred Hammer[2], O.V. (Alyona) Ivanova[2] and Hugo J.W.M. Hoekstra[2]
[1] *PhoeniX Software, P.O. Box 545, 7521PA Enschede, The Netherlands*
remco.stoffer@phoenixbv.com
[2] *MESA+ Institute for Nanotechnology, Univ. of Twente, P.O. Box 217, 7500AE Enschede, The Netherlands*

Recent Near-field Scanning Optical Microscopy (NSOM) experiments with slit metal coated probes claim to measure the out-of-plane optical magnetic field around a dielectric sample waveguide [1]. The observations can also be explained by mode overlap calculations.

Summary

Measurements [1] of electromagnetic fields around an optical waveguide, by means of Near-field Scanning Optical Microscopy (NSOM) with a metal-coated tapered fiber tip with a slit in the coating, seem to indicate that the in-plane electric and out-of-plane magnetic components of the optical field can be determined independently. We consider the structure shown in Figure 1(a) as a simplification of the configuration of [1]. The probe is assumed to be purely cylindrical; any effects related to the tapering to the much wider, non-slit probe fiber are thus not taken into account. Interest is in the polarized optical signal that is detected at the upper end of the probe, if the lower end scans through the evanescent optical field over the surface of the sample waveguide. The tip supports two guided, though lossy, modes, one with a major x-oriented electric field component that is localized in the glass core (b), and another with a dominant y-oriented electric field that is located mainly in the probe slit (c). We create a standing wave pattern in the sample waveguide by interfering counter-propagating versions of its fundamental TE (x-polarized) mode. Under the assumption that the probe does not significantly perturb the sample field, the optical signals associated with the two modes propagating upward in the probe are given by inner products with the sample field at the end facet of the tip, 20 nm above the surface. These overlap integrals involve only the x and y components of the fields. Figures 1(d) and (e) show that, just as in the experiments [1], the maxima of the power picked up by the two probe modes are shifted by half a period.

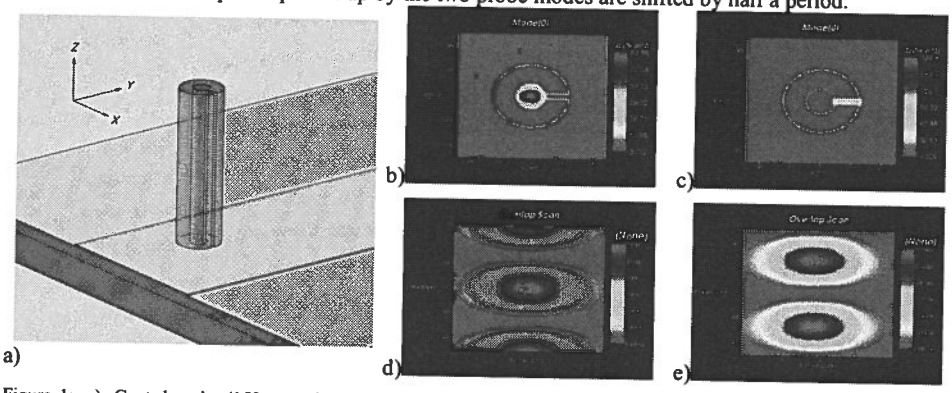

Figure 1:, a): Coated probe (150 nm Al on a 100 nm radius glass core, with a 40 nm slit) above a silicon nitride waveguide [1]. b),c): Intensities of the two modes supported by the slit probe. d), e): Signal power associated with the x- and y-polarized probe modes vs the position (x,y) of the tip.

[1] M. Burresi et al., *Science* **326**, 550-553 (2009)

Enhanced transmission of electromagnetic radiation through subwavelength apertures beyond the cutoff wavelength

S. Carretero-Palacios[1], S. G. Rodrigo[1], L. Martin-Moreno[1], F.J. Garcia-Vidal[2]

[1] *Instituto de Ciencia de Materiales de Aragón (ICMA) and Departamento de Física de la Materia Condensada, CSIC-Universidad de Zaragoza, E-50009 Zaragoza, Spain*

sol@unizar.es

[2] *Departamento de Física Teórica de la Materia Condensada, Universidad Autónoma de Madrid, E-28049 Madrid, Spain*

Introduction

Sub-wavelength apertures periodically arranged may transmit electromagnetic waves beyond the cut-off wavelength with a much higher intensity than if they were isolated. Confined electromagnetic modes at each side of a metal film may provide an efficient tunneling channel for photons passing through such array of holes. This is the so-called Extraordinary Optical Transmission **[1]**.

Results

We analyze theoretically resonances appearing at wavelengths red-shifted from the cut-off of the holes **[2]**, **[3]**. We name this phenomenon Localized Extraordinary Optical Transmission (LEOT). Interestingly, since no surface modes are involved, the physical mechanism is valid for both isolated (SH) and periodically arranged holes (2DHA).

In particular, we will give analytical expresions for the LEOT peak position as a function of the film thickness (h), and the dielectric constants of the cover, the substrate, and inside the holes, (ε_1, ε_3, ε_2, respectively) for both symmetric ($\varepsilon_1 = \varepsilon_3$) and asymmetric ($\varepsilon_1 \neq \varepsilon_3$) configurations, for any hole shape of high aspect ratio **(See Fig.1)**. Furthermore, the peak position is not the only spectral property affected by the dielectric environment, but also LEOT peak intensities are drastically modified.

These results explain the unexpected fact reported by recent experiments in the THz regime about enhanced transmission **[4]** through isolated holes at wavelengths beyond the cutoff wavelength.

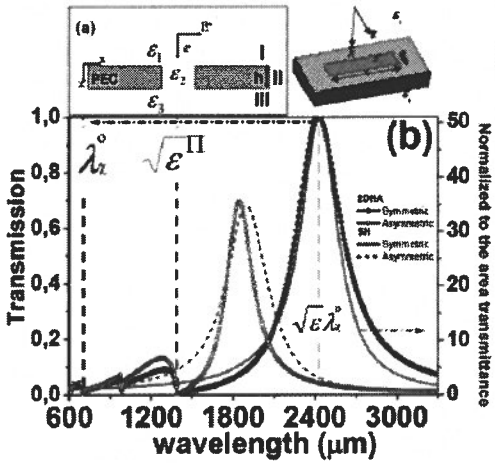

FIG.1: (a) Schematic of the investigated structure. Panel (b): for h = 1μm, rectangular holes with: a_x = 10 μm, a_y = 350 μm, and ε_2 = 1.0, the figure shows transmission curves through a 2DHA (P=400 μm) placed in a symmetric environment (full symbols) and on a substrate (empty symbols). With solid line it is shown the normalized to the area transmission of a SH in the symmetric configuration. The dashed line depicts the same but for the asymmetric case. The dielectric constant of either the cover and/or the substrate is chosen to be 12.

References

[1] T. W. Ebbesen et al. *Nature (London)* **391**, 667 (1998)

[2] A. Degiron et al., *Opt. Commun* **239** (2004)

[3] K. J. Klein Koerkamp et al., *Physs. Rev. Lett.* **92**, 1839901 (2004)

[4] M. A. Seo et al., *Opt. Express*, **16**, 20484, (2008)

Plasmonic resonant modes in coupled and overlapping nanowires

Andrzej Stefanski[1], Alejandro Manjavacas[2], Viktor Myroshnychenko[2], Dorota Anna Pawlak[1] and Javier Garcia de Abajo[2]

[1] *Institute of Electronic Materials Technology, ul. Wolczynska 133, 01-919 Warsaw, Poland*
andrzej.stefanski@itme.edu.pl, dorota.pawlak@itme.edu.pl
[2] *Instituto de Optica, CSIC, Serrano 121, 28006 Madrid, Spain*
viktor@io.cfmac.csic.es, ama@io.cfmac.csic.es, jga@io.cfmac.csic.es

Analysis of the electromagnetic field propagation in two coupled nanowires and two overlapping nanowires is presented. So-called gap mode found in two nanowires placed in close proximity is compared with phenomena found in overlapping nanowires.

Introduction

Gap plasmon resonant mode in structures containing nanowires placed in close proximity has been recently reported [1,2]. Similar kind of modes have been expected for overlapping wires. Investigations of structures containing overlapping nanowires are presented here.

Results

Analysis of the electromagnetic field propagation in two coupled nanowires and two overlapping nanowires has been performed. The silver (Ag) nanowires in a silica (SiO_2) host have been calculated at the first stage. The modeling has been carried out by 2D boundary element method and 2D multiple-elastic-scattering multipolar expansion method [3,4]. The two approaches result in coinciding normalized plots.

The photonic density of states (DOS) as a function of energy and momentum parallel to the wires is presented for various distances between the wires. It is compared with photonic local density of states calculated as a function of energy and momentum parallel to the wires for various values of the overlapping depth. In the structure with overlapping nanowires two modes similar to the gap modes can be observed.

Similar analysis has been carried out for polaritonic (ionic crystals as potassium chloride, KCl) wires. Ionic crystals can support optical phonons that couple to photons and result in surface polaritons. In contrast to metallic materials the polaritonic materials show a dispersion behavior in THz range but properties and behavior of metallic nanowires with plasmons in an optical region can be extrapolated to polaritonic cylinders in a THz region. Such kind of materials made of polaritonic wires as KCl, can be easily made by directional solidification of eutectic [5].

References

[1] A. Manjavacas and F. J. García de Abajo, *Robust plasmon waveguides in strongly interacting nanowire arrays,* Nano Letters **9**, 1285-1289 (2009).

[2] A. Manjavacas and F. J. García de Abajo, *Coupling of gap plasmons in multi-wire waveguides*, Optics Express **17**, 19401-19413 (2009).

[3] F. J. Garcia de Abajo and A. Howie, *Relativistic electron energy loss and electron-induced photon emission in inhomogeneous dielectrics*, Phys. Rev. Lett. **80**, 5180-5183 (1998).

[4] F. J. Garcia de Abajo and A. Howie, *Retarded field calculation of electron energy loss in inhomogeneous dielectrics*, Phys. Rev. B **65**, 115418 (2002).

[5] V.M. Orera et al., *Novel Photonic Materials Made from Ionic Eutectic Compounds*, Acta Phys. Slovaca **55**, 261-269, (2005).

Accurate Time Domain Simulation of Optical Microcavity Ring Resonators

Nabeil Abujnah, R. Letizia, S. S. A. Obayya
Faculty of Advanced Technology, University of Glamorgan, Pontypridd CF37 1DL, UK
sobayya@glam.ac.uk

Introduction

Microcavity Ring Resonators (MRRs) based on high-index-contrast waveguide are presented. The impact of the structure parameters on the structure performance is investigated. The numerical technique used for the analysis is the multiresolution time domain (MRTD) combined with uniaxial perfectly matched layer (UPML) absorber to truncate the computational domain.

Results

MRRs are critical optical components that can be used in a variety of applications ranging from quantum electrodynamics to telecommunication device and optical sensor [1]. Thank to recent advances in material technology and fabrication techniques, MRRs with physical dimensions comparable to optical wavelength have been made possible to be fabricated with negligible bending loss [2]. The analysed parameters are the coupling coefficients between the input/output waveguides and the ring, the resonant frequencies, and the free spectral range (FSR). The effect of the structure geometry parameters such as the gap between the ring and input/output waveguides, the ring radius, and the width of the input/output waveguides and the ring resonator are thoroughly investigated. The numerical technique used is MRTD [3] which provides high numerical precision without the strict limitation on the step size in space compared with commonly used finite difference time domain (FDTD). The considered two-dimensional coupled MRR is shown in Fig. 1. The variation of coupling coefficients with frequency is shown in Fig. 2 and compared to the result obtained on the same structure when FDTD is used. Fig. 3 illustrates the result of electric field pattern of propagation around the ring. More results will be presented to show the dependence of MRR performance on optical design performances.

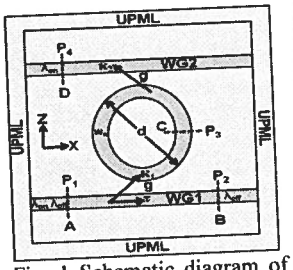

Fig. 1 Schematic diagram of MRR

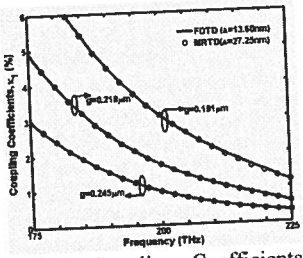

Fig. 2 Coupling Coefficients variation calculated with FDTD and MRTD

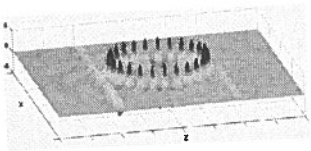

Fig. 3 resonance mode profile inside MRR

References

[1] K.J. Vahala, *Nature*, **424**, 839-846 (2003)
[2] Taflove A., Hagness S. C., *Computational electrodynamics:The finite-Difference Time-Domain Method*. Norwood: Artech House, Inc. 2005.
[3] Letizia, R., and Obayya, S.S.A, *IET Optoelectronics*, **2**, 241-253 (2008)

New design of Directional Polarising Beam Splitter

Gebriel. A. Gannat and S. S. A. Obayya
Integrated Communications Research Centre. Faculty of Advanced Technology
University of Glamorgan, Pontypridd CF37 1DL, UK
Email: sobayya@glam.ac.uk

A new design of a photonic crystal directional Polarizing Beam Splitter (PBS) is proposed and realised using Finite Difference Time Domain (FDTD). From obtained results the performance of the PBS is improved and 18.2μm coupling length is achieved.

Introduction

Separating TE from TM using polarised beam splitter (PBS) [1] and polarization channel drop filter (PCDF) [2] has been an area of interest for researchers over the last decades. The scientist interest is driven by the fact that communication systems have an increasing demand for the extremely wide transmission bandwidth in optical frequencies and the utilisation of Polarisation splitting devices may help to increase the spectral efficiency. The focus in this work is on the polarised beam splitter (PBS) where a novel design of directional beam splitter (PBS) based on Photonic Crystal (PhC) is proposed and realized using Finite Difference Time Domain (FDTD).

Results

The proposed structure in Fig. 1 represents new design of directional polarised beam splitter (PBS). The aim of this new proposed is to reduce the length of polarised beam splitter. This is achieved by using rectangular air holes instead of circular holes for the directional coupler between the two channels. Rectangular holes can be discretised by high accuracy and can be simulated using relatively large mesh cells compared with the circular holes directional coupler proposed in [5]. The radius of the air holes of the PhC is $r = 0.147\mu m$, the lattice constant a =0.457 μm, the length of the rectangular holes in the coupling region is = 0.294μm and the width =0.1.206μm. The refractive index for the waveguides n_g =3.32. As shown in Fig. 1, the three white lines in ch-1 and ch-2 are line detectors to record the incident fields at the input and transmitted power in both channels for TE and TM modes.

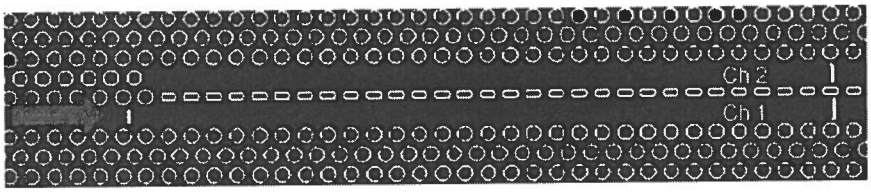

Fig. 1 proposed structure with coupling length 18.2 μm

References

[1] T. Liu, et al., *IEEE Photon. Technol. Lett.*, **17**, 1435-1437 (2005)
[2] H. Ren et al., *J. Opt. Quantum Electron.*, **38**, 645-654 (2006)

An HCMT model of optical microring-resonators

Manfred Hammer,
MESA+ Institute for Nanotechnology, University of Twente, Enschede, The Netherlands
m.hammer@ewi.utwente.nl

Analytical modes of the bus and cavity cores are combined into a 2-D hybrid analytical / numerical coupled mode theory (HCMT) model of integrated optical ring-resonators. The variational technique generates 1-D FEM-discretized solutions for the amplitude functions in their natural Cartesian and polar coordinates.

Summary

Optical microresonator configurations with a circular cavity between two parallel bus waveguides are considered in the frequency domain. Given the analytical modes of the two bus cores and the bend mode(s) [1] supported by the curved waveguide profile that constitutes the cavity, and restricting to unidirectional (clockwise) wave propagation, one readily writes the following ansatz for the time harmonic electromagnetic field, using Cartesian coordinates x, z and polar coordinates r, θ as in the figure:

$$\begin{pmatrix}\boldsymbol{E}\\ \boldsymbol{H}\end{pmatrix}(x,z) = f(z)\begin{pmatrix}\boldsymbol{E}\\ \boldsymbol{H}\end{pmatrix}^{\mathrm{u}}_{\mathrm{s}}(x)\,\mathrm{e}^{-\mathrm{i}\beta z} + b(z)\begin{pmatrix}\boldsymbol{E}\\ \boldsymbol{H}\end{pmatrix}^{\mathrm{l}}_{\mathrm{s}}(x)\,\mathrm{e}^{\mathrm{i}\beta z} + a(\theta)\begin{pmatrix}\boldsymbol{E}\\ \boldsymbol{H}\end{pmatrix}_{\mathrm{b}}(r)\,\mathrm{e}^{-\mathrm{i}\kappa R\theta}.$$

Indices $_{\mathrm{b}}$ and $_{\mathrm{s}}$ indicate the bend mode profile of the cavity, and the directional profiles of the upper ($^{\mathrm{u}}$) and lower ($^{\mathrm{l}}$) bus waveguide with propagation constants $\pm\beta$. κ (real) is selected close to the real part of the complex bend mode propagation constant, such that κR is a natural number, with R the cavity radius. In line with the HCMT approach [2] one now discretizes the so far unknown amplitude functions $f(z)$, $b(z)$, and $a(\theta)$ by linear 1-D finite elements over a suitable z-interval, and for $\theta \in [0, 2\pi]$. Then a Galerkin procedure is applied on a computational window that covers the entire resonator structure. One obtains a dense, but small size algebraic system of equations for the element coefficients. The numerical solution yields approximations for the amplitude functions and permits to reassemble the overall optical field. The figure shows an example. Extension towards bidirectional wave propagation along all channels, and towards other, also multi-cavity configurations, is straightforward.

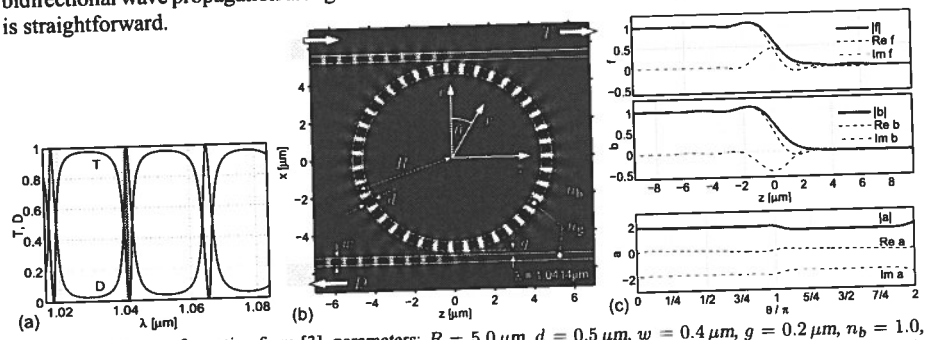

A microresonator configuration from [3], parameters: $R = 5.0\,\mu$m, $d = 0.5\,\mu$m, $w = 0.4\,\mu$m, $g = 0.2\,\mu$m, $n_b = 1.0$, $n_g = 1.5$. (a): relative power transmission T and drop D versus the excitation wavelength λ; (b): principal electric component of the TE polarized field at $\lambda = 1.0414\,\mu$m; (c): HCMT amplitudes f, b, and a at the resonance (b).

References

[1] K. R. Hiremath, M. Hammer, R. Stoffer, L. Prkna, J. Čtyroký. *Opt. Quant. Elect.*, 37(1-3):37–61, 2005.
[2] M. Hammer. *Journal of Lightwave Technology*, 25(9):2287–2298, 2007.
[3] K. R. Hiremath, R. Stoffer, M. Hammer. *Optics Communications*, 257(2):277–297, 2006.

Oscillations in plasma sphere after its instant formation

Alexander Nerukh[1], Tatyana Remayeva[1] and Nataliya Sakhnenko[1]
[1]*Kharkov National University of Radio Electronics, 14 Lenin Ave., Kharkov, 61166, UKRAINE*
nerukh@ddan.kharkov.ua

The transformation of a plane harmonic wave caused by instant creation of a plasma sphere is investigated. The exact expression for the transformed field is obtained by virtue of the solution of an initial and boundary value electromagnetic problem for Maxwell's equations.

Introduction

The paper is devoted to the investigation of the key processes in the interaction of an electromagnetic field with a spherical plasma particle after its creation. An unconditioned ratio of the sphere radius and the spatial scale of the electromagnetic field is assumed. The investigation takes into account the full vector nature of the electromagnetic field by using the expansions over the set of the orthogonal vector spherical functions.

Results

A 3-D initial problem for the Maxwell's equations, when a medium permittivity changes in time inside a sphere, is formulated in the form of the Volterra integral equation in time domain [1]. Solution of this equation uses the Laplace transformation together with the known method of the spherical vector functions $\mathbf{M}_{mn}(r,\theta,\varphi)$ and $\mathbf{N}_{mn}(r,\theta,\varphi)$ [2, 3]. Transformation of a plane wave caused by the instant ionization of the medium inside the sphere is considered.
Analysis of the obtained expressions for the transformed electromagnetic field shows that instead of an initial wave with the frequency ω the transformed field gets a whole spectrum. First of all the wave with the transformed frequency $\omega_1 = \sqrt{\omega^2 + \omega_e^2}$, ω_e is the plasma frequency, appears. The frequency of this wave is as in unbounded medium and its spatial distribution remains unchanged as compared to the initial wave [4]. This wave exists only in the contractive sphere region until the moment of collapse this region at the sphere centre. In the other part of the sphere, the broadened spherical layer, there are the waves with the initial wave frequency but with changed spatial dependence. These waves are excited by the wave impinging onto the sphere after the ionization. There are also infinite spectra of the waves $\bullet\ e^{p_{nk}t}\mathbf{M}_{\pm 1n}(-ip_{nl}r/v_1,\Omega)$ and $\bullet\ e^{\bar{p}_{nk}t}\mathbf{N}_{\pm 1n}(-i\bar{p}_{nl}r/v_1,\Omega)$ with complex eigen-frequencies $p_{nk} = i\omega_{nk} - \alpha_{nk}$. These spectra are different for various spherical vectors and depend on the number n of the partial spherical vector.
The exterior field contains the wave with the initial wave frequency and the waves of the spectra provided by the eigen-frequencies $p_{nk} = i\omega_{nk} - \alpha_{nk}$. The cross-section for the partial wave has a decaying temporal dependence and deexcitation of the different partial waves is going on with different rates. The waves with the frequencies ω_1 are absent in the exterior field.

References

[1] Nerukh, A. G. and Khizhnyak, N. A. *Modern problems of transient macroscopic electrodynamics (in Russian)*, Test-Radio, Kharkov, Ukraine, 1991.
[2] Morse P.M. and Feshbach H., *Methods of theoretical physics*, McGraw-Hill, 1953.
[3] Kokkorakis G. C. and J. G. Fikioris, *IEEE Trans. on Antenn. and Propag.*, 55, 3178-3190 (2007).
[4] Morgenthaler F. R. *IRE Trans. Microwave Theor. Tech.* 6, 167-172 (1958).

Numerical Simulation of Arbitrarily Shaped Dielectric Bodies

A. Al-Jarro, P. Sewell, T. Benson, A. Vukovic, J. Paul
George Green Institute for Electromagnetics Research, The University of Nottingham, University Park, Nottingham NG7 2RD, UK
ahmed.aljarro@nottingham.ac.uk

An accurate and flexible three-dimensional Volterra Time Domain Integral Equation (TDIE) algorithm capable of running on both structured rectangular grids and unstructured tetrahedral meshes is implemented here to model the time-dependent electromagnetic field of arbitrarily shaped volumetric dielectric bodies.

Introduction

The ability to accurately and cost-effectively simulate electromagnetic wave interactions with penetrable bodies containing a diverse range of feature sizes or boundaries that are curved or non-tangential to the coordinate axes of complex and/or time varying material response is of significant practical interest for many applications in photonics. Typically, these interactions can be analyzed using methods that are based on the differential or integral form of the Maxwell equations. Common volumetric differential equations techniques such as the finite difference time domain, FDTD [1] and transmission line modeling, TLM [2] require discretisation of the full problem space and to explicitly construct absorbing or perfectly matched boundary conditions. In contrary, time domain integral equation, TDIE, techniques only require the direct discretisation of regions whose material properties differ from a background material and inherently satisfy radiation conditions. While continuous effort has been employed to further advance numerical techniques involving volume integral equations in the frequency domain for various applications, however, to our knowledge, limited progress has been reported in the time domain. In this work we progress on such a scheme with the development of a novel 3D Volterra TDIE [3, 4] that is capable of running on an arbitrary volumetric mesh. Stability, accuracy and convergence of the algorithm are discussed and validated by means of canonical working examples. For the case shown in Fig 1 validation is performed analytically; whereas for the more general case using in house built TLM solvers.

Results

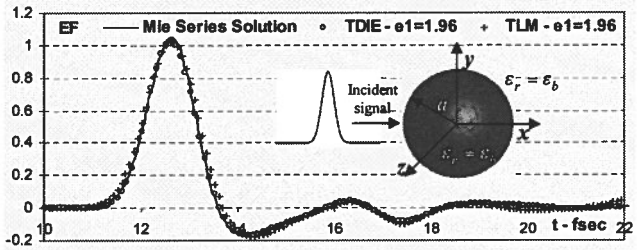

Fig 1: Electric field distribution (Vm^{-1}) at the centre of a microsphere of radius a=0.5μm and relative permittivity ε_r=1.96 placed in an otherwise homogeneous background of relative permittivity ε_b =1.0.

References

[1] A. Taflove, et al., Artech House, (2000)
[2] C. Christopoulos, IEEE Press, (1995)
[3] A. Al-Jarro, et al., *25th Inter. Review of Progress in ACE*, 8 – 12 March 2008, Monterey, Cal
[4] A. Al-Jarro, et al., *Inter. Sym. on Ant. and Prop.*, 20-23 October 2009, Bangkok, Thai

Accuracy Issues in the Numerical Modelling of Micro & Nano Cavities

Harshana G. Dantanarayana, Phil Sewell, Ana Vukovic and Trevor M. Benson
George Green Institute for Electromagnetics Research, The University of Nottingham, University Park, Nottingham, NG7 2RD, UK
eexhgd@nottingham.ac.uk

Some accuracy issues associated with modelling circular micro and nano resonators with time domain rectangular mesh numerical methods is presented regarding the resonant frequency, field profile and Q factor.

Introduction

Micro- and nano-scale resonators have become important components for integrated photonic & biophotonic applications such as filters, sensors, novel light sources [1]. Numerical techniques are widely used for the study of these structures, with time domain methods proving particularly valuble in the study of nonlinear problems. However, some deviations of resonant frequencies derived from Finite Difference Time Domain (FDTD) method, from the analytical results for circular resonators has been previously presented [2]. In this paper, we investigate the accuracy of the time domain rectangular mesh Transmission Line Method (TLM) when modelling circular resonators in two dimensions in search of the roots for such discrepancy. Parameters of practical interest include resonant frequecy, field profile and Q-factor of the resonances.

Results

Time domain TLM method was applied to the study of the resonant modes of TE & TM polarisations of a circular cylinder of very small dimensions comparable to the wavelength of interest. We discuss techniques for the extraction of resonant frequencies and Q factors from the time domain data. Comparison with analytical solution for the circular resonator shows a generally good agreement and convergence as the mesh size is reduced as shown in figure, but depending on the exact problem discretisation chosen. Determining the high Q factors associated with the low radial order modes proves problematic with the extraction methods used.

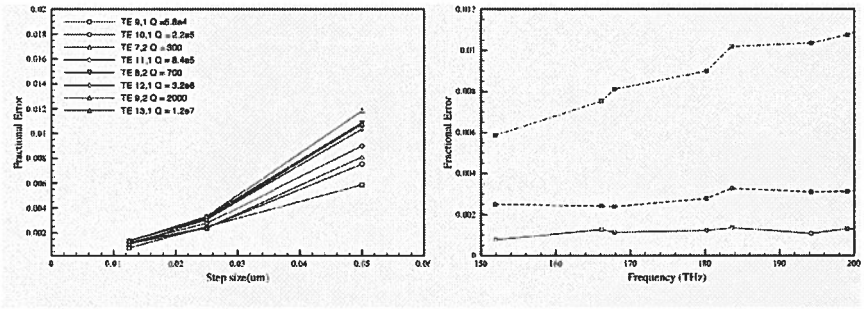

(a) (b)

Figure 1: Fractional Error of extracting resonant frequencies with the discretisation step size for TE resonant modes

References

[1] V.Ilchenko et al., *IEEE J. Sel. Top. Quant.*, **12(1)**, 15-32, (2006).
[2] A.Boriskin et al., *J. Opt. Soc. Am. A*, **25**, 1169-1173, (2008).

Step approximation of oblique boundaries to compute band structures of photonic crystals

S. F. Helfert
FernUniversität in Hagen, Chair of Optical Information Technology, Universitätsstr. 27 58084 Hagen, Germany
stefan.helfert@fernuni-hagen.de

In this presentation we describe the step approximation of an oblique boundary. This requires the transformation of points that are outside the computational window into the computational domain.

Introduction

As well known, the boundaries of elementary cells of hexagonal photonic crystals are parallelograms. For the analysis oblique coordinates were introduced into the method of lines (MoL) and in finite difference (FD) methods [1]–[3]. However, the size of the appearing matrices is twice as large as the number of discretization points, which can cause a high numerical effort.

Numerical algorithm and results

In this presentation, a staircase approximation of the oblique boundaries is introduced (see Fig. 1a). Since a step approximation of waveguide structures is commonly used one might wonder about the novelty of this approach. It is important to point out that the computational window itself has to be modelled with staircases here - not only an inner region. Hence, points outside the computational window must be taken into account, (e.g., point $k+1$ (Fig. 1a) for an FD–discretization of derivatives with respect to z). For band structure computations the periodicity in horizontal direction can be utilized permitting to "fold" the fields from the right boundary to the left one. Now, the PhC is periodic in oblique directions. Therefore, the points "1" and "3" (see Fig. 1a) must be related and not "1" and "2" as in Cartesian coordinates. In the algorithm a "virtual layer" is introduced for this purpose, to cause a "shift" of the fields. The algorithm was used to determine the band structure of a well known structure from the literature [4] with the MoL with oblique coordinates and with a step approximation (Cartesian coordinates). The results in Fig. 1b show a very good agreement.

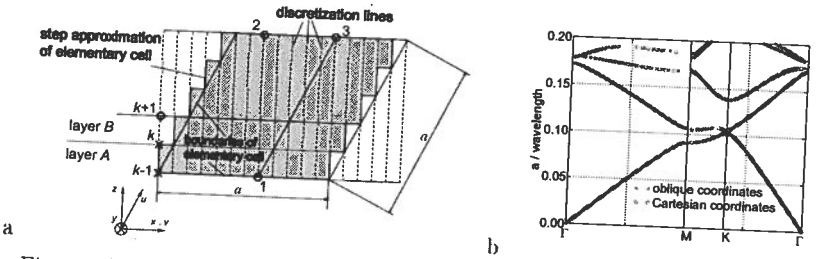

a b

Fig. 1. a) Elementary cell of a hexagonal photonic crystal; b) determined band structure

References

[1] S. F. Helfert, *Prog. Electrom. Res., PIER*, **61** (2006) 271–278.
[2] S. F. Helfert, in *ICTON Conf.*, Rome, Italy, (2007), **2**, 80–83.
[3] A. G. Edelmann and S. F. Helfert, to appear in *Opt. Quantum Electron.*, (2010).
[4] P. R. Villeneuve et al., *IEE Proc.-Optoelectron.*, **145** (1998), 384–390.

A Fourier-based WA-BPM with Complex Jacobi Iteration

Rafael Godoy-Rubio, Sebastián Romero-García, Alejandro Ortega-Moñux and J. Gonzalo Wangüemert-Pérez

Dpto. Ingeniería de Comunicaciones, Universidad de Málaga, Campus Teatinos s/n, 29071, Málaga, Spain

faligr@ic.uma.es

In this contribution we propose a new Fourier-based wide-angle beam propagation method (WA-BPM) incorporating complex Jacobi (CJ) iterative schemes. It is shown that the convergence of this Fourier domain two-step complex iterative technique is highly improved with respect to previous space domain implementations without needing to use preconditioners.

Introduction

Fourier-based beam propagation methods differ from finite differences implementations (FD-BPM) in the transverse discretization strategy. In Fourier-based BPMs the unknown transverse fields are expanded into Fourier series [1] instead of applying a central difference approach.

Recently, a new Complex-Jacobi iterative method has been introduced to efficiently solve the Helmholtz equation [2], and has been extended to FD-WA-BPM schemes in [3]. This technique has been proved to be highly competitive in terms of execution speed.

In this work, we present a reformulated complex Jacobi iterative method to solve the beam propagation equation in the domain of Fourier coefficients. We establish new requirements for the iteration parameters to ensure stability and to optimize convergence rate.

Results

The application of this Fourier domain reformulated complex Jacobi method to WA-BPM schemes results in higher convergence rates with respect to the previously reported finite difference versions. In Table 1, runtime and number of iterations required by the complex Jacobi method to converge per propagation step are listed for two 2D problems (with numerical parameters chosen to achieve the same accuracy). For the finite difference approach, the mean value (μ) and deviation (σ) of the number of iterations are given. For Fourier-based schemes this number remains constant and significantly lower.

TABLE 1. Comparison of average runtime and number of iterations required by CJ-based FD-WA-BPM and Fourier WA-BPM in free space and waveguide structure

	Runtime/Number of iterations of Complex Jacobi (per propagation step)	
	FD-WA-BPM	**Fourier-based WA-BPM**
Gaussian beam in free space	0.32 s / $\mu = 446$, $\sigma = 10$	0.07 s / 34
Polymer Waveguide Crossing	0.2 s/ $\mu = 244$, $\sigma = 11$	0.04 s / 9

References

[1] J. G. Wangüemert-Pérez, et al. *Opt. Quantum Electron.*, **36**, 285-301, (2004).

[2] G. R. Hadley, *J. Comp. Phys.*, **203**, 358-370, (2005).

[3] Khai Q. Le, et al. *Opt. Express.*, **16**, 17021-17030, (2008).

Absorbing Boundaries for Structure Related Beam Propagation Methods

Ken Chan[1], Phillip Sewell and Ana Vukovic
George Green Institute for Electromagnetic Research, University of Nottingham, NG7 2RD, UK
[1]eexkc1@nottingham.ac.uk

Structure-Related Beam Propagation Methods (SR-BPM) employ non-orthogonal sampling grids in order to minimize non-physical scattering caused by staircasing of material boundaries. A modified Perfectly Matched Layer (PML) has been developed for the SR-BPM for the first time and it is shown that it successfully eliminates non-physical reflections from open radiation boundaries.

Introduction

Modern photonic circuits typically contain a number of bends and curved or tilted waveguides. Modelling boundaries that are not aligned to orthogonal, usually Cartesian, coordinates will typically require the use of small mesh sizes in order to achieve good accuracy and to minimize non-physical staircasing noise. The advantage of the SR-BPM is that because the local coordinate system is defined to be conformal to the local device structure, staircasing noise is eliminated and faster and more memory efficient simulations are possible due to a relaxation in the field sampling density [1]. However, implementations of the Du-Fort Frankel (DFF) [2] algorithm in conjunction with the SR-BPM method exhibit unwanted reflections from conventional Cartesian coordinate PML boundaries. In this work a novel PML boundary condition is developed in order to properly match the boundary interface with the SR coordinates and this provides a stable and computationally efficient algorithm.

Results

The new PML boundary has been demonstrated for a range of tilted waveguide problems. Fig.1 shows the output power as a function of the tilt angle of a 3μm wide leaky waveguide when employing a conventional Cartesian coordinate PML and with the new SR PML boundary condition. The waveguide has core refractive index of 3.44, an air superstrate and substrate and an operating wavelength of 1.15μm. It can be seen that with the conventional PML the accumulation of spurious reflections from the boundary leads to a rapid non-physical gain in power, whilst the new phase shifted PML minimizes the unwanted reflections and thus stabilizes the algorithm over a wider range of tilt angles.

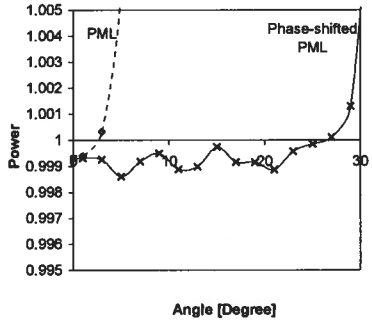

Fig.2 Output power of the titled waveguide after 512 μm of propagation for the case of conventional and phase shifted PMLs. Waveguide is sampled with $\Delta x=\Delta z=0.025\mu m$.

References

[1] D.Z. Djurdjevic, et al., J. Lightwave Technology, **22**, 10, Oct. 2004
[2] Phillip Sewell, et al., J. Lightwave Technol. **23**, 1, Jan. 2005

BPM simulation of polarization rotator based on near Z-axis propagation in curved and straight anisotropic channel waveguides in $LiNbO_3$

Andrey V. Tsarev
Institute of Semiconductor Physics SB RAS, Novosibirsk, 630090, Russia
tsarev@isp.nsc.ru

A new passive polarization rotator based on anisotropic Ti:$LiNbO_3$ diffused channel waveguide is proposed and examined by 3D BPM. The 1.2 cm structure provides TE-TM conversion with internal loss 0.4 dB and included both straight and curved sections for simpler use this polarization rotator in integrated optic devices.

Introduction

Polarization rotators are widely used for polarization diversity of optic elements. Recently, polarization rotator based on straight Ti:$LiNbO_3$ diffused channel waveguide aligned at near Z-axis on Y-cut $LiNbO_3$ had been theoretically studied [1]. This paper further develops this conception by implementation the curved sections which provides additional features of polarization rotator.

Results

The new passive polarization rotator had been designed and simulated by the fast BeamPROP commercial software [2] utilizing 3D BPM anisotropic paraxial approximation. General structure features are also verified by competitor OptiBPM software [3] that uses wide angle 3D anisotropic BPM with the high page order (4,4). Variable radius (R > 2.5 cm) curved structures are chosen in order to provide small transmitting loss (< 0.4 dB) for Ti:$LiNbO_3$ diffused channel waveguides with small 0.015 increment of refractive index. The optimal structure length is 1.2 cm which provides efficient TE-TM conversion (see Fig. 1) by straight section about 0.5 cm aligned at angle 6.36° related to Z-axis on Y-cut $LiNbO_3$. Input and output straight sections of arbitrary length are oriented along Z-axis and are intended for simpler fitting this device with other optic elements on the same substrate.

The author thanks companies RSoft Design Group , Inc. [2] and Optiwave [3] for providing BPM software.

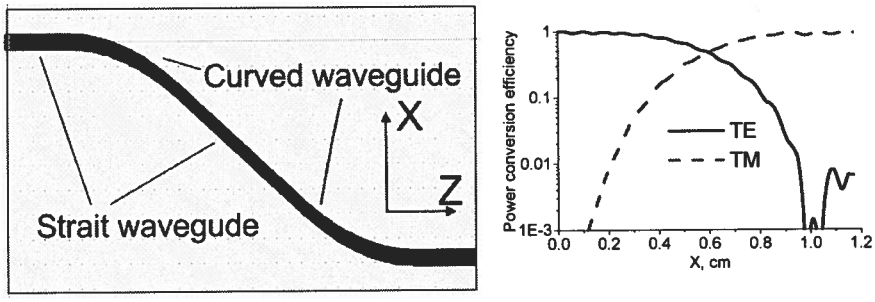

a) b)

Fig. 1. 3D BPM simulation [2] of near Z-axis polarization rotator. a) General design (not in scale); b) TE-TM polarization conversion efficiency (TM transmittance - 0.0065, TE transmittance - 0.918).

References

[1] A. V. Tsarev, *Optics Express*, **16**, 1653-1658 (2008).
[2] BeamPROP 8.0 by RSoft Design Group, Inc., *www.rsofdesign.com*.
[3] OptiBPM 10 by Optiwave, *www.optiwave.com*.

Simple and Fast Algorithm for Calculation of Optical Fiber Chromatic Dispersion Approximate Estimates

Vladimir A. Burdin[1], Anton V. Bourdine[1]
[1]*Department of Communication Lines, Povolzhskiy State University of Telecommunications and Informatics (PSUTI), 67, Moscow Av., Samara, Russia;*
burdin@psati.ru

Simple and fast algorithm for calculation of coaxial optical fiber chromatic dispersion approximate estimates is presented. This approach is based on the combination of well known rigorous stratification method and perturbation method. Proposed approach numerical results, FEM numerical results and experimental data are compared.

Introduction

By using stratification method it is usual to construct the dispersion function as the determinant matrix system. While this is theoretically correct, it is not the most prescription. Worse, the determinant is not the most convenient construction for locating the zeros, particularly in the case where two zeros are very close to each other. Presented computer algorithm is easy to implement, fast in execution time, and more reliable in the finding zeros of modes.

Results

We propose a simple and fast algorithm for calculation of optical fiber mode chromatic dispersion approximate estimates. Represented approach is adopted for optical fiber with an arbitrary coaxial index profile. Introduced method is based on the combination of rigorous stratification method [1-7] and perturbation method [8, 9]. There are three steps in proposed algorithm. The first by well known 4x4 matrix method coarse propagation constant estimates are calculated. On second step more precise approximation is calculated from dispersion equation at integral form. Third estimate correction is calculated by using perturbation method as described in [8]. To estimate an accuracy of proposed method, some sample of optical fiber was considered. Doped silica glass refraction indexes with respect to wavelength are calculated by method based on Sellmeier equation [10]. Also the same fiber sample chromatic dispersion was computed by FEM algorithm [11]. A good agreement between proposed approach numerical results, FEM numerical results and experimental data is demonstrated.

References

[1] P.J.B. Clarricoats, K.B. Chan, *Electronic Letters*, **6(22)**, 694 – 695 (1970).
[2] C. Yeh, G. Lindgren, *Applied Optics*, **16(2)**, 483 – 493 (1977).
[3] J.M. Arnold, *Electronic Letters*, **13(22)**, 660 – 661 (1977).
[4] P. Yeht, A. Yariv, E. Marom, *J. Opt. Soc. Am.*, **68(9)**, 1196 – 1201 (1978).
[5] K. Thyagarajan, et al., *Applied Optics*, **30(27)**, 3877 – 3879 (1991).
[6] T. Kawanishi, M. Izutsu, *Optics Express*, **7(1)**, 10 – 22 (2000).
[7] U. Langbein et al., *Opt Quant Electron.*, DOI 10.1007/s11082-009-9344-8.
[8] R.Sammut, A. W. Snyder, *Applied Optics*, **15(2)**, 477 – 482 (1976).
[9] A. W. Snyder, J. D. Love, *Optical Waveguide Theory*, London, Chapman and Hall (1983).
[10] V. Burdin, *Infocomminication Technologies*, **6(2)**, 37 – 41 (2008).
[11] V. Burdin et al., *Infocomminication Technologies*, **7(2)**, 13 – 20 (200p).

Analysis of Multiplexer-Demultiplexer Based On Nematic Liquid Crystal Photonic Crystal Fiber Coupler

M. F. O. Hameed and S. S. A. Obayya
Integrated Communications Research Centre, Faculty of Advanced Technology, University of Glamorgan, UK; Email: sobayya@glam.ac.uk

Abstract

A novel design of 1.3μm/1.55μm wavelength multiplexer-demultiplexer (MUX-DEMUX) is proposed and analyzed using the full vectorial finite difference method and the full vectorial finite difference beam propagation method. The reported MUX-DEMUX as shown in Fig.1 is based on soft glass photonic crystal fiber coupler infiltrated by a nematic liquid crystal of type E7 (NLC-PCF). The infiltrated holes are arranged in a soft glass of type SF57 (lead silica). The refractive index of the SF57 material is greater than the ordinary and extraordinary refractive indices of the E7 material. Therefore, the propagation through the suggested coupler has been taken place by the modified total internal reflection. In addition, the use of the soft glass background material and the nematic liquid crystal (NLC) offer unique and uncommon propagation and polarization properties which cannot be achieved in the conventional silica PCF coupler [1].

Results

The numerical results reveal that the proposed MUX-DEMUX of length 3.265mm can provide crosstalks of as low as -20dB with great bandwidths of 24nm and 40nm around the wavelengths of 1.55μm and 1.3μm, respectively. In addition, the suggested MUX-DEMUX has a tolerance of ±3% in its length which makes the design more robust to the perturbation introduced during the fabrication process. Figure 2 shows the normalized power transfer for the quasi TE modes at wavelengths of 1.3μm and 1.55μm in the left core of the NLC-PCF coupler. More results will be presented in the conference

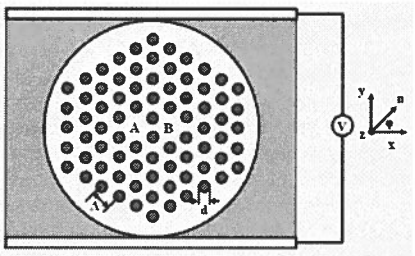

Fig 1. Cross section of the NLC-PCF coupler sandwiched between two electrodes and surrounded by silicone oil. The director of the NLC with a rotation angle φ is shown at the right.

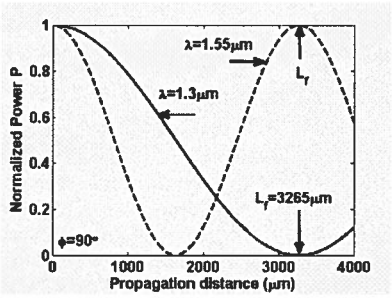

Fig. 2. Evolution of the normalized powers at core A for the quasi TE modes at different wavelengths, 1.3μm and 1.55μm along the propagation direction.

Reference

[1] K. Saitoh, et al, *Opt. Express*, **11**, 3188-3195 (2003)

Progress in Finite Element Analysis of Photonic Crystal Fibers

B.M.A. Rahman, A. Agrawal, N. Kejalakshmy, R. Uthman, Y. Azabi and K. T. V. Grattan

School of Engineering and Mathematical Sciences,
City University London
London EC1V 0Hb, UK
b.m.a.rahman@city.ac.uk

Abstract
The vector Finite Element Method (FEM) analysis of Photonic Crystal Fibers (PCF) is presented and simulation results for leakage/bending loss in optical and THz regime, high nonlinearity and flat dispersion for Supercontinuum Generation and plasmon-dielectric modes for sensing are shown.

Introduction

Photonic crystal fibers are important specialized optical waveguides due to their inherent advantages arising from modal properties, such as controllable spot-size, birefringence and dispersion properties, achieved through tailoring their structural parameters. The optical modes in a PCF with two dimensional confinement and high index contrast are hybrid in nature, with all six components of the E and H fields being present. Hence, only a vectorial formulation should be used to calculate accurately their modal solutions. The H field formulation with the augmented penalty function technique is given below:

$$\omega^2 = \frac{\left(\int (\nabla \times \vec{H})^* \cdot \hat{\varepsilon}^{-1} (\nabla \times \vec{H})\, d\Omega\right) + \left(\int (\eta/\varepsilon_0)(\nabla \cdot \vec{H})^* (\nabla \cdot \vec{H})\, d\Omega\right)}{\int \vec{H}^* \cdot \hat{\mu}\, \vec{H}\, d\Omega} \qquad (1)$$

where $\vec{H}$ is the full-vectorial magnetic field, $\hat{\varepsilon}$ and $\hat{\mu}$ are the permittivity and permeability respectively of the waveguide, ε_0 is the permittivity of the free-space, ω^2 is the eigenvalue, ω is the angular frequency of the wave. The dimensionless parameter η is used to impose the divergence-free condition of the magnetic field in a least squares sense to eliminate spurious solutions.

Results

We present results on FEM analysis of a few novel PCF designs. These include: single mode operation, optimization of birefringence, optimization of dispersion properties, leakage and bending losses of silica, soft glass, Teflon, and Topas PCF for both the optical and THz frequencies. It is also show that a PCF with a small defect hole (coated with a thin metal layer) in the core area to enable supermode formation by coupling of the surface plasmon modes with PCF modes is useful for sensing applications. Spiral PCF in which air-holes are arranged in different spiral patterns optimized for high birefringence (0.22 at 1550nm in Silica); large non-linearity (γ>5250 $W^{-1}.km^{-1}$ at 1064*nm* and γ>2150 $W^{-1}.km^{-1}$ at 1550*nm*) with a low and flat dispersion (D~0.8 *ps/km.nm* and Dispersion slope ~-0.7*ps/km.nm*^{2} at 1060*nm*) in SF57 soft glass for SCG are presented.

Acknowledgements
A large part of these numerical simulations were carried out under the support of an UK and India Education and Research Initiatives (UKIERI) Major Project.

Modelling backscattering in optical waveguides

A. Canciamilla[1], F. Morichetti[1,2], A. Artuso[1], and A. Melloni[1]
[1]*POLICOM – Dipartimento di Elettronica e Informazione, Politecnico di Milano, via G. Colombo 81, 20133 Milano, Italy*
[2]*Fondazione Politecnico di Milano, p.zza Leonardo da Vinci 32, 20133 Milano, Italy*
melloni@elet.polimi.it

The properties and the statistics of backscattering induced by sidewall roughness in optical waveguides are modelled and compared with experiments. The presented model is effectively employed to evaluate the impact of backscattering on the performance of optical circuits.

Summary

Backscattering due to rough sidewalls in optical waveguides can originate strong impairments in optical devices and systems [1]. In this work we investigate the properties and the statistics of waveguide backscattering and their dependence on the waveguide parameters. In our model, sidewall roughness is decomposed as a spatial superposition of random sinusoidal perturbations. Any spatial harmonic of amplitude δw produces (at the Bragg wavelength λ_B) a field backreflection $H_r(\lambda_B)= \kappa dz$, where dz is the waveguide length,

$$\kappa = \frac{\pi}{\lambda_B}\delta n_{eff} = \frac{\pi}{\lambda_B}\frac{\partial n_{eff}}{\partial w}\delta w \qquad (1)$$

is the grating coupling coefficient and δn_{eff} is the effective index perturbation. Given a roughness degree δw, backscattered power depends only on the squared derivative $(\partial n_{eff}/\partial w)^2$, indipendently of the waveguide shape and index contrast Δn. Figure 1 shows the agreement of the theoretical model (dashed lines) with experiments for two different types of waveguides, fabricated in silicon on insulator (SOI, squares) and silicon oxynitride (SiON, diamonds) technology, respectively. The core width w is normalized to the width w_0 of the single mode waveguide, that is w_0 = 480 nm in SOI (height 220 nm, Δn = 140%), and w_0 = 2.2 μm in SiON (height 2.2 μm, Δn = 4.5%).

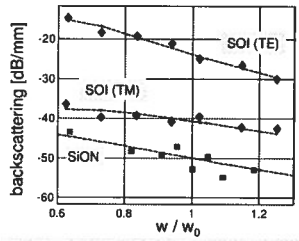

Fig. 1: Theoretical (dashed lines) and measured (marks) backscattering of 1-mm long waveguides in SOI and SiON technology.

We found that the statistics of backscattering is independent of the shape, size, and technology of the waveguide. Figure 2 shows that the (a) real and (b) imaginary part of backscattering (normalized to the standard deviation σ_r) of a 2.2 x 2.2 μm^2 SiON waveguide (diamonds, $\sigma_r^2 = 5\cdot10^{-6}$) and a 480 x 220 nm^2 SOI waveguide (squares, $\sigma_r^2 = 1.5\cdot10^{-3}$) follow both a gaussian probability density function (PDF).

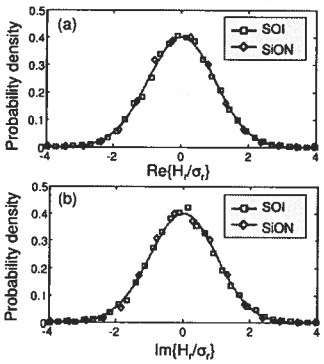

Fig. 2: PDF of the (a) real and (b) imaginary part of backscattering of a SOI (squares) and a SiON waveguide (diamonds).

These results can be used for modelling realistic waveguides and for evaluating the impact of backscattering in integrated devices and circuits.

References

[1] F. Morichetti, A. Canciamilla, C. Ferrari, M. Torregiani, A. Melloni, and M. Martinelli, "Roughness induced backscattering in optical silicon waveguides", Physical Review Letters, vol. 104, 033902, Jan. 2010.

Chebyshev Collocation Dirichlet-to-Neumann Map Method for Lamellar Diffraction Gratings in Conical Mounting

Dawei Song[1,2,3] and Ya Yan Lu[3]

[1]*Joint Advanced Research Center of USTC and CityU, Suzhou, Jiangsu, China*
[2]*Department of Mathematics, University of Science and Technology of China, Hefei, Anhui, China*
[3]*Department of Mathematics, City University of Hong Kong, Kowloon, Hong Kong*

For lamellar diffraction gratings in conical mounting, the widely used Fourier modal method involves the time-consuming step of solving eigenvalue problems. The eigenvalue problems can be avoided using Chebyshev collocation and Dirichlet-to-Neumann (DtN) map techniques.

Introduction

The Fourier modal method (FMM) [1,2] is widely used for diffraction gratings consisting of uniform layers, but it usually is quite expensive to calculate the eigenmodes in each layer. In a previous work [3], we developed the Chebyshev collocation Dirichlet-to-Neumann (DtN) map method to avoid the eigenvalue problems for gratings in classical mounting. In this paper, we extend the method to gratings in conical mounting.

The method

We consider a lamellar grating which is periodic in x and invariant in z. The grating layer, which is assumed to be uniform in y, is given by $0 < y < d$. If the grating is in conical mounting, then the electromagnetic field depends on z as $e^{i\gamma_0 z}$ for a given γ_0. To solve the problem, we set up a system of equations for E_x and H_x at $y = 0$ and $y = d$. These equations are derived from the continuities of E_x, H_x, E_z and H_z. Notice that E_x and H_x satisfy scalar Helmholtz equations, but E_z and H_z are related to the x and y derivatives of E_x and H_x. More precisely, E_z is a sum of $E_z^{(1)}$ and $E_z^{(2)}$ which are related to the x derivative of E_x and y derivative of H_x, respectively. For $E_z^{(2)}$, we need the DtN map of H_x which can be efficiently calculated [3]. For $E_z^{(1)}$, we need a suitable discretization in x. The case for H_z is similar. Therefore, we can express E_z and H_z in terms of E_x and H_x, and set up the system of equations.

Results

We consider a metallic lamellar grating, where the dielectric constant of the metal is $\varepsilon = (0.1 + 5.0i)^2$, L is the period in x, $d = L$, the width of the metal in the grating layer is $L/2$, the wavelength of the incident wave is $L/2$, and the angles of incidence are $\theta = 30°$ and $\phi = 45°$. Retaining $N = 500$ Fourier modes, FMM gives the reflected diffraction efficiencies $R_1 = 0.31108$, $R_0 = 0.44157$, $R_{-1} = 0.13265$, $R_{-2} = 0.075546$. For the same N, the Chebyshev collocation DtN map method requires much less computation time. Since finite difference approximations are also used in the method, the results appear to be less accurate.

References

[1] M. G. Moharam, E. B. Grann, and D. A. Prommet, J. Opt. Soc. Am. A **12**, 1068-1076 (1995).
[2] P. Lalanne and J.-P. Hugonin, J. Opt. Soc. Am. A **17**, 1033-1042 (2000).
[3] D. Song and Y. Y. Lu, J. Opt. Soc. Am. A **26**, 1980-1988 (2009).

Influence of scattering layers on waveguide modes and the external efficiency of OLED structures

Shcherbakov Alexey[1,2] and Alexandre Tishchenko[1,2]

[1] *Laboratory Hubert Curien, University Jean Monnet, Rue du ProfesseurBenoit Lauras 18, 42000 Saint-Etienne, France*

alex.shcherbakov@phystech.edu

alexandre.tishchenko@univ-st-etienne.fr

[2] *Moscow Institute of Physics and Technology, Institutsky 9, 141701 Dolgoprudny, Russia*

Introduction

Light emitting structures based on organic materials represent a promising technology for lightning applications [1]. An organic light emitting device (OLED) conventionally consists of several optically transparent lossy plane layers and possibly a metallic electrode [1]. An important part of the optimization of such structure requires the improvement of the external efficiency which highly depends on the electromagnetic energy redistribution inside OLEDs. The possible mechanisms of energy loss include heat loss, excitation of surface plasmons and waveguide modes. The attempts of exact analysis of OLEDs in terms of these mechanisms were undertaken in [2, 3]. Regarding waveguide modes an OLED represents a planar multilayer lossy waveguide. The means of analysis of the modal structure of such waveguides are well established [4, 5]. However this analysis implies the coherency of the sources exciting these waveguides which is obviously not the case when dealing with OLEDs. Additionally with the aim of increasing the output efficiency OLEDs are sometimes supplemented with a scattering layer containing low index nanoparticles [6]. It results in extra loss of coherency. These two effects are seem to be important and should be included in any rigorous electromagnetic analysis of OLEDs.

Results

In the present paper a model of light propagation in a plane layered structures in terms of plane waves is revisited. Instead of conventionally used T-matrices we apply S-matrix algorithm which allows to avoid the growth of numerical errors and hence for more accurate calculation of variables sensitive to these errors (e.g. mode propagation constants). Exact formulae for power losses are derived which include implicitly the power transferred by evanescent waves. The modes of OLED structures are calculated with an improved algorithm of pole search [7]. The influence of limited source coherency on modes is analyzed by introducing a nonzero linewidth of each photon emitting exciton. The presence of scattering layer is simulated as auxiliary effective sources calculated by $\mathbf{J} = -i\omega\Delta\varepsilon\mathbf{E}$. Such expression gives a reasonable first-order approximation in the case of small contrast layers.

References

[1] M. T. Bernius, M. Inbaserkaran, J. O'Brien, W. Wu, *Adv. Mat.*, **12**, 1737-1750 (2000)

[2] K. A. Neyts, *J. Opt. Soc. Am. A*, **15**, 962-971 (1998)

[3] K. Celebi, T. D. Heidel, M. A. Baldo, *Opt. Exp.*, **15**, 1762-1772 (2007)

[4] J. Chilwell, I. Hodgkinson, *J. Opt. Soc. Am. A*, **1**, 1742-1753 (1984)

[5] L.M. Walpita, *J. Opt. Soc. Am. A*, **2**, 595-602 (1985)

[6] J. J. Shiang, T. J. Faircloth, A. R. Duggal, J. Appl. Phys. 95, 2889-2895 (2004)

[7] A. V. Tishchenko, M. Hamdoun, O. Parriaux, Opt. and Quantum Electron. **35** 475-491 (2003)

Dimensionality reduction for 3D vectorial optical scattering problems

O.V. (Alyona) Ivanova[1], Remco Stoffer[2], and Manfred Hammer[1]
[1] *MESA+ Institute for Nanotechnology, Univ. of Twente, P.O. Box 217, 7500AE Enschede, The Netherlands*
[2] *PhoeniX Software, P.O. Box 545, 7521PA Enschede, The Netherlands*
o.v.ivanova@math.utwente.nl

The spatial dimensionality of vectorial 3D frequency domain optical scattering problems is reduced by means of a global expansion of the field in one direction in slab modes of some reference slice(s). A variational formalism yields the equations in the other two directions. These coupled partial differential equations are solved using a Finite Element Method with modified Transparent Influx Boundary Conditions with PMLs.

Summary

By means of a global expansion over TE and TM slab modes in one direction, the dimensionality of vectorial 3D scattering problems is reduced. A Finite Element Method solves the resulting system of 2D equations; the boundaries of the calculation window are made to be transparent to outgoing light by utilizing modified Transparent Influx Boundary Conditions with PMLs. At the top and bottom of the window, PMLs are used to absorb vertically scattered radiation. We demonstrate that in case of a photonic crystal waveguide the current method with one mode in the expansion predicts the location of the bandgap and other spectral features much more precisely than a standard Effective Index Method, at more or less the same computational cost. More modes in the expansion allow radiation loss to be taken into account, and bring the results closer to a 3D FDTD reference result. Figure 1 summarizes some example results.

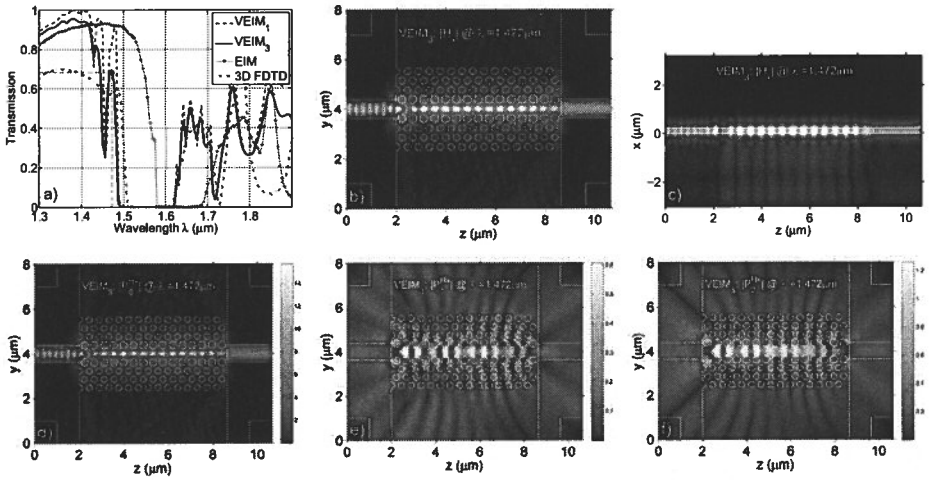

Figure 1: a) Transmission spectrum of a photonic crystal waveguide; results with 1 ($VEIM_1$) and 3 ($VEIM_3$) TE slab modes in the expansion, compared with 3D FDTD results. b)-f) are plots for $VEIM_3$ at λ=1.472μm. b) $|H_x|$ in a y-z cross-section through the middle of the waveguide (x=0.11μm). c) $|H_x|$ in an x-z cross-section along the waveguide axis at y=4μm. d)-f): coefficient-functions P_j^{Hx} of the fundamental, first and second order slab mode j=0,1,2 used in the expansion.

Loss Reduction at Resonances in a Grated Waveguide Cavity

H. Alatas[1,2,#], A. A. Iskandar[1], M. O. Tjia[1] and H. J. W. M. Hoekstra[3]

[1]Physics of Magnetism and Photonics Reserach Group, Faculty of Mathematics and Natural Sciences, Institut Teknologi Bandung, Jl. Ganesha 10, Bandung 40132, Indonesia. [2]Theoretical Physics Division, Department of Physics, Bogor Agricultural University, Jl. Meranti, Kampus IPB Darmaga, Bogor 16680, Indonesia. [3]Integrated Optical MicroSystems Group, MESA+ Research Institute for Nanotechnology, University of Twente, 7500 AE Enschede, The Netherlands

[#]alatas@ipb.ac.id

We present considerable loss reduction for TE electromagnetic waves at resonance in a Grated Waveguide (GWg) cavity by introducing a variety of structural modifications near the boundaries of the grated section

Summary

The modified GWg is described in Fig 1, with the core GWg structure having eight uniform teeth of $g = 100$ nm, $\Lambda = 200$ nm and 0.5 duty cycle, in a slab of $h = 160$ nm.

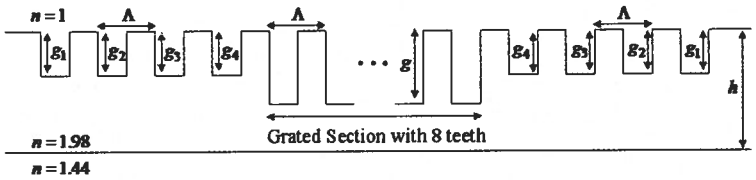

Fig. 1

The transmittance, reflectance and loss of the propagating wave were calculated by means of Green's function approach [1]. The results are presented in Figs. 2 for ten different GWg structures by the combined parameters (g_1, g_2, g_3, g_4) consisting of the following varieties: 1. $(0,0,0,0)$ nm, 2. $(20,20,20,20)$ nm, 3. $(40,40,40,40)$ nm, 4. $(60,60,60,60)$ nm, 5. $(80,80,80,80)$ nm, 6. $(60,60,80,80)$ nm, 7. $(60,60,60,80)$ nm, 8. $(40,40,60,80)$ nm 9. $(20,40,60,80)$ nm. and 10. $(100,100,100,100)$ nm. Note that the GWg structures 1 and 10 correspond to the uniform grated section with 8 and 16 teeth, respectively. Depicted in the Figs. 2 are the non-monotonous variations of transmittance, reflectance and loss, with respect to different GWg structures, at the right-edge resonance of the photonic stop-band, along with the associated resonance wavelengths. It is observed that the structural modification introduced on the grated section generally lead to the reduction of loss, in conjuction with transmittance enhancement while leaving the reflectance relatively unaffected. The optimal result featuring a loss reduction from 9.98% to 2.95% (or 70.44% reduction) is achieved by the modified grated section of $(60,60,80,80)$ nm structure with the transmitted waves at the observation point increased from 89.68% to 97.04%.

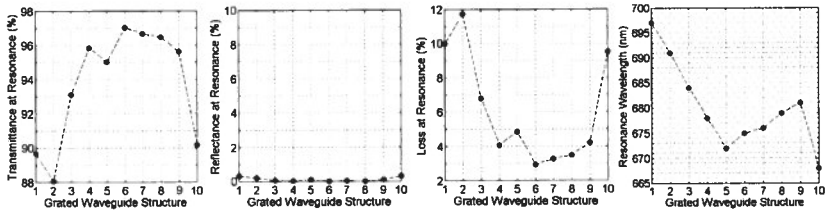

Fig. 2

References

[1] M. Paulus and O. J. F. Martin, *Phys. Rev. E* **63** 066615 (2001)

True-modal approach for 2D grating calculation

I.F.Gushchin[1], A.V.Tishchenko[1]

[1] *Laboratory Hubert Curien, University Jean Monnet, Rue du ProfesseurBenoit Lauras 18, 42000 Saint-Etienne, France*

alexandre.tishchenko@univ-st-etienne.fr

Introduction

The micro-optical and metallic nanostructures encountered a huge interest today. So far the metals were used frequently as mirrors, they make their return in the form of micro-and nanostructures by their eventual confinement properties of light and genesis of refractive indices that nature has placed at our disposal. The physical phenomena at the basis of these new effects are collective oscillations in form of plasmons. Since they are placed in the form of complex structures, metals and their properties must be modeled before as it is difficult to fabricate such small structures. The current problem is that no method is able to model safely the optical behavior of such microstructures with two or three dimensions.

The "true" modal method can model a 1D metallic periodic structure in the case of TM polarization with accuracy even when other methods do not converge or give incorrect results [1]. The modal method could be therefore a reference method also for the case of two or three dimensional structure.

Results

We present an implementation of 2D true-modal method to the diffraction problem. Our approach includes the same steps as the 1D true-modal method does: the modal basis definition; writing dispersion equation including the periodicity condition and the incidence condition; calculating propagation constants of 2D modes; the overlap integrals; the transmission matrices and the final scattering matrix calculation.

Benefits of such approach arise from the fact that the final precision is quite good even for a small number of modes under consideration. It allows to speed up scanning over a wide range of parameters with predictable accuracy.

Reference:

1. M. Foresti, L. Menez, and A. V. Tishchenko, "Modal method in deep metal–dielectric gratings: the decisive role of hidden modes," J. Opt. Soc. Am. A **23**(10), p. 2501-2509 (2006)

Long Period Gratings in Tapered Fibers and Equivalent Chirped Gratings

Enakshi K. Sharma and Krishna Ch. Patra
Department of Electronic Science, University of Delhi South Campus, New Delhi 110021, India
enakshi54@yahoo.co.in

We present a general numerical procedure to simulate LPGs in tapered fibers and chirped, apodized LPGs and establish their equivalence. The equivalent chirp and apodization are shown to vary with wavelength, choice of coupled cladding mode and taper angle.

Summary

Although LPGs in tapered fibers have been fabricated for sensor applications [1] the procedure to analyse and obtain the transmission characteristics of such gratings is not reported in literature. In an LPG written in a fiber that is dragged tapered, since, the core and the cladding radii change along the propagation length, the effective indices of the core guided mode and cladding guided modes also change along the propagation length. As a result for a given grating period the phase matching condition can be satisfied to a given mode at different wavelengths or at one wavelength to different modes as it propagates through the grating in the tapered fiber. Hence, the study of transmission characteristics now necessarily requires that all these cladding modes be included simultaneously in the coupled mode analysis. The 'matrix method', often used for two mode coupling, cannot be used for gratings in tapered fibers [2]. Since the mode fields change along the taper, the coupling coefficients also change slightly along the taper length. The coupled equations for amplitudes of modes have to be solved numerically and we show that in the numerical solution process a correction for the change in effective indices of the coupled modes along the grating length needs to be applied.

In the LPG in a tapered fiber the coupling coefficient and phase matched wavelength for mode coupling to each cladding mode changes along the length. This behavior is similar to that of a slightly apodized chirped grating. We establish this equivalence and show that the equivalent chirp function and apodization are different for each wavelength, each coupled cladding mode and also depend on taper angle. We have also developed the procedure for numerical solution of the multiple coupled mode equations with these equivalent chirp functions.

Effect of tapering on the transmission spectra for a grating with index modulation $\Delta n^2 = 10^{-4}$, $\Lambda = 565\mu$m in a typical taper[1] with $n_{co} = 1.458$, $n_{cl} = 1.454$ and tapering defined by $a_{co}(z) = a_{co}(o) - z/z_1$, $a_{cl}(z) = S\, a_{co}(z)$, S=13.3, $a_{co}(0) = 4.6\mu$m $a_{cl}(0) = 62.5\mu$m is shown in Fig.(1). The wavelength dependent chirp function of the equivalent chirped grating for a taper defined by z_1=10cm/μm and coupling to the LP_{05} mode is shown in Fig.(2).

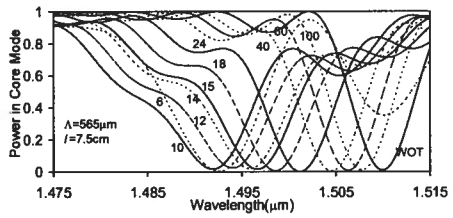

Fig. 1: Effect of tapering; z_1 marked, WOT: untapered

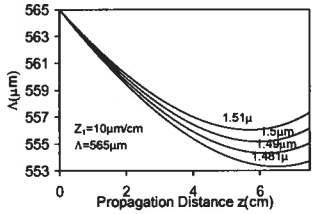

Fig. 2: Equivalent chirp function

References

[1] T. Allsop et al., *J. Lightwave Technol.* **24**, 870 (2006); T. Allsop et al., *Electronics Letts.* **41**, 471 (2005)
[2] T. Erdogan, *J. Lightwave Technol.* **15**, 1277 (1997).

2-D Metallic Photonic Crystal Waveguide Bends for Terahertz Range

Elif Degirmenci*, Frederic Surre and Pascal Landais
Research Institute for Networks and Communications Engineering (RINCE)
Dublin City University, Glasnevin, Dublin 9 Ireland
*elif@eeng.dcu.ie

Abstract

Metallic photonic band-gap crystals are used to design waveguide and waveguide bends in order to operate at terahertz frequencies. Transmission characteristics are obtained and compared for different 60° and 90° bends using Finite Element Method.

Introduction

Terahertz (THz) waves refer to electromagnetic (EM) radiation in a frequency band between 0.3 THz and 10THz, corresponding to wavelengths in the sub-millimeter range. THz science and technology have been developing very rapidly for their potential applications in variety of areas, such as imaging, security, spectroscopy and communication. With the rise of THz frequency based technologies and new developments in generating THz radiation, guiding THz waves in an efficient way with low-loss, high performance become of a key relevance.

For interconnection to other devices, waveguides are required to have flexibility of bending. However, bends introduce losses arising from total internal reflection. Conventional waveguides support guided modes with high efficiencies but transmission is limited in the case of bends as conventional waveguides need large radius of curvature to keep the bending losses at a reasonable level. To overcome this problem, photonic crystals have been studied with the advantages of low losses and low dispersion properties and almost perfect transmission has been obtained around sharp bends [1][2]. Nevertheless, metallic band-gap crystals are preferred for advantages over the dielectric photonic crystals, such as wider band-gaps and smaller sizes [3]. They have also shown good transmission characteristics at THz frequencies [4].

Conclusion

We simulated 2-D metallic photonic crystal waveguides and bend structures based on square lattice array using copper rods at THz frequency range. Transmission characteristics have been obtained for various waveguide designs. With the proposed bend designs level of reflection have been decreased and over 98.5% transmission performance have been obtained for a wide frequency range in the THz spectrum.

References

1. S. Lin, et.al., *Science*, **282**, 274-276 (1998)
2. A. Mekis, et.al., *Phys. Rev. Lett*, **77**, 3787-3790 (1996)
3. V. Kuzmiak, et.al., *Physical Review B*, **50**, 16835-16844 (1994)
4. Y. Zhao, et.al., *IEEE Trans.Micro. Theory and Techniques*, **55**, 656-663 (2007)

Terahertz Ring Resonator Based Photonic Crystals

R. Selim, D. Pinto, and S. S. A. Obayya
Integrated Communications Research Centre, Faculty of Advanced Technology
University of Glamorgan, Pontypridd CF37 1DL, UK
sobayya@glam.ac.uk

Introduction

A terahertz (THz) Photonic Crystal (PhC) Ring Resonator (PCRR) design is presented. The numerical technique used for the design is the Complex Envelope Alternating Direction Implicit Finite Difference Time Domain (CE-ADI-FDTD).

Results

The Terahertz wavelength range of $30\mu m$ to $3mm$ has gained much attention among researchers over the last decade. This is due to the lack of existing devices in that range, and the wide scope of potential applications of the THz wave such as high speed communications, medical diagnosis, and military detection. The lack is because of the poor response properties of the many natural materials in the THz range. PhCs with the appropriately determined photonic bandgap (PBG) can provide strong confinement and flexible control for THz waves [1]. The numerical technique used is the CE-ADI-FDTD. This method overcomes the limitation in the time step size introduced by the Courant limit in the conventional FDTD method without sacrificing the accuracy of the results. In this work, a particular design of an optical photonic crystal ring resonating is investigated. The PhC structure is a 13 × 13 square lattice, with a 5 × 5 semi-square ring as shown in Fig.1. The arrangement of uses polyaniline holes of radius $r = 0.185a$ where a is the lattice constant, $a = 68.75\mu m$, with the highlighted holes set at $r = 0.18a$. The holes have a refractive index $n_h = 4.848$ placed in dielectric background of Silicon Oxide (SiO2) $n = 1.5$. The PBG ranges from the normalised frequency units (a/λ) 0.20 to 0.3, where λ is the wavelength in vacuum. A pulse set covering the entire PBG shows the resonant modes inside the ring resonator as in Fig.2. Fig.3 illustrates the lightwave propagation in the structure. More results will be presented in the conference about the huge potential of this structure in the development of further designs for switching devices in the THz range.

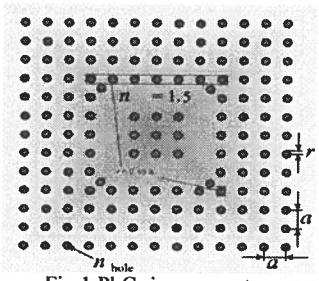

Fig.1 PhC ring resonator

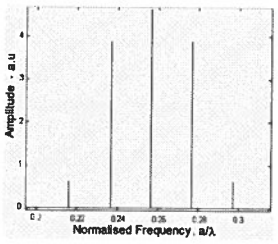

Fig.2 Ring resonator modes

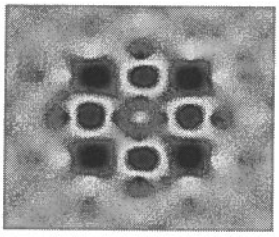
Fig.3 Lightwave propagation

References

[1] A.R. Maleki Javan, et al., *Opt Quant Electron*, **40**, 695-705 (2008)

Design of high sensitive photonic crystal based sensors

J. Derbali[1], F. AbdelMalek[1], S.S.A Obayya[2], H. Bouchriha[3]
[1] *National Institute of Applied Sciences and Technology, BP 676.Cedex 1080, Tunis. Tunisia*
[2] *Faculty of Advanced Technology, University of Glamorgan. Pontypridd CF37 1DL, Wales. UK*
[3] *Unité de Physique Quantique et de Photonique. Faculté des Sciences de Tunis. Campus universitaire 2092 Manar II Tunisia*
Email: sobayya@glam.ac.uk

Introduction

Photonic crystals (PCs) are periodic structures that have been formed due to the Bragg scattering. Introducing defects in PCs that consists of breaking the periodicity of the dielectric function is the key behind increasing demand on PCs. Electromagnetic fields in PCs with defects are well localized therefore can be used for several applications [1, 2]. Due to their ability to confine and control light propagation, PCs could play a major role in designing an optical platform. PCs are able to localize the electric field in the cladding region rather than the core where its refractive index is much larger. Therefore PCs with defects are sensitive to a small refractive index change produced by the presence of biomolecules in air hole based defects [1]. In this work, a novel biosensor based on photonic crystal (PC) containing several defects is proposed. The multidefect is arranged in a hexagonal shape along the line defect of the PC. The sensing region of the proposed sensor consisting of the multidefect area is exposed to different analytes. It is shown that the size of the defect, and defect to defect spacing and surface area of the multidefect region influence the performance of the sensor. The interaction between the resonant mode and attached molecules in the multidefect region is studied in terms of field overlap with molecules. Finite difference time domain is applied to calculate the transmission spectrum, field plots and sensitivity of the proposed sensor.

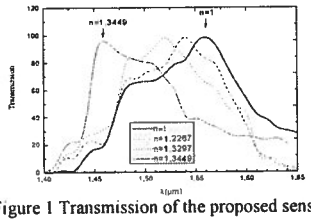

Figure 1 Transmission of the proposed sensor for different analytes

The transmission spectrum in Figure 1, shows that the peak shifts when the air hole multidefcts ar filled with analytes rather than air. It indicates that the biosensor is more sensitive to the analyte of refractive index n =1.3449 compared to the other analytes. This is due to a strong binding of molecules and an enhancement of the electric field when this analyte is present.

References

[1] M. Lee and P. M. Fauchet, *Opt. Express*, **15**, 4530, (2007)
[2] O. Painter, et al., *Science*, **284**, 1819 (1999)

Bandgaps in One-Dimensional Dissipative Photonic Crystals

Gregory V Morozov and Frank Placido
Thin Film Centre, School of Engineering, University of the West of Scotland, Paisley PA1 2BE, Scotland, United Kingdom
gregory.morozov@uws.ac.uk

Bandgaps of one-dimensional (1D) photonic crystals are analyzed, taking dissipation into account. Accurate analytical expressions for band edges are derived. The derivation is based on a perturbative expansion of the dispersion equation, which remains valid at the band edges of available 1D photonic crystals.

Introduction

In the recent paper [1], we have derived simple and accurate analytical expressions for all bandgaps (not only for the first one) of transparent bi-layer photonic crystals. The purpose of this paper is to extend the results to bi-layer photonic crystals with dissipation, i.e. to photonic crystals with complex refractive indices / dielectric permittivities.

Results

The analysis of bandgaps in a transparent (non dissipative) 1D photonic crystal is usually performed with the aid of the dispersion equation for the Bloch wave number K. This equation takes different forms for s - waves (electric field perpendicular to the plane of incidence) and p - waves (magnetic field perpendicular to the plane of incidence) correspondingly. For a bi-layer photonic crystal those two forms are

$$\cos Kd = \cos k_{1z}d_1 \cos k_{2z}d_2 - \frac{1}{2}\left(\frac{k_{2z}}{k_{1z}} + \frac{k_{1z}}{k_{2z}}\right)\sin k_{1z}d_1 \sin k_{2z}d_2 ,$$

$$\cos Kd = \cos k_{1z}d_1 \cos k_{2z}d_2 - \frac{1}{2}\left(\frac{n_1^2 k_{2z}}{n_2^2 k_{1z}} + \frac{n_2^2 k_{1z}}{n_1^2 k_{2z}}\right)\sin k_{1z}d_1 \sin k_{2z}d_2 ,$$

with $k_{1z,2z} = k\sqrt{n_{1,2}^2 - n_{\text{in}}^2 \sin^2\theta_{\text{in}}}$. Here $k = \omega/c$ is the wave number in vacuum of the impinging wave, $n_{1,2}$ and $d_{1,2}$ are the refractive indices and thicknesses of the basic layers, n_{in} is the refractive index of the incident medium ($n_{\text{in}} = 1$ in case of vacuum), θ_{in} is the angle of incidence. One can see that in case of normal incidence of the impinging wave the two equations become identical.
According to Floquet-Bloch theory, the Bloch wave number K is complex in forbidden bands (bandgaps) and real in allowed bands. Therefore, the bandgap edges can be found by setting

$$\left|\cos K(k)\, d\right| = 1 .$$

In this paper we modify the dispersion equation for a bi-layer crystal to include layers with complex dielectric permittivities (for example, metal layers [2]), and then obtain accurate analytical expressions for the bandgaps. To achieve the second goal we expand the modified dispersion equation in powers of a newly constructed parameter, selected because it remains relatively small around the band edges of most available photonic crystals.

References

[1] G. V. Morozov and F. Placido, *Jornal of Optics*, **12**, to be published, (2010)

[2] M. Bergmair and K. Hingerl, *ICTON 2007: Proceedings of the 9th International Conference on Transparent Optical Networks*, Vol. 2, pp. 58-61, (2007)

Linear and Tringle Order Placement of Optical Directional Couplers

Saktioto[1,2], Dedi Irawan[1], Nor Faridah Hanim[1], Jalil Ali [1]

[1]Advanced Photonics Science Institute, Faculty of Science, Universiti Teknologi Malaysia

Johor, Malaysia. nfhanim@gmail.com

[2]Physics Dept, Math and Sciences Faculty, University of Riau, Pekanbaru, Indonesia

Abstract

Optical waveguide couplers are well known devices used to direct light from one light source to a one or more waveguides. An important aspect of optical fibre technology is the coupling of an optical fibre to an optoelectronic device for transmitting information conducted by the optical fibre. In optical networks, optical couplers playing important key component for the application of optical coupler, optical switches and optical power splitters. Generally for switching purpose, one or two optical switch junction of optical fibre coupler is commonly used. The major obstacle in fabricating more than two coupling parameter is to obtain desired coupling ratio. To overcome this matter, the transfer matrix model is proposed so that we can calculate power splitting in fibre coupling. The results show a good agreement with 1X2 and 1X3 single mode fibre coupler. Power was transferred completely in to other waveguides at odd multiples of $z = \pi / (2\kappa)$. The optical parametric is held to be constant such as spaced waveguides, propagation constants, and coupling constant. This simulation can be modified for more than one input power sources.

Comparison of Resonant Coupling and Adiabatic Mode Transfer for Integrated Mode Adapters

A. Wieczorek[1], B. Roycroft[1], F. H. Peters[1,2] and B. Corbett[1]
[1] *Tyndall National Institute, University College Cork, Lee Maltings, Cork, Ireland*
andreas.wieczorek@tyndall.ie
[2] *Department of Physics, University College Cork, Cork, Ireland*

The resonant coupling principle [1] for the transition of the optical field between two waveguides of a passive asymmetric twin waveguide (ATW) [2] is compared with an adiabatic transition. The commercial available Film Mode Matching (FMM) tools Fimmwave/Fimmprop are used.

Introduction

In the ideal case in photonic integrated circuits (PIC), different waveguides are required for the maximum efficiency of the circuit. ATW´s offer the opportunity to include two vertically separated waveguides designed for different needs. Resonant and adiabatic coupling between these waveguides were investigated.

Results

The resonant coupler has a total length of 211 µm and consists of three different sections, two for power transfer between the modes and one for mode interference. The adiabatic mode adapter has three taper sections with different taper angles. The total length is 450 µm. In Fig 1a, b the power in the fundamental TE and TM modes on the output side is displayed. Fig. 1a clearly shows that resonant coupling offers only a width variation of ± 50 nm without causing significantly higher losses especially in the TE mode. In Fig 1b the insensitivity of adiabatic transfer to a higher refractive index can be seen. However the single mode waveguide comes close to cut-off at lower refractive index in both cases and therefore the losses increase. This work was sponsored by Science Foundation Ireland (SFI) under grant 07/SRC/I1173.

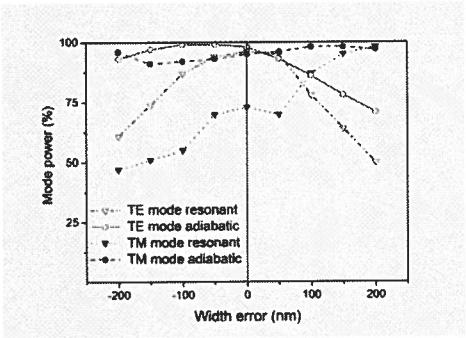

Fig. 1a: Error of the ridge width of the upper waveguide

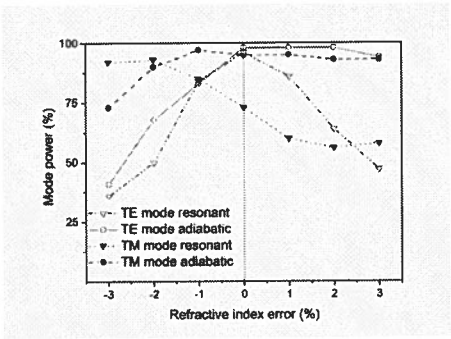

Fig. 1b: Error of the refractive index of the lower waveguide quaternary

References

[1] Suematsu, et. al., *IEEE J. Quantum Electron.*, vol. QE-11, no. 7, pp. 457-460, Jul. 1975.
[2] P. V. Studenkov, et. al., *IEEE Photon. Technol. Lett.*, vol. 10, pp. 1088–1090, Aug. 1998

Compound Waveguide on the Photorefractive Crystal

Boris Usievich, Jamil Nurligareev and Vladimir Sychugov
General Physics Institute, Vavilov streey 38,, 119991, Moscow, Russia
borisu@kapella.gpi.ru

New compound waveguide structure is proposed consisting of dielectric layer on top of the nonlinear photorefractive crystal.

Introduction

Photorefractive affect was found by Ashkin et al. in 1966 [1]. This is a complex phenomenon that allows to obtain numerous nonlinear effects at relatively low power levels (<1W/cm^2). It is known that nonlinear surface wave can propagate along the surface of photorefractive crystal [2]. Due to the fact that surface wave penetration in the crystal is determined by the nonlinear properties of the crystal only, this kind of surface wave has a continuous spectrum contrary to the ordinary waveguide modes. In this paper we study the propagation of light in the compound structure consisting of linear dielectric layer placed on top of the photorefractive crystal.

Results

The consider structure consists of linear dielectric slab (n=1.46, h=0.6 μm) placed on top of the photorefractive crystal (n=2.36, r_{eff}=1340 pm/V) and is similar to the Bragg waveguide as the effective refractive index of the mode is lower than that of the dielectric layer. We study the propagation of TE-polarised light with 0.441 μm wavelength along the structure. Equation for the amplitude of the guided wave in the crystal can be written as follows for diffusion type nonlinearity:

$$\frac{d^2A(x)}{dx^2}+\gamma\frac{dA(x)}{dx}+k_0^2(n^2-n_{eff}^{\ 2})A(x)=0,$$

Where $\gamma = 2k_0^{\ 2}n^4r_{eff}k_BT/q$ and n_{eff} is the effective refractive index of the mode. Combining this equation with the air-dielectric boundary condition and wave equation for the linear layer we can calculate the distribution of the mode field for different values of n_{eff}. Formally the mode can exist at any given n_{eff} but the part of the mode power propagating in the dielectric layer strongly depends on it (Fig. 1). Figure 2 shows the field distribution of the fundamental mode having the highest concentration of power in the linear dielectric layer. We suppose that our structure can be useful in studying nonlinear effects near the surface of photorefractive crystals.

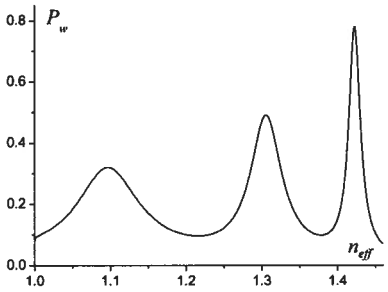

Figure 1. Power in the linear layer

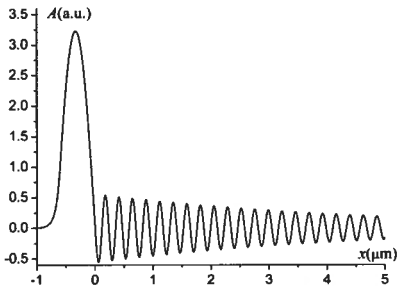

Figure 2. Mode field distribution

References

[1] A. Ashkin et al., *Appl. Phys. Lett*, **9**, p.7, (1966)
[2] G.S. Garcia Quirino et al., *Phys. Rev. A*, **51**, 1571, (1995)

Analysis of Leakage loss in Very Deeply Etched Ridge Waveguides

Qiaoyin Lu, Weihua Guo, Diamuid Byrne, and John F. Donegan
Semiconductor Photonics Group, School of Physics, Trinity College, Dublin 2, Ireland
luqi@tcd.ie

Leaky modes in very deeply etched ridge waveguides have been analyzed by the compact 2D FDTD technique combined with the Padé approximation transform. Results show that the loss of leaky modes tends to saturate when the etching depth under the waveguide core is very deep. Leakage cancellation behavior at specific ridge widths has also been observed.

Introduction

Leaky mode analysis in optical waveguides is very important for designing optical waveguide based devices. Recently we employed a model which combined the compact 2D FDTD method with the Padé approximation transform to analyze the leaky modes in optical waveguides [1]. This model is simple to implement, and it can provide reliable analysis because it calculates the real part and imaginary part of the leaky mode effective index separately. Because of the time domain simulation, this model can account for all mode coupling effects naturally. In the following we will use this model to analyze the leaky loss behavior in very deeply etched ridge waveguides.

Results

The ridge waveguide we analyzed has the same structure as in [1] with the etching depth now extended to 6 μm. In the simulation, only half of the structure is considered by employing a perfect magnetic (electric) wall at the vertical symmetry plane to simulate the TE_{10} (TE_{20}) mode. UPML ABCs with a 1 μm thickness are applied on all the other outer boundaries. A uniform space cell of 0.02 μm is used in the simulation. Fig.1 (a) plots the calculated leaky loss versus the etching depth, which shows that the loss of both TE_{10} and TE_{20} modes tends to saturate when the etching depth is very deep. Fig.1 (b)-(c) plot the calculated leaky loss as a function of ridge width with the etching depth from shallow to deep for the TE_{10} and TE_{20} mode, respectively. It is observed that at specific ridge widths, the leaky loss nearly disappears. For the etching depth of 6 μm, the cancellation peaks become very sharp and the leaky loss is generally several order of magnitude lower than normal values. Similar phenomena have been observed in [2-3].

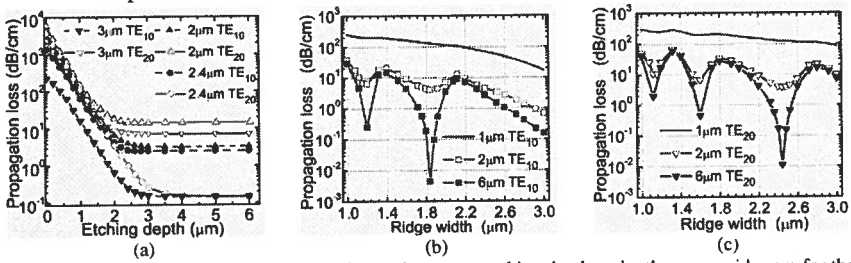

Fig. 1. (a) Calculated propagation loss of leaky modes versus etching depth under the waveguide core for the ridge width of 2, 2.4, and 3 μm. (b)-(c) Calculated propagation loss of leaky modes versus ridge width with the etching depth under the core as 1, 2 and 6 μm for the TE_{10} and TE_{20} mode, respectively.

References

[1] Q. Lu, et al., *Electron. Lett.*, **45**, 700-701, (2009).
[2] M. A. Webster, et al., *IEEE Photon. Technol. Lett.*, **19**, 429-431, (2007).
[3] S. T. Peng et al., *Trans. Inst. Electron.* Jpn., **E61**, 151-154, (1978).

Synthesis of Gradient Refractive Index Profile Waveguides with Desired Propagation Properties

Nikolai E. Nikolaev
Peoples' Friendship University of Russia,6 Miklukho-Maklaya Str., Moscow 117198, Russia
ne_nikolaev@mail.ru

We demonstrate effective and accurate procedure of finding optimal refractive index profile of planar waveguides having desired frequency range of single-mode regime.

Summary

Gradient index profile waveguides, like, for example, polymer ones, has many applications due to possibilities to provide advanced propagation properties. Their fabrication and usage widened during recent years [1]. However, as the fabrication process is too complicated to make an exact profile, some further adjustments are often needed to provide the required propagation properties.

We reported previously on rigorous semi-analytical approach to design the waveguides with complex gradient profiles of refractive index using Shift Formulae Method (SFM) [2]. This method allows solving the problem of synthesis by using the results of direct problem solution.

In this communication, we elaborated the technique of finding optimal refractive index profile of waveguides with desired characteristics. We implemented the technique to find gradient index profile of the waveguide having desired frequency range of single-mode regime.

Shift Formulae Method uses mathematical model to describe the profile [3-5]. This model is flexible enough to represent smooth profiles as Gaussian one, complementary-error function profile and many others, as well as buried profiles. Owing to the model flexibility the SFM makes the synthesis easy and not time-consuming. We show that this technique allows one to determine the refractive index profile of the waveguide with desired properties.

Applying some additional demands to the waveguide characteristics, such as a desired propagation constant at certain frequency, narrows search and allows finding exact refractive index profile of the waveguide.

References

[1] 1. K. Kuriki, T. Kobayashi, N. Imai, T. Tamura, S. Nishihara, A. Tagaya, Y. Koike and Y. Okamoto, *IEEE Photonics Technology Letters*, **12**, No. 8, 989-991 (2000).

[2] N.E. Nikolaev and V.V. Shevchenko, *Proc. XVth International Workshop on Optical Waveguide Theory and Numerical Modelling*, April 20-21, Varese, Italy (2006).

[3] N.E. Nikolaev and V.V. Shevchenko, *Optical and Quantum Electronics*, **39**, No 10-11, 891-902 (2007).

[4] N.E. Nikolaev and V.V. Shevchenko, *J. of Commun. Technology and Electronics*, 43, No 6, 651 (1998).

[5] V.V. Shevchenko, *Sov. J. of Commun. Technology and Electronics*, **31**, No 9, 28 (1986).

Effective-Index-based Matrix Method: a Semi-Analytical Tool to Design Graded-Index Waveguides and Directional Coupler Devices

Pranabendu Ganguly[1], Juran C. Biswas[1], Samir K. Lahiri[1], and Rajib Chakraborty[2]
[1] *Advanced Technology Development Centre, Indian Institute of Technology, Kharagpur, 721302, India*
pran@ece.iitkgp.ernet.in
[2] *Department of Applied Optics and Photonics, University of Calcutta, 92, A. P. C. Road, Kolkata, 700009, India*

Transfer matrix method along with the WKB approximation has been successfully applied to analyse graded-index channel waveguides, bent waveguides, and coupled waveguide devices.

Introduction

Beam propagation method (BPM) in different forms is the mostly used numerical technique to assess 3D graded-index waveguide structures, since an exact analytical solution does not exist for these complex, asymmetric refractive index distributions. This paper highlights a semi-analytical effective-index based matrix method (EIMM) applicable to diffused channel waveguide structures, for quick computation of design parameters with fair accuracy. EIMM can handle both week and strong coupling between the waveguides for any arbitrary lateral refractive index distribution and it determines the radiation loss associated with the guided mode quantitatively.

Theoretical Approach

The eigenvalue equation or WKB quantization condition of the guided modes confined within the depth direction of a waveguide having a refractive index distribution $n(z,x)$ can be written as [1]:

$$\frac{4\pi}{\lambda}\int_0^{z_b}\sqrt{n^2(z,x)-n_{eff}^2(x)}\,dx+\phi_t+\phi_b=2m\pi, \qquad m=0,1,2,\ldots \tag{1}$$

Where z and x are the depth and lateral axes, $z = 0$ and $z = z_b$ are the total internal reflection points in the depth direction associated with ϕ_t and ϕ_b phase changes. This equation has been solved numerically to determine the lateral effective-index profile, $n_{eff}(x)$. In the next step $n_{eff}(x)$ has been discretised into a layered structure and a hypothetical high refractive index medium has been introduced as a 1st layer. 2x2 transfer matrices [2] corresponding to each interface of the layers have been computed. The electric field in the guiding layer has been determined in terms of the incident electric field in the 1st layer by simple matrix multiplication, and excitation efficiency (η) has been computed for different incident angles (θ_I). This prism-coupling approach indicates the guided mode propagation constants (β) (both real and imaginary parts) in terms of resonance peaks (Lorentzian) in η versus θ_I spectra, and finally the mode profiles have been computed using these β values. The accuracy of the method depends on the validity of the slowly varying refractive index approximation in the depth direction, as well as on the optimised separation of the 1st medium from the actual discretised $n_{eff}(x)$ structure. The increment of θ_I during the computation is also a critical parameter for the required accuracy of the β values for further mode profile calculations. EIMM has been successfully applied to design single-mode continuous and segmented waveguides, bent waveguides, two-mode interference (TMI) structures, and coupled waveguide devices, for Ti:$LiNbO_3$ technology. Some of the design results are validated with BPM and experimental data.

References

[1] K.T. Koai, et al., *J. Lightwave Technol.*, **7**, 533- 539, 1989.

[2] A.K. Ghatak, et al., *J. Lightwave Technol.*, **5**, 660- 667, 1987.

Improved Variational Effective Index Approximation for Photonic Crystal Slabs

Pushpa Bindal* and Anurag Sharma
Physics Department, Indian Institute of Technology Delhi, New Delhi – 110 016
asharma@physics.iitd.ac.in

We present an improved variational effective index method for reduction of 2-D Bragg grating problems to 1-D and show significant improvements particularly at smaller wavelengths. The method is based on the optimal variational (Vopt) method, which we have earlier used successfully for conventional waveguides.

Summary

In a recent paper, Hammer and Ivanova [1] have examined the applicability of the effective index method (EIM) and of its improved form, the variational effective index (vEIM), for obtaining the reflection and transmission characteristics of photonic crystal slab waveguides. It has been concluded that the methods are largely inadequate, particularly for the region of smaller wavelength. In the EIM, the effect of the transverse waveguide is used only to modify the index of the high index region (film) and the low-index regions (air-holes) are left unmodified (or given an index on the basis of an 'educated guess'). In the vEIM [1], the indices of the both low and the high index regions are also modified on the basis of a common transverse waveguide. In both cases, transverse waveguide used does not take into account the presence of index variational along the length of the Bragg structure. Our approach takes this into account by making the variational effective index method iterative as in the case of optimal variational method (Vopt) [2]. In this approach, the method of Hammer and Ivanova [1] can be considered as the zeroeth order iteration, while we have shown significant improvement by the use one more iteration. We have used earlier the Vopt method for successfully reducing 3-D conventional waveguiding structures to equivalent 2-D structures [2].

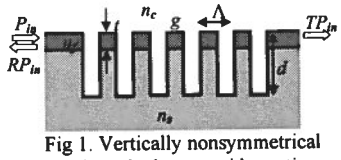

Fig 1. Vertically nonsymmetrical deeply etched waveguide grating; n_f=2.0; n_c = 1.0; n_s=1.45; (Λ, g, t, d) = (0.21, 0.11, 0.2, 0.6) μm

As an example, we include results for the structure studied in [1] shown in Fig.1. The results for the reflectance (R) and transmittance (T) are shown in Fig.2 where we have also included the results of the QUEP method [3] taken from [1] as reference for comparison. These results show that for smaller wavelength region, where the vEIM performed poorly, significant improvement are obtained. More examples and analysis would be presented at the Workshop.

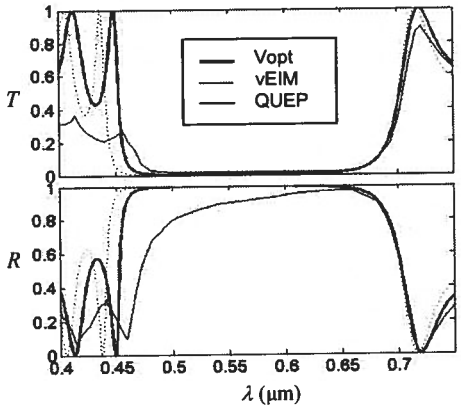

Fig 2. Reflectance (R) and Transmittance (T) of the grating shown in Fig.1 as a function of wavelength

This work was partially supported by a grant from the CSIR, Govt. of India and through UKIERI Project.

References

[1]. M. Hammer, O. V. Ivanova, *OWTNM 2009*, Jena, Germany, April 17-18, 2009; also *Opt. Quantum. Electron.* DOI 10.1007/s11082-009-9349-3 (2009).
[2] A. Sharma, P. Bindal, *Opt. Quantum. Electron.* **24**, 1359 (1992); A.Sharma, *ibid* **21**, 517 (1989).
[3] M. Hammer. *Optics Commun.* **235**, 285 (2004).

* *On leave from Kalindi College, Delhi University.*

Parallel Simulation of Non-Local Non-Linear Schrödinger Systems Using Multithreaded Graphical Processing Unit

Mandana Baregheh, Vladimir Mezentsev, and Holger Schmitz
Photonics Research Group, Aston University, Birmingham B4 7ET, UK
bareghem@aston.ac.uk

We present a scalable solution for parallel integration of the non-local non-linear Schrödinger equations using a multithreaded parallel hardware. Specific implementation has been performed using the highly parallel capabilities of a programmable graphics processor.

Introduction

Non-Linear Schrödinger Equation (NLSE) and its generalisations are generic mathematical models typically describing narrow bandwith wave propagation in envelope approximation. In this paper we consider a parallel numerical solution for a specific model which describes femtosecond laser pulse propagation in transparent media [1], [2]. However our approach can be extended to similar models. We compare performance of the described below parallel code implementated for Nvidia Graphics Processing Units using CUDA programming interface [3] with a serial CPU version used in [1], [2].

Efficient use of GPU's parallel resources requires radical revision of the current pipelined method. In the following model the first equation is the NLSE describing an envelope amplitude u of the laser wave coupled to the equation for a concentration of plasma carriers ρ (the notation and parameters are described in [1], [2]):

$$\partial_z u - i\kappa\Delta_\perp u = i\sigma|u|^2 u - id\partial_{tt}u - i(\gamma\Omega\tau)\rho u - \mu|u|^{2(K-1)}u\,; \quad \partial_t\rho = \nu\rho + \left(\frac{u}{u_0}\right)^{2K} \tag{1}$$

Coupling between the equations makes NLSE non-local which results in impossible straightforward parallel implementation.

To simplify the problem, the splitting operator method is used here similar to that in [1] to reduce it into a succession of linear and nonlinear steps. The linear term is solved in frequency domain using `cufft`, the Fast Fourier Trasform (FFT) implemented in Nvidia CUDA's Fourier transform Library [4]. The parallel simulation of the nonlinear term is not straightforward due to non-locality. A different approach is adopted which parallelises the solution by splitting the nonlinear problem as an integral equation in time domain. Partial integrals are delegated for calculation performed by concurrent threads. Trapeziodal integration is used to calculate the integral terms.

Results

We have managed to successfully parallelise solution of NLSE using CUDA. We have tested the accuracy of the results which gave us a satisfactory 10^{-6} difference between GPU and CPU results. As for performance time, we have 10x speed up on a modest Quadro FX 570.

References

[1] V. Mezentsev, et al., *SPIE, Laser-based Micropackaging*, **6107**, 241–250 (2006)
[2] V. Mezentsev, et al., *SPIE, Laser-based Micro- and Nanopackaging and Assembly.* **6459**, 64590B (2007)
[3] Nvidia Corporation, *Nvidia CUDA Programming Guide*, http://developer.download.nvidia.com/
[4] Nvidia Corporation, *CUDA CUFFT Library*, http://developer.download.nvidia.com/compute/cuda/

Fundamentals of multi-reflector filtering technology

Andrey V. Tsarev
Laboratory of Optical Materials and Structures
Institute of Semiconductor Physics SB RAS,
Novosibirsk, 630090, Russia
tsarev@isp.nsc.ru

Abstract—**The paper discusses different basic photonic structures which built the fundamentals of multi-reflector filtering technology aimed to develop optical tunable devices with multi-hundreds reconfigurable wavelength channels.**

Keywords-component: Integrated optics; silicon photonics; nanophotonics; acousto-optics; BPM and FDTD methods.

I. INTRODUCTION

Modern society is based on growing information exchange providing by fiber optics networks. Different technologies (ring resonators, Brag gratings, thin film filters, AWG, acousto-optics (AO), etc.) that are currently used for manufacturing tunable filters and reconfigurable Add/Drop multiplexes (ROADM) supports the assumption that at date we have not got an optimal solution for optical devices adjusting the growing market demands. One of the most important tasks is to develop technologies which can flexibly handle 1000 WDM-wavelength channels in the single fiber.

This paper discuss different basic photonic structures which built the fundamentals of multi-reflector (FR) filtering technology studded in order to rich this ambitious challenger.

II. ACOUSTOOPTICS IN MULTI-REFLECTOR STRUCTURES

Acousto-optics is among perspective technologies as it provides wide tuning, high switching time and unique opportunity of flexible redirection into a single fiber of multiple wavelength optical signals by launching the multi-frequency acoustic signals. Unfortunately this technology has principal limitation in filtered linewidth thus the best AO devices could work only with 100 GHz channel spacing [1].

By the use of multi-reflector (MR) beam expanders [2] (with strong dispersion) the wavelength channel spacing could be increased in several times [3-5]. Unfortunately this technology approach has not been demonstrated due to extremely complicate problem to manufacture partial reflectors on good AO material like $LiNbO_3$. One can show that photonic row of holes [6] deeply etched through $Ti:LiNbO_3$ waveguide (see Fig.1) are the best candidate for this AO devices. Alternative technology is based on utilizing chalcogenide As_2S_3 thin films where partial strips reflectors could be written by electron beam our by ultraviolet radiation. AO devices are inherently polarized depending. In order to provide polarization diversity one can use polarization splitters and polarization rotators. Among other different technologies we propose to use the set of deep trenches as polarization splitter [7] and use channel waveguide [8] tilted at small angle respect to Z axis on Y-cut of $LiNbO_3$ as a polarization rotator.

III. ROADM ON SOI

Alternative and very perspective technology to develop widely tunable devices is based on CMOS-compatible silicon nanophotonics [9, 10]. Multi-reflector filtering approach [11] inherently uses wide and single mode waveguides which need to decrease parasitic signals. In order to build such waveguide in high-contrast silicon-on-insulator (SOI) structures with thin (~ 220 nm) silicon core we set up the novel waveguide designs. General idea is to construct the wide waveguides with strong mode-dependent properties (that depends on mode distribution) in those manner that fundamental mode will have small optical loss and all other modes – very high. Heterogeneous [12-14] waveguide (see Fig.3a) provides mode-dependant loss by additional loss regions with high concentration of electrons and holes on the sides of SOI rib. Thus it has different propagation loss for zero and first modes: Loss0 ~ -1.4 dB/cm, Loss1 ~ -8.6 dB/cm [12]. Even better optical properties (Loss0 ~ -0.7 dB/cm, Loss1 ~ -10.7 dB/cm) has new strip and grating loaded (SGL) waveguide [15] shown in Fig.3b. The central silicon nitride strip forms conventional strip loaded waveguide and additional side gratings produce strongly mode dependent loss due to coupling to radiation modes [15]. Depending of the case study and available technology both of these quasi-single mode waveguides could be used to manufacture MR-filtering devices. Partial reflectors can be developed as thin (40 nm) grooves [12, 13] or photonic crystal row of subwavelength holes [6, 16] that cross the waveguide core and aligned at close to Brewster angle (to provide small reflection coefficient in high-contrast waveguide). To provide high efficiency, crosstalk and sidelobe suppression, one has to optimize the reflection coefficient of different partial reflectors. It could be done by varying the reflector thickness or diameter of holes [16] or tilting the angle orientation of reflectors [12]. From the other side this courses undesirable phase change in transmitted and reflected sub-beams which interfere and construct output signals. Compensation of these parasitic changes is done by changing the reflector position. Principal view of MR-ROADM is shown on Fig.4a. The part of the structure (in the large scale) is shown in Fig.4b where also presents alternative variants of basic photonic structures, namely, heterogeneous and SGL - waveguides, different type of partial reflectors (as trenches or rows of holes).

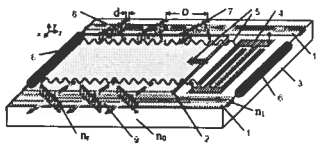

Figure 1. Noncollinear MR-AO fillter built by the rows of holes: (1) channel waveguide; (2) planar waveguide; (3) piezoelectric substrate; (4) interdigital transducer; (5) surface acoustic wave (SAW); (6) SAW absorber; (7) partial reflector; (8) first beam expander; (9) second beam expander.

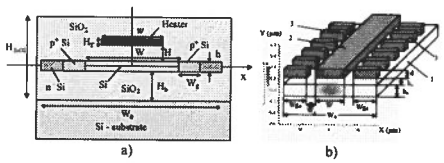

Figure 2. Wide SOI waveguides. (a) Heterogeneous; (b) SGL-waveguide and field distribution of TE_0 mode; 1 – slab Si; 2 – silicon nitride strip over the silica buffer; 3 – grating;

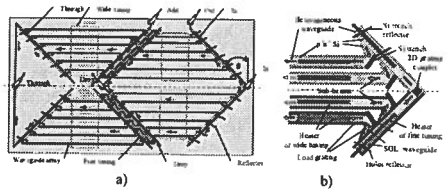

Figure 3. Thermo-optic MR-ROADM on thin SOI. (a) General view; (b) different possible structure design in the vicinity of input 2D grating.

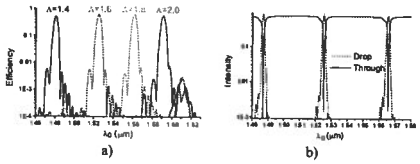

Figure 4. 2D FDTD simulation of MR-devices with 32 reflectors. (a) Response of AO filter built by row of holes at the different acoustical wavelength Λ (in μm); (b) Response of ROADM built by deep trences.

Tuning of filtered wavelength could be done by thermo optic phase shifters for wide and fine tuning. Note that device can be tuned within total FSR = 40 nm by moderate change of temperature ($\Delta T < 65°$) in the appropriate waveguides [12-14]. Polarization diversity provides by 2D grating couplers [17] with the aperture ideally fitting both the fiber core and novel waveguides. Technical parameters of MR-AO filters and MR-ROADMs had been examined [5, 12, 13] by direct simulation by FDTD and FEM methods by commercial software (for small number of reflectors N_r=32) to make prove the concept of MR-technology, as well by in-house software [4, 12] which demonstrate wide tuning of 200 wavelength channels.

Conclusion

This paper makes a short review of basic photonic structures which can be used to manufacture multi-reflector filtering devices as well to construct other optical elements. MR-technology had not been demonstrated experimentally but has a lot of advantages as it gives the principal possibility to develop tunable acousto-optic filters and thermo-optic ROADM with control of multi-hundred wavelength channels.

Acknowledgment

The author thanks Company RSoft Design Group, Inc. for providing user license for BPM and FTDT software [18].

References

[1] T.Nakazawa, M.Doi, S.Taniguchi, Y.Takasu, and M.Seino, "Ti:LiNbO3 AOTF for 0.8 nm Channel-Spaced WDM," Proc. OFC'98, PD1, 1998.

[2] A. V. Tsarev, "Beam-expanding device," United States Patent No 6,836,601, December 28, 2004.

[3] A.V.Tsarev "Acousto-optical variable filter," United States Patent No. 7,092,139, August 15, 2006.

[4] A.V.Tsarev, E.A.Kolosovsky "A Compact narrow linewidth acousto-optic tunable filter," Avtometriya (Optoelectronics, Instrumentation and Data Processing), vol. 42, No 6, pp. 93-104, 2006.

[5] A.V. Tsarev, "Finite-difference time-domain simulation of compact acousto-optic filters based on multireflection beam expanding," Quantum Electronics, vol. 37, pp. 393-398, 2007.

[6] Pierre Pottier, Sara Mastroiacovo, and Richard M. De La Rue, "Power and polarization beam-splitters, mirrors, and integrated interferometers based on air-hole photonic crystals and lateral large index-contrast waveguides," Optics Express, vol. 14, pp. 5617- 5633, 2006.

[7] Andrei V. Tsarev. Simulation of New Integrated-Optics Polarisation Controller in SOI Technology, in Proceedings XV International Workshop on Optical Waveguide Theory and Numerical Modelling, Varese, Italy, 20 and 21 April 2006, poster P27, p.43, 2006.

[8] Andrei V. Tsarev, "New compact polarization rotator in anisotropic $LiNbO_3$ graded-index waveguide," Optics Express, Vol. 16, pp. 1653-1658, February 2008.

[9] G. T. Reed, Silicon Photonics. State of the art (John Wiley & Sons, Ltd, 2008).

[10] W. Bogaerts, et al., "Nanophotonic Waveguides in Silicon-on-Insulator Fabricated With CMOS Technology," J. Lightwave Technol. 23, pp. 401-412, 2005.

[11] A. V. Tsarev, "Tunable optical filters," United States Patent No 6,999,639, February 14, 2006.

[12] A. V. Tsarev, "Thin heterogeneous optical silicon-on-insulator waveguides and their application in reconfigurable optical multiplexers," Quantum Electronics, vol. 38, pp. 445-451, 2008.

[13] A. V. Tsarev, F. De Leonardis, and V.M.N. Passaro, "Thin heterogeneous SOI waveguides for thermo-optical tuning and filtering," Opt. Express, vol. 16, pp. 3101-3113, 2008.

[14] Francesco De Leonardis, Andrei V. Tsarev, Vittorio M. Passaro, "Optical properties of new wide heterogeneous waveguides with thermo optical shifters," Optics Express, vol. 16, pp. 21333–21338, 2008.

[15] Andrei V. Tsarev, "New wide strip and grating loaded quasi-single-mode waveguide on SOI," Opt. Express, vol. 17, pp. 13095-13101, 2009.

[16] A.Tsarev, "Power beam-splitter based on photonic crystal row of holes and Brewster effect in SOI waveguides" Optics Letters, in press.

[17] W. Bogaerts, D. Taillaert, P. Dumon, D. Van Thourhout, R. Baets, "A polarization-diversity wavelength duplexer circuit in silicon-on-insulator photonic wires," Opt. Express, vol. 15, pp. 1567-1578, 2007.

[18] www.rsoftdesign.com, Rsoft Photonic CAD Suite, ver. 8.

Numerical simulation of power beam-splitter based on photonic crystal row of holes and Brewster effect

Andrey V. Tsarev
Institute of Semiconductor Physics SB RAS,
Novosibirsk, 630090, Russia
tsarev@isp.nsc.ru

***Abstract*—A power beam splitter built in a silicon-on-insulator (SOI) ridge waveguide by photonic crystal row of holes at close to the Brewster angle had been examined by 3D FDTD method. It provides a small splitting ratio (< 0.04) for silica filled holes with diameter 200 nm and spacing 300 nm.**

Keywords-component: Integrated optics; silicon photonics; nanophotonics; photonic crystal row of holes, power splitter; Brewster effect; FDTD method.

I. Introduction

Recently, photonic crystal rows of holes at 45° were used as the power and polarization beam-splitters in the large index-contrast waveguides [1]. It was shown that the single row of air-holes at 45° can provide typical splitting ratio 0.2-0.8 by changing the period of holes (a) and/or filling-factor (f), defined as the ratio of the area of the air discs to the total area. Multi-reflector filtering devices [2-4] have to use much smaller splitting ratio (< 0.04) which needs a small filling factor (f < 0.3) for the current design [1] based on 45° row of holes. Alternative 45° air-slot configuration (working in a frustrated total internal reflection regime) requires ultra narrow (< 20 nm) slot width [1]. Thus both of these technologies are expected to have difficulties in fabrication of beam-splitters with small splitting ratio. During the study of multi-reflector filtering elements we have shown [3, 4] that for TE polarization (electric field in the plate of waveguide) the air-slots built at close to Brewster angle could provide desired splitting ratio by changing the angle and/or the slot width (> 40 nm).

This paper joints together both of these approaches and for the first time examines the Brewster effect for TE guided wave which is propagated through compact photonic splitter built by subwavelength row of holes (see Fig.1) [5]. Note, that TE polarization is typically used by two dimensional gratings to provide the polarization diversity [6]. Thus this case of TE polarization is the most important for CMOS compatible photonic structures on silicon-on-insulator (SOI) that utilized thin (~0.2 μm) silicon waveguide core.

Photonic beam-splitters based on the Brewster effect are properly working only with wide optical beam [3, 4]. In the case of narrow beam, the different spectrum components have to be reflected with different amplitudes and thus strongly disturbs reflected field. From the other side, the wide channel waveguide in the large index-contrast structures is always multimode which could produces multiple ripples in the transmitted signal due to multimode interference [1]. In order to suppress the parasitic higher order modes we propose to use heterogeneous [3, 4] or strip and grating loaded (SGL) [7] waveguides which are quasi-single-mode even for large waveguide width (4-12 μm). Their single-mode behavior is due to the effect of strongly mode-dependent optical loss produced by special side regions with additional loss coursed by the free carrier dispersion (in heterogeneous waveguide) or by the coupling to radiation modes (by the subwavelength side grating in SGL waveguide). Both of these waveguides are possible to approximate by ridge waveguide structure with small complex variation of refractive index at both sides of waveguide strip. It means that these waveguides on thin SOI structures can be correctly simulated as the low index-contrast strip waveguides in lateral direction and the large index-contrast waveguides in transverse direction.

II. Photonic Crystal Row of Holes

General structure of intersecting ridge waveguides crossed by row of holes is presented on Fig.1. The silicon waveguide core (height $h = 0.24$, width $W = 4$ μm and refractive index $n_1 = 3.478$) is bounded with the side regions of width $W_g = 4$ μm and the smaller refractive index $n_2 = 3.378$. Holes of period $a \sim 300$ nm and diameter $d \sim 200$ nm are etched through the total silicon core. The surrounding media and holes are filled by silica with refractive index $n_r = 1.4$. This structure is a good analogy with heterogeneous or SGL waveguides except the smaller width W and the larger index increment $\Delta n = n_1 - n_2$, which are artificially chosen in order to decrees the guided mode size and thus to minimize 3D FDTD simulation region.

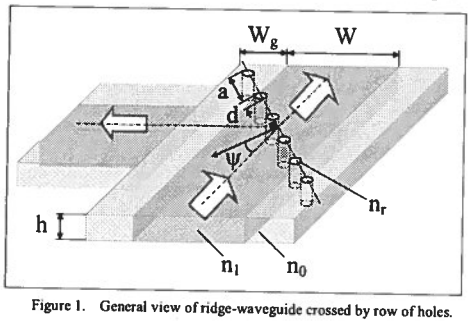

Figure 1. General view of ridge-waveguide crossed by row of holes.

Results of 3D FDTD simulation of the reflecting (R_0) and transmitting (T_0) power coefficients for the fundamental TE_0 mode measured at different incident optical wavelength λ_0 and angle Ψ are presented on Fig.2b. The scattering loss is determined as $Loss = 1 - R_0 - T_0$.

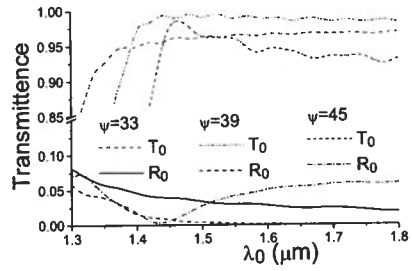

(a)

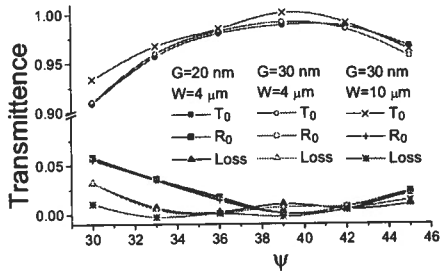

(b)

Figure 2. Transmittence of TE_0 mode in ridge-waveguide crossed by row of holes. (a) Spectrum response at different Ψ. d = 180 nm, a = 280 nm, W = 4 μm. (b) Dependence on incident angle at different W and grid size G at λ_0 = 1.55 μm. d = 200 nm, a = 300 nm.

These results prove that row of holes possesses the Brewster effect, namely, reflected power of fundamental mode goes to zero at the Brewster angle (~ 39°). Note, that TE_0 guided mode has a moderate divergence (~ 7.5°) in the plate of waveguide that courses a strong beam-distortion effect [8] at and close to the Brewster angle. As a result, reflected wave is slightly tilted in opposite directions for the incident angle Ψ smaller and larger the Brewster angle. Just at Brewster incident angle the reflected wave contains two optical beams of small and almost equal amplitudes which courses moderate loss of power of TE_0 mode in the vicinity of 39° (see Fig.2b). Taking into account the beam-distortion effect, the FDTD Time Monitors [9] are tilted about ±3° in order to maximize the reflected power of TE_0 mode. As the beam-distortion is coursed by angular divergence of reflected beam, thus for wider waveguide (W = 10 μm) this effect is insufficient (see Fig.2b). Slanted row of holes also shifts transmitted beam by value $\delta W \sim 8$ nm, thus part of waveguide section after reflector is shifted by δW. Besides, the larger waveguides provides the less radiation loss due to the smaller angle divergence.

Analysis of Fig.2b shows that we have three mechanisms of power loss which are the most essential in different ranges of incident angle Ψ. The first one is coursed by beam-distortion effect [8] in a vicinity of the Brewster angle. The next one is the effect of back scattering (for large Ψ) in the -1st order diffraction by the Bragg grating formed by row of holes. The last mechanism of loss is taken place for angles $\Psi \leq 30°$ due to strong radiation of scattering power into surrounding (up and down) silica media by row of holes that work as scattering source (by refractive index discontinue in the holes boundary).

For the illustration Fig.2b also presents result for different simulation grid. It shows that for the most interesting angle range $30° < \psi < 39°$ the grid 20 nm and 30 nm give similar results which prove the high accuracy of 3D FDTD simulation.

SUMMARY

To summarize, the guided mode reflection by photonic crystal row of holes in large index-contrast ridge waveguide is examined by 3D FDTD. It was shown that TE wave possess a typical Brewster effect and thus row of holes could be used as a power divider with small splitting ratio (< 0.04). Row of holes (filled by silica) in wide 10 μm waveguide provides the small scattering loss. Incorporation of row of holes in single-mode heterogeneous [3, 4] or strip and grating loaded waveguide [7] with the CMOS compatible multi-reflector filtering technology [3-4] provides the possibility to develop novel tunable filters and multiplexes which can handle multi-hundreds wavelength channels in DWDM optical networks.

ACKNOWLEDGMENT

The author thanks Company RSoft Design Group, Inc. [9] for providing user license and technical support for Rsoft Photonic CAD Suite 8.0 for BPM and FDTD simulations.

REFERENCES

[1] Pierre Pottier, Sara Mastroiacovo, and Richard M. De La Rue, "Power and polarization beam-splitters, mirrors, and integrated interferometers based on air-hole photonic crystals and lateral large index-contrast waveguides," Optics Express, vol. 14, pp. 5617- 5633, 2006.

[2] A. V. Tsarev, "Tunable optical filters," United States Patent No 6,999,639, February 14, 2006.

[3] A. V. Tsarev, "Thin heterogeneous optical silicon-on-insulator waveguides and their application in reconfigurable optical multiplexers," Quantum Electronics, vol. 38, pp. 445-451, 2008.

[4] A. V. Tsarev, F. De Leonardis, and V.M.N. Passaro, "Thin heterogeneous SOI waveguides for thermo-optical tuning and filtering," Opt. Express, vol. 16, pp. 3101-3113, 2008.

[5] A.Tsarev, "Power beam-splitter based on photonic crystal row of holes and Brewster effect in SOI waveguides" Optics Letters, in press.

[6] W. Bogaerts, D. Taillaert, P. Dumon, D. Van Thourhout, R. Baets, "A polarization-diversity wavelength duplexer circuit in silicon-on-insulator photonic wires," Opt. Express, vol. 15, pp. 1567-1578, 2007.

[7] Andrei V. Tsarev, "New wide strip and grating loaded quasi-single-mode waveguide on SOI," Opt. Express, vol. 17, pp. 13095-13101, 2009.

[8] C. Chiu Chan, and T. Tamir, "Angular shift of a Gaussian beam reflected near the Brewster angle," Optics Letters, vol. 10, pp. 378 -380, 1985.

[9] www.rsofdesign.com, Rsoft Photonic CAD Suite, ver. 8.0.

Design and simulation of photonic crystal thin film photovoltaic cells

Guillaume Gomard[1,2], Emmanuel Drouard[1], Ounsi El Daif[1,2], Xianqin Meng[1,2], Anne Kaminski[2], Alain Fave[2], Mustapha Lemiti[2] and Christian Seassal[1]

Université de Lyon, Institut des Nanotechnologies de Lyon (INL), UMR 5270 CNRS- INSA-ECL-UCBL

[1] Ecole Centrale de Lyon, 36 avenue Guy de Collongue, 69134 Ecully Cedex, France

[2] INSA de Lyon, Bat. Blaise Pascal, 7 avenue Capelle, 69621 Villeurbanne, France

guillaume.gomard@ec-lyon.fr

We report on an increase of the absorption efficiency of thin film photovoltaic solar cells, by periodically patterning the absorbing layer as a planar photonic crystal (PC). This can be achieved through holographic lithography or nanostamping, two low-cost techniques yielding to large patterned areas. Concepts are introduced by focusing on amorphous silicon (a-Si:H) as the absorbing medium.

First theoretical studies conducted on 100 nm thick single 1D-PC membranes made of a-Si:H predicted a solar light absorption efficiency of nearly 44% between 300 nm and 750 nm, against 33% for a non-patterned layer [1]. This enhancement was experimentally confirmed in a good agreement with optical simulations [2]. Then, the absorption properties of 2D-PC membranes with a square symmetry were investigated. A relative increase of 25% for the absorption efficiency occurs when replacing the 1D-PC by a 2D-PC, together with a less polarization dependence. Hence, we introduce a complete cell as shown in Fig. 1.

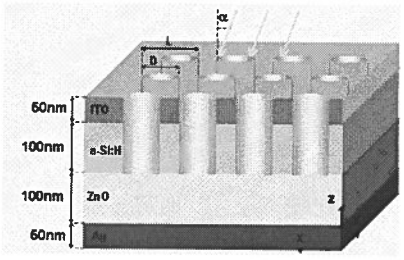

Fig. 1: Schematic illustration of a complete stack patterned as a 2D-PC

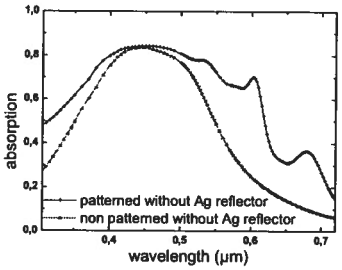

Fig. 2: Effect of 2D patterning on the simulated absorption spectra of the a-Si:H layer in the complete stack (without Ag back-reflector)

Such a stack would present 70% of its solar light integrated absorption in the active layer, instead of barely 54% in the case of the non-patterned stack. As shown on Figure 2, a significant absorption efficiency increase is expected between 500 nm and 700 nm, where the absorption of the a-Si:H is usually low.

This gain should result in an equivalent increase of the conversion efficiency, since the thickness of the a-Si:H layer is lower than the mean free path of the minority carriers, leading to a low level of bulk carrier recombination. The global electro-optical characteristics of those "photonised" solar cells will thus be discussed. Carrier generation rate maps from optical simulations are introduced in electrical simulation software. It is aimed at the optimization of the device from an electrical point of view and at the derivation of such characteristics as the conversion efficiency, for sake of comparison with experimental values.

References

[1] Y. Park, E. Drouard, O. El Daif, X. Letartre, P. Viktorovitch, A. Fave, A. Kaminski, M. Lemiti, C. Seassal, *Optics Express* **17** 14312 (2009)

[2] O. El Daif, E. Drouard, A. Fave, A. Kaminski, M. Lemiti, X. Letartre, P. Viktorovitch, C. Seassal, *Proc. 24th European Photovoltaic Solar Energy Conference* 548 (2009)